Thèse n° 9682

Resilient drones with morphing wings

Présentée le 20 mars 2023

Faculté des sciences et techniques de l'ingénieur
Laboratoire de systèmes intelligents
Programme doctoral en robotique, contrôle et systèmes intelligents

pour l'obtention du grade de Docteur ès Sciences

par

Charalampos VOURTSIS

Acceptée sur proposition du jury

Prof. F. Mondada, président du jury
Prof. D. Floreano, directeur de thèse
Prof. . M. Kovac, rapporteur
Prof. A. Ollero, rapporteur
Prof. S. Mintchev, rapporteur

École
polytechnique
fédérale
de Lausanne

2023

To myself.

Acknowledgments

This work would not have been possible without the financial support from EPFL and the EPFLinnovators fellowship program. I would like to express my deepest gratitude to my thesis director Prof. Dario Floreano for welcoming me to the Laboratory of Intelligent Systems and allowing me to participate in a state-of-the-art, diverse and stimulating environment with incredible and inspiring people.
I would also like to thank my thesis committee members Prof. Anibal Ollero, Prof. Mirko Kovac, Prof. Stefano Mintchev, and Prof. Francesco Mondada, who have taken the time to review this thesis and contributed in providing constructive criticism to improve it further. I would like to extend my sincere thanks to the NCCR Robotics and the Aerial Core EU project for actively supporting the work in this thesis.
Words cannot express my gratitude to the people who collaborated with me throughout these years. I am extremely thankful to Prof. William Stewart for being an excellent advisor and friend. I am also grateful to the students I supervised all these years and especially Victor Casas Rochel and Francisco Ramirez Serrano. In particular, I would like to express my special thanks to Nathan Müller, who not only actively contributed to this work but also continues to support me in promoting my vision for aerial robotics.
I would also like to express my gratitude to Michelle Wälti, Corinne Lebet, and Michèle Jaccoud Ramseier for their administrative help and support throughout these years.
In addition, I would like to thank my friends and colleagues, Dr. Fabrizio Schiano and Dr. Przemyslaw Kornatowski, that helped me throughout these years with stimulating discussions, helpful feedback, and advice. Thanks should also go to Olexandr Gudozhnik for his outstanding engineering support.
Moreover, I would like to thank all my colleagues in the Laboratory of Intelligent Systems for the time we spent in and out of the lab and helped to create a friendly, inclusive, and supportive environment to work in.
Continuing, I would like to thank my long-lasting friends George, Eirini, Loukas, Nikos, William, Fabrizio, and their families, who supported me and continue to support me for all these years.
Next, I would like to thank my partner Georgia for her love and support in my journey to achieve the best possible version of myself.
Last but not least, I would like to thank my family for their unconditional love and support for

about 30 years, during the good and bad times — my parents, Giota and Sakis, and my sister Marvina.

Lausanne, February 24, 2023 Charalampos Vourtsis.

Abstract

Winged aerial robots and Unmanned Aerial Vehicles (UAVs) commonly referred to as winged drones and drones, are increasingly used in a wide range of professional and non-professional applications today, spanning from civilian to military. As a result, they have to operate in diverse and challenging environments throughout their mission. However, these flying robots suffer from design limitations that reduce their operational envelope in such environments, increasing cost and restricting their mission advantage over other vehicles. Moreover, current winged drones' fixed geometry limits their operational versatility due to their inability to adjust to the requirements dictated by their diverse, complex, and often changing environments.
For example, strong and sustained wind currents can tip over or push off-course small-sized drones with exposed wings. Once tipped over, fixed-wing drones will be unable to continue their mission. In addition, when a mission might require ground operations, these winged drones may be prone to damage caused by contact between their exposed wings and electronics with ground objects.
Drones that are resilient to challenging conditions exist in the literature and on the market, although they are restricted to rotorcrafts with limited range and operational endurance. The purpose of this thesis is to develop the next generation of resilient, autonomous, winged aerial robots. The focus will be on addressing operational requirements that a wing drone might face during routine industrial missions, for example, inspection, monitoring, reconnaissance and search and rescue. Different methodologies and design strategies will be presented to allow next-generation winged drones to operate in these challenging conditions, including adverse wind currents and changes from open, wide to cluttered, confined, and unstructured environments.

Keywords: aerial robotics, bio-inspiration, morphing, shape-shifting, winged drones, VTOLs, hybrid UAVs

Résumé

Les robots aériens ailés et les véhicules aériens sans pilote (UAV), communément appelés drones ailés et drones, sont aujourd'hui de plus en plus utilisés dans un large éventail d'applications professionnelles et non professionnelles, du secteur civil au militaire. Par conséquent, ils doivent opérer dans des environnements divers et difficiles tout au long de leur mission. Cependant, ces robots volants souffrent de limitations de conception qui réduisent leur enveloppe opérationnelle dans de tels environnements, ce qui augmente leur coût et limite leur avantage par rapport à d'autres véhicules. De plus, la géométrie fixe des drones ailés actuels limite leur polyvalence opérationnelle en raison de leur incapacité à s'adapter aux exigences dictées par ces environnements divers, complexes et changeants.

Par exemple, des vents forts et soutenus peuvent faire basculer ou pousser hors trajectoire des drones de petite taille dont les ailes sont exposées. Une fois renversés, les drones à ailes fixes seront incapables de poursuivre leur mission. En outre, lorsqu'une mission nécessite des opérations au sol, ces drones ailés peuvent être sujets à des dommages causés par le contact de leurs ailes et de leur électronique avec des objets au sol.

Des drones résistants aux conditions difficiles existent dans la littérature et sur le marché, bien qu'ils soient limités à des appareils à rotor avec une portée et une endurance opérationnelle limitées. L'objectif de cette thèse est de développer la prochaine génération de robots aériens ailés, autonomes et résilients. L'accent sera mis sur le traitement des exigences opérationnelles auxquelles un drone ailé pourrait être confronté lors de missions industrielles de routine, par exemple, l'inspection, la surveillance, la reconnaissance et la recherche et le sauvetage. Différentes méthodologies et stratégies de conception seront présentées pour permettre aux drones ailés de la prochaine génération de fonctionner dans ces conditions difficiles, comprenant les courants de vent défavorables et les changements d'environnements ouverts et larges à des environnements encombrés, confinés et non structurés.

Mots-clés : robotique aérienne, bio-inspiration, morphing, shape-shifting, drones ailés, VTOLs, drones hybrides

Περίληψη

Τα εναέρια ρομπότ με φτερά και τα μη επανδρωμένα εναέρια οχήματα (UAV) που συνήθως αναφέρονται ως φτερωτά drones ή και drones χρησιμοποιούνται όλο και περισσότερο σε ένα ευρύ φάσμα επαγγελματικών και μη επαγγελματικών εφαρμογών σήμερα, στον πολιτικό και τον στρατιωτικό τομέα. Ως αποτέλεσμα, πρέπει να λειτουργούν σε ποικίλα και απαιτητικά περιβάλλοντα καθ΄ όλη τη διάρκεια της αποστολής τους.

Ωστόσο, αυτά τα ιπτάμενα ρομπότ πάσχουν από σχεδιαστικούς περιορισμούς που μειώνουν το επιχειρησιακό τους πεδίο σε τέτοια περιβάλλοντα, αυξάνοντας το κόστος και περιορίζοντας τα πλεονεκτήματα της αποστολής τους έναντι άλλων οχημάτων. Η στατική γεωμετρία των σημερινών φτερωτών ρομπότ περιορίζει την επιχειρησιακή τους ευελιξία λόγω της αδυναμίας τους να προσαρμοστούν στις απαιτήσεις που υπαγορεύουν τα ποικίλα, πολύπλοκα και συχνά μεταβαλλόμενα περιβάλλοντα.

Για παράδειγμα, τα ισχυρά και συνεχή ρεύματα ανέμου μπορούν να ανατρέψουν ή να σπρώξουν εκτός πορείας αεροσκάφη μικρού μεγέθους με εκτεθειμένα φτερά. Μόλις ανατραπούν, τα μη επανδρωμένα αεροσκάφη στατικής πτέρυγας δεν θα μπορούν να συνεχίσουν την αποστολή τους. Επιπλέον, όταν μια αποστολή μπορεί να απαιτεί επιχειρήσεις στο έδαφος, αυτά τα φτερωτά μη επανδρωμένα αεροσκάφη μπορεί να είναι επιρρεπεπείς σε ζημιές που προκαλούνται από την επαφή των εκτεθειμένων φτερών και των ηλεκτρονικών τους με αντικείμενα στο έδαφος.

Τόσο στη βιβλιογραφία όσο και στην αγορά υπάρχουν μη επανδρωμένα αεροσκάφη ανθεκτικά σε δύσκολες συνθήκες, ωστόσο περιορίζονται σε ελικόπτερα με περιορισμένη εμβέλεια και επιχειρησιακή αντοχή. Σκοπός της παρούσας διατριβής είναι η ανάπτυξη της επόμενης γενιάς ανθεκτικών, αυτόνομων, φτερωτών εναέριων ρομπότ. Έμφαση θα δοθεί στην αντιμετώπιση των επιχειρησιακών απαιτήσεων που μπορεί να αντιμετωπίσει ένα φτερωτό drone κατά τη διάρκεια βιομηχανικών αποστολών ρουτίνας, για παράδειγμα, επιθεώρηση, παρακολούθηση, αναγνώριση και έρευνα και διάσωση. Θα παρουσιαστούν διαφορετικές μεθοδολογίες και στρατηγικές σχεδιασμού που θα επιτρέψουν στα φτερωτά ρομπότ επόμενης γενιάς να λειτουργούν σε αυτές τις δύσκολες συνθήκες, συμπεριλαμβανομένων των δυσμενών ρευμάτων ανέμου και των αλλαγών από ανοικτά, ευρύχωρα σε ακατάστατα, περιορισμένα και αδόμητα περιβάλλοντα.

Λέξεις-κλειδιά: εναέρια ρομποτική, βιο-έμπνευση, μορφοποίηση, αλλαγή σχήματος, φτερωτά μη επανδρωμένα αεροσκάφη, VTOL, υβριδικά UAVs

Table of contents

List of figures

List of tables

1 Introduction

The introductory section highlights the limitations of existing winged drones, presents the sources of inspiration for possible improvements, and underlines three of the most significant challenges state-of-the-art drones are facing.

1.1 Motivation

1.1.1 Existing limitations

Winged drones have been used in a wide variety of applications with mission profiles spanning from civilian to military. Currently, these drones can operate efficiently in a single environment with fixed mission requirements. As future mission complexity increases, aerial vehicles will be required to adapt their operations to diverse or mixed environments with several and even contradictory mission requirements [41]. Currently, adaptation in diverse mission profiles requires operators to deploy different vehicles specific to the mission type. For example, when precision and ease of deployability are required for a mission, the operators will deploy a copter vehicle that can hover. In contrast, in the case where long-range and high altitudes are needed, the operators will deploy a fixed-wing vehicle.

However, there are mission types that require both precision and long-range operations. For example, in a search and rescue mission scenario where rapid reconnaissance is of paramount importance, a vehicle will be needed that has the characteristics of being able to travel long distances and be precise enough to operate in hovering in a confined environment to perform the reconnaissance task. In this scenario, being able to travel long distances ensures that the operators can remain at a safe distance while being able to operate in a confined environment enables reconnaissance of a possible damaged infrastructure in a short time. This is only one example that highlights the need for vehicles that are able to combine diverse and contradicting mission requirements.

There are drones that can operate both for long distances and in hovering. As will be discussed in the next chapters, these vehicles are named Vertical Take-Off and Landing (VTOL) due to their ability to combine the features of a plane in horizontal flight and a copter in hovering flight [17]. Examples of VTOL aircrafts are presented in Figure 1.1. Despite the operational versatility of such vehicles, there are still conditions that limit their performance and safety when operating in modern missions. The challenge of adverse weather conditions during flight and the challenges of ground locomotion or survivability after a crash are yet to be addressed in the current design of these drones. Operational robustness will be a critical milestone for drones with Level 5 autonomy (Annex B), which will require the drone to constantly adapt its operation for mission success. However, how does someone design vehicles that can adapt to highly diverse and challenging environments?

1.1.2 Natural flyers

Natural flyers have evolved for millions of years to increase their survivability rate in their natural habitats. Birds, bats, and insects are not only able to endure challenging environments, but they are also able to do so while demonstrating substantial energy efficiency and flight performance. For example, many species from the *Coleoptera* order, commonly known as beetles, are flying creatures with several protective features that have allowed them to survive

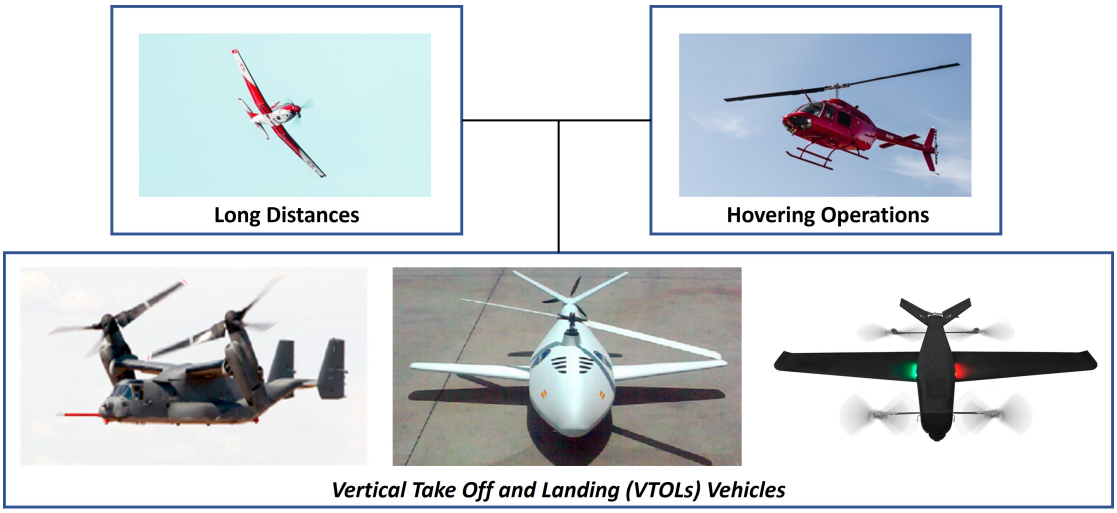

Figure 1.1: Vertical Take-Off and Landing Vehicles. Adapted from [1, 2, 3, 4, 5]

for millions of years. Beetles employ protective wings that, when folded, endow them with collision-resilient properties on the ground. In flight, the beetles deploy their protective wings to assist the main wings by generating lift to offset their weight and even increase flight performance [42, 43, 44, 45].

Another example is the *Anisoptera* insects, which belong to the *Odonata* order and are commonly known as Dragonflies [46]. These insects evolved to independently control their four wings for over 400 million years to achieve better flight performance and increase their predatory capabilities [47, 48]. Similar to insects, birds have also evolved for better flight performance in diverse environments, demonstrating exceptional energy efficiency [49, 50, 51].

There are numerous examples of how animals evolved to survive in their ever-changing natural habitats, although there is a common feature that distinguishes the evolution of most flying animals. Adaptive morphology is the common denominator in the evolution of flight that allows flying animals to morph their shape depending on the required mode of operation [52]. Several insects, bats, and birds adapt their wings, tails, and bodies to achieve configurations that can either increase their flight efficiency or protect them from the environment and predators (Figure 1.2).

1.1.3 Adaptive morphology and morphing wings

Due to its prevalence in nature, wing morphing is believed to be a promising design principle that can be used to develop drones with extended flight performance, and better energy efficiency [53, 54]. In the literature, morphing wing strategies are categorized based on the orientation of the morphing plane. An overview and classifications of morphing strategies for aircraft are illustrated in Figure 1.3. According to Li et al., the highest level of morphing in terms

Figure 1.2: Most birds (A), bats (B), and insects (C) are flying animals capable of adapting their morphology [6, 7, 8].

of initial to the final surface is achieved by planform, and out-of-plane morphing techniques [9]. Concilio et al., mentioned that morphing wing systems are composed of three basic components that form their structural system. These components are the actuation system, the skeleton, and the skin. A high-level overview of a morphing wing system is presented in Figure 1.5:

- Actuation system: The actuation system is responsible for morphing the skeleton and the skin. It is usually composed of one or many mechanical or electrical passive or active actuation components
- Skeleton: The skeleton is the main load-bearing structure. It is the structural component responsible for maintaining the structural loading during flight.
- Skin: The skin is responsible for transferring the aerodynamic loading to the structure.

Although morphing during flight has been widely investigated, aggressive morphing techniques of more than a few degrees are usually limited to static prototypes and proof of concept mechanisms [55, 56, 57].

There is a lot of work around the investigation of adaptive morphology and morphing wings in robotics [53]. The use of state-of-the-art morphing wings is restricted to investigating novel locomotion concepts or improvements in aerodynamic performance. Meanwhile, there are no applications that use morphing wings for protection and safety purposes. Examples of vehicles featuring morphing wings are presented in Figure 1.4.

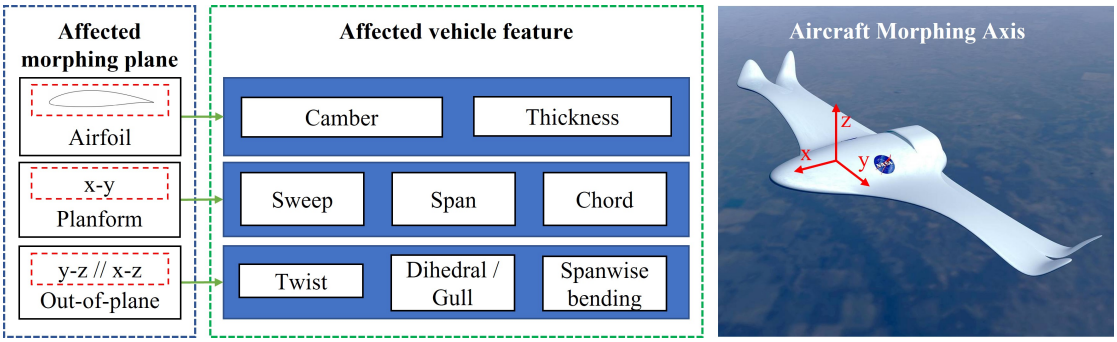

Figure 1.3: Classification of morphing wing strategies (adapted from [9, 10]).

The hypothesis in this work is that, similar to nature, morphing wing concepts can be used for improvements in energy efficiency, gains in flight performance, and advancements in the out-of-flight resilience properties.

This thesis is focused on the development of methodologies for increasing the resilience of current drones with the goal of enabling them to operate in challenging environments with diverse requirements. This work investigates the proposed resilience concepts on winged drones because of their increased performance compared to copter drones. In particular, the concepts presented are proposed as adaptations of fixed-wing and fixed-wing VTOL drones. As discussed in section 1.1.1, VTOL drones are vehicles that combine the advantages of rotorcrafts and fixed wings. However, their current design limits their operational benefits and flight performance operations. Despite that, VTOLs are platforms that can easily adapt to diverse requirements, namely limited space take-off and landing, fast forward flight, or low-speed hovering flight. Thus, improving on VTOL limitations is a significant part of the work of this thesis which will present methodologies that will leverage VTOLs to achieve higher operational resilience.

1.1.4 Winged VTOL drones

There are two main types of flying vehicle categories that dominate the literature and the market. These are the rotorcrafts and the fixed wings. As discussed, there is one subcategory that combines the best from both these conventional categories (Figure 1.1). This category is the Vertical Take Off and Landing vehicles, also referred to as Hybrid Unmanned Aerial Vehicles (HUAV). VTOLs are hybrid platforms that are capable of both hovering and long-range flight. VTOLs have been used for several decades, with a broad range of missions and applications for civilian and military purposes [18].

These vehicles are classified by their transition strategy from horizontal to vertical flight. According to Saeed et al., these hybrid vehicles are categorized into two types: convertiplane and tail-sitter [18]. A convertiplane preserves its airframe orientation in different flight modes

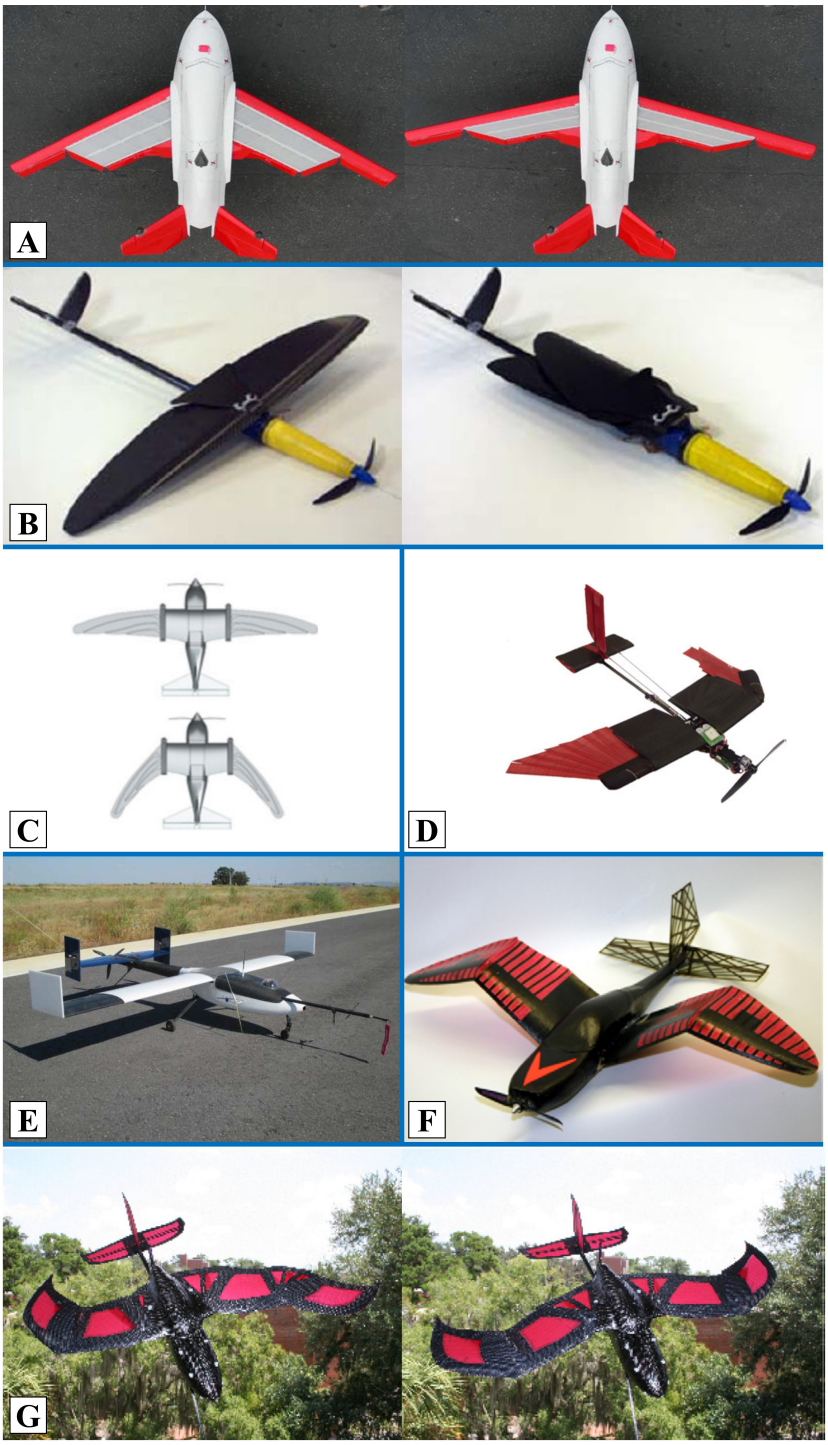

Figure 1.4: Examples of drones with morphing wings. (A) NextGen MFX-1 and (B) AquaMAV are examples of variable wing sweep [11, 12]. (C) Roboswift and (D) LisHawk, feature wingtip morphing [13, 14]. (E) An aircraft with variable span wing [15]. (F) An example of out-of-plane morphing and (G) a variable multi-joint sweep drone [16].

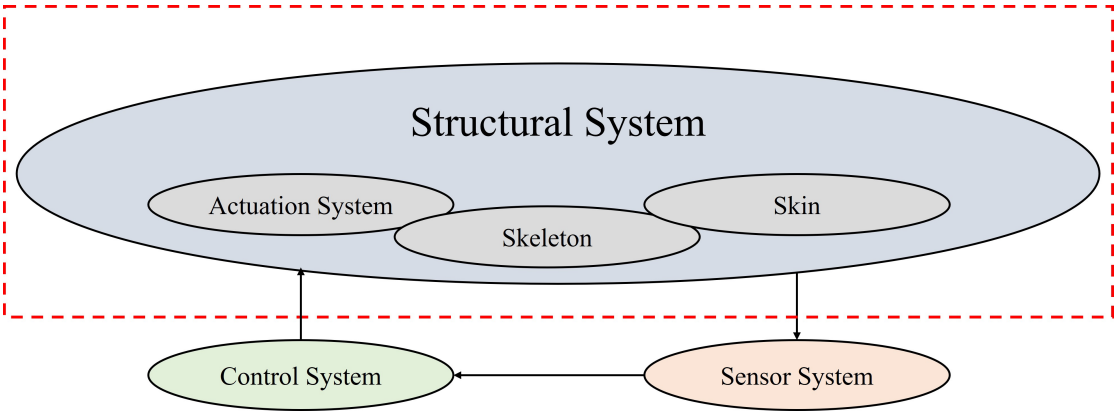

Figure 1.5: Schematics of a general adaptive structure (adapted from [9]).

[12–15], and different mechanisms are engaged to achieve the transition. On the other hand, tail-sitters [16–19] take off and land vertically on their tail, and the entire airframe is required to rotate to achieve cruise flight mode. The VTOL classification is adapted from [18] and presented in Figure 1.6. There are several VTOL designs in academia and the industry, although current designs suffer from design limitations due to their fixed geometric configuration.

1.2 General approach

As highlighted in the introduction and will be discussed in the next sections, resilience is one of the main limitations of current winged drones. Resilience refers to the operational robustness of a drone in diverse environments with different properties, whether spatial, atmospheric, or mission specific. Future winged drones will have to overcome rapid changes in atmospheric phenomena during operation, pass from wide open to cluttered and confined spaces or recover from an unpredicted collision. Existing drones operate successfully in specific operational profiles, although fully autonomous missions of Level 5 (Annex C) require resilient drones that can adapt and overcome any environment or operational challenge.

Currently, drones are getting smaller to enable flight in confined spaces while energy storage devices are improving in capacity to allow for long-range operations. However, abrupt winds remain challenging for outdoor missions; thus, vehicles designed for indoor operations cannot perform outdoors. While size reduction and performance improvements can allow for long-range indoor or outdoor missions, flying is still significantly more energetically expensive than other modes of locomotion. Future drones will be required to operate on the ground or water to save energy and fly when needed to overcome obstacles or cover long distances. Exposed wings of small UAVs would restrict maneuverability and increase the risk of collisions when not operating in the air and, in particular, on the ground when in cluttered confined spaces. However, assuming that a vehicle is capable of safe operations indoors, outdoors, and on different modes of locomotion, transitioning between these operational profiles can be

Figure 1.6: Categorization of hybrid UAVs, adapted from [17, 18]. Hybrid UAVs, or winged VTOLs will be referred to as VTOLs throughout this work.

challenging and dangerous. Currently, most flight vehicles and especially winged vehicles, are threatened by overturns during their operation either in wide open or cluttered confined spaces. Self-righting of future drones would be a mandatory function, the same as it is on most living animals capable of operating in such environments.

This thesis is structured with the goal of identifying the significant challenges during the operation of a winged drone and proposing solutions to overcome them. These methodologies address drone operations during flight and multi-modal operations in flight and on the ground after a catastrophic event. The challenges identified and addressed are the following:

- *Winds*
  Either abrupt winds or sustained wind effects can significantly deteriorate the performance of a winged drone. The additional drag generated from the exposed wings is a challenge for aircraft of all sizes, which can be destabilized or even crash as a result of a strong and continuous wind effect.

- *Collisions*
  As drone operations get more and more complex, vehicles will be required to operate in different environments that necessitate air, water, or ground locomotion. Collisions are challenging for all multi-modal drones, especially those operating on the ground. Exposed wings and electronics usually require strong reinforcements that induce additional drag and weight penalties to protect them from collisions.

- *Overturns*
  Wing drones operating in cluttered environments can easily get destabilized and crash. Although there are various methods to increase their collision resilience, an overturn after a crash might be catastrophic for their mission. Self-righting methods exist, although they require additional mechanisms which increase weight and drag.

In the subsequent section, the thesis outline will be presented along with abstracts from each chapter that will briefly introduce the problem, highlight the proposed solution and summarize the key achieved results.

1.3 Thesis outline

Chapter 1: Introduction

The introductory section highlighted the limitations of existing winged drones, presented the sources of inspiration for possible improvements, and underlined three of the most significant challenges state-of-the-art drones are facing.

Chapter 2: Wind Defiant Morphing Drones

The second chapter of this work focuses on addressing the limitations of winged VTOLs' in-flight resilience. Intense winds are challenging for vertical take-off and landing drones (VTOLs) with wings. In particular, in the hovering regime, wings are sensitive to wind currents that can be detrimental to their operational and energetic performances. Tail-sitters are particularly prone to those wind currents because their wings are perpendicular to the incoming wind during hovering. This wind generates a large amount of drag and can displace and destabilize the vehicle, possibly leading to catastrophic failures. Here a morphing strategy is demonstrated in a custom-built 1.8 kg tail-sitter with morphing wings that can actively resist winds and leverage them to increase its aerodynamic efficiency. It is shown that adaptive wing morphing during hovering in adverse wind conditions can reduce normalized energy consumption up to 85%, increase attitude and positional stability, and leverage wind energy to increase its yaw angular rate up to 200% while decreasing motor saturation levels.

Chapter 3: Ultra Wind Defiant Morphing Drones

In the previous chapter, the benefits of morphing wings were demonstrated. Namely, they could be used to reduce the normalized energy consumption and increase the attitude and positional stability of a tailsitter VTOL drone. Despite the experimental outcomes, it was also observed that the proposed design suffered from limitations on the amount of wind force it could sustain (Level 3, (Annex C)) due to the exposed surface of the fuselage. In this chapter, a new design is proposed that can sustain a wind force of Level 5 (Annex C) while operating in hovering mode. The drone's design is inspired by the insect order *Odonata*, which includes the *Zygoptera*, which are commonly known as Damselflies, and the *Anisoptera*, which are commonly known as Dragonflies. Similar to these types of insects, the vehicle features four independently actuated morphing wings that allow different amounts of wing surface exposure to the perpendicular wind during hovering or horizontal flight.

Chapter 4: Robotic *Elytra*: Insect-Inspired Protective Wings

What happens, though, when drones are required to operate both in the air and on the ground? Winged drones that fly in close proximity to obstacles or that are capable of aerial and terrestrial locomotion can benefit from protective systems that prevent damage to delicate aerial structures. Existing protective solutions focus on multi-copter drones and consist of adding structures, such as cages, mechanisms, and instruments that add weight and drag. Here, a protective strategy is described for winged drones that mitigate the added weight and drag by means of increased lift generation and stall delay at high angles of attack. The proposed structure is inspired by the wing system found in beetles and consists of adding an additional set of retractable wings, named *elytra*, which can rapidly encapsulate the main folding wings when protection is needed.

Chapter 5: Insect Inspired Self-Righting for Fixed-Wing Drones

It is evident now that winged drones can be required to perform in different types of environments. While in the air or on the ground thought, an overturn can compromise an operation. Micro Aerial Vehicles (MAVs) are being used in a wide range of applications such as surveillance, reconnaissance, inspection and search and rescue. However, due to their small size and complex mission profile, they are prone to tipping over, jeopardizing their operation. Self-righting is an open challenge for fixed-wing drones since existing research focuses on terrestrial and multicopter flying robots with solutions that increase drag and structural weight. Until now, solutions for winged drones remained largely unexplored. Inspired by beetles, a robust and elegant solution is proposed. In the previous chapter, it was presented that when retrofitting a drone with elytra, they can be used to protect it during ground locomotion. In this work, a fixed-wing drone is retrofitted with elytra to assist it in self-righting during an overturn incident. It is shown that artificial elytra provide additional lift during flight to mitigate their structural weight while also being able to self-right the MAV when it has been flipped over. Simulations were performed along with dynamic and aerodynamic experiments to validate our results.

Chapter 6: Beyond

In this thesis, various methodologies were investigated for developing the next generation of resilient, autonomous flying robots capable of operating in challenging, diverse environments. These methodologies focused on developing solutions for applications in routine industrial missions, namely inspection, monitoring, reconnaissance and search and rescue missions. The methodologies developed for featuring a wide range of applicability from conventional fixed-wings planes to morphing VTOL platforms.
In this chapter, the main achievements of the work presented in this thesis are summarized, along with the limitations of the technologies and methodologies described in the previous chapters. Concluding, an outlook for possible industrial applications is presented along with potential avenues for future research avenues.

Appendix A: Publications

The work presented in this thesis is based on the following publications:

- C. Vourtsis, V. C. Rochel, N. S. Müller, W. Stewart, and Dario Floreano, “Wind Defiant Morphing Drones,” in *Advanced Intelligent Systems*, 2200297, Jan. 2023, [58].
- C. Vourtsis, W. Stewart, and D. Floreano, “Robotic Elytra: Insect-Inspired Protective Wings for Resilient and Multi-Modal Drones,” in *IEEE Robotics and Automation Letters (RA-L)*, vol. 7, no. 1, pp. 223-230, Jan. 2022, [59].
- C. Vourtsis, V. C. Rochel, F. R. Serrano, W. Stewart, and D. Floreano, “Insect Inspired Self-Righting for Fixed-Wing Drones,” in *IEEE Access*, in *IEEE Robotics and Automation*

Letters (RA-L), vol. 6, no. 4, pp. 6805-6812, Oct. 2021, [60].

- C. Vourtsis, V. C. Rochel, N. S. Müller, W. Stewart, and Dario Floreano, "Method for wind harvesting and wind rejection in flying drones", *Patent Pending*, Sep. 2022.

Appendix B: Drone Autonomy Levels

Characterization of the drone autonomy levels as presented in the drone industry.

Appendix C: Wind Force Levels: The Beaufort Scale

Presentation of the Beaufort wind force scale.

2 Wind Defiant Morphing Drones

The second chapter of this work focuses on addressing the limitations of winged VTOLs' in-flight resilience. Intense winds are challenging for vertical take-off and landing drones (VTOLs) with wings. In particular, in the hovering regime, wings are sensitive to wind currents that can be detrimental to their operational and energetic performances. Tail-sitters are particularly prone to those wind currents because their wings are perpendicular to the incoming wind during hovering. This wind generates a large amount of drag and can displace and destabilize the vehicle, possibly leading to catastrophic failures. Here a morphing strategy is demonstrated in a custom-built 1.8 kg tail-sitter with morphing wings that can actively resist winds and leverage them to increase its aerodynamic efficiency. It is shown that adaptive wing morphing during hovering in adverse wind conditions can reduce normalized energy consumption up to 85%, increase attitude and positional stability, and leverage wind energy to increase its yaw angular rate up to 200% while decreasing motor saturation levels.

- The work presented in this chapter is adapted from [58]:
  C. Vourtsis, V. C. Rochel, N. S. Müller, W. Stewart, and Dario Floreano, "Wind Defiant Morphing Drones," in *Advanced Intelligent Systems*, 2200297, Jan. 2023, [58].

- Supportive video material can be found at:
  https://www.youtube.com/watch?v=uLdlixtffEk&ab_channel=EPFLLIS

- Supportive dataset material can be available upon request.

2.1 Introduction

Hybrid Unmanned Aerial Vehicles (UAVs) refer to drones that combine the benefits of fixed-wing and rotary-wing aircraft in that they are capable of both horizontal and vertical (hovering) flight operations [26]. Most hybrid UAVs reorient the entire propulsion system or use a dedicated propulsion unit for each flight mode [17, 26]. The reorientation of the propulsion system, or the presence of additional propulsion units, increases the mechanical complexity and weight of these UAVs, resulting in reduced energy efficiency. Tail-sitters are a type of hybrid UAV with fixed wings capable of hovering and transitioning to horizontal flight without reorienting the propulsion system or dedicated propulsion units. The tail-sitter design has the lowest mechanical complexity, but the exposed wings leave the vehicle particularly prone to crosswinds in hovering flight [17].

In nature, flying animals, like birds and insects, operate in diverse wind conditions by adapting their wing morphology or body configuration according to the flight performance they need to achieve [61]. Birds change the shape of their wings to increase or decrease their agility, and insects rapidly change their flapping angles to perform highly agile maneuvers [62, 63, 64]. Wing morphing is a commonly adopted strategy by engineers, although current vehicles fail to achieve the performance of natural flyers [53]. Nevertheless, different approaches have already been proposed as solutions for gust rejection and increased maneuverability in the hovering regime of VTOL platforms. Sweeping wings are retracted during hovering to reduce the moment of inertia, thus increasing maneuverability [65, 66]. However, in the work of Ang et al., the area of the wings remains unchanged throughout the flight, and therefore, the vehicle's performance in crosswinds does not change [65]. In contrast, in the work of Heredia et al., the wings are entirely retracted in hovering, thus not providing any possible aerodynamic benefit as it would be in the cases where the drone is flying with the wind [66]. Another solution for wind rejection is to adapt the wing design to enforce flow detachment in the airfoil's leading edge to mitigate turbulent perturbations. However, this solution would not be applicable in wings oriented perpendicular to crosswinds where the wings are in deep stall, and the drag effects are predominant to the lift generation [67]. Furthermore, biologically inspired morphing wings attract interest to make winged drones more agile in wind conditions, but these do not specifically address the problem of withstanding adverse winds or hovering flight [67, 68, 69].

Other topics of work that focus explicitly on mitigating wind effects concentrate on controller development, although they do not address wind energy harvesting [70, 71, 72]. Rather than simply reducing the adverse wind effects, other studies show the possibility of harvesting energy to increase range and endurance by exploiting thermal wind currents. This approach is widely investigated for powered and unpowered fixed-wing soaring [73, 74, 75, 76]. However, this particular strategy requires the aircraft to continuously pass through air masses with different speeds and at specific angles of attack, which is not the primary mode of operation profile of VTOL platform in hovering, where it is required to fly for long periods at angles of attack of more than 60°.

In this work, we describe a strategy where we utilize the morphing wings of a VTOL platform in such a way that we increase stability against adverse winds while leveraging wind energy for efficient hovering flight and increased maneuverability in the yaw axis (Figure 2.1).

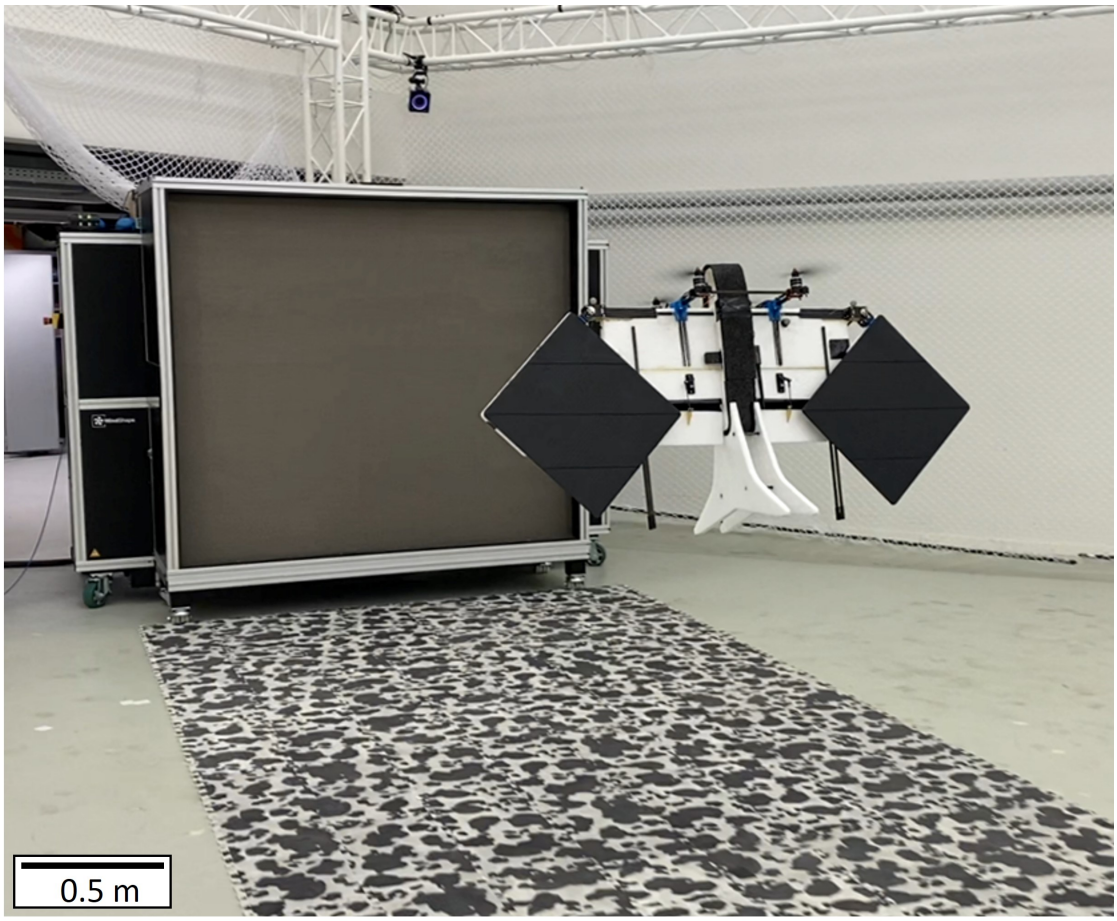

Figure 2.1: A morphing Vertical Take-Off and Landing (VTOL) tailsitter drone in front of the Windshape wind generator [19]. The drone was tested in up to Level 3 wind force (Annex C).

The wing area has a strong impact on flight performance. A large wing area increases the vulnerability to cross winds during hovering operations due to large amounts of generated drag. Therefore, VTOLs with fixed wings usually face a design compromise. There is a trade-off between small wing size for smaller drag during hovering flight and larger wing size for increased lift during horizontal flight.

We overcome this compromise by either symmetrically or asymmetrically changing the drone's wing area based on the wind direction. This is accomplished with a wing controller that can adjust the wing area of the drone using simple servo actuators. The principle is based on minimizing the overall energy consumption and not solely on drag reduction or lift maximization. This means that the controller can exploit crosswinds in a beneficial manner depending on if

the next commanded waypoint is upwind or downwind of the vehicle. Similarly, we utilize asymmetric morphing to exploit wind currents for yaw control or to increase the drone's maximum achievable yaw rate when used in conjunction with motor actuation. By commanding wing asymmetry in windy conditions, yaw control can be decoupled from maintaining altitude or assisted by the wing morphing. Controlling yaw only through deferentially actuated motors exhibits a yaw rate threshold that occurs due to the motors needing to maintain altitude and turn the vehicle simultaneously.

2.2 Morpho - A morphing VTOL drone

Morpho is a quad tail-sitter UAV with morphing wings that adapt their surface depending on the flight mode and wind conditions (Figure 2.2). The drone's extended and retracted configurations, along with the effects of wing morphing in the center of gravity and the moments of inertia, are presented in Figure 2.3. For simplicity, the wing has a rectangular airfoil profile with a thickness of approximately 15 mm.

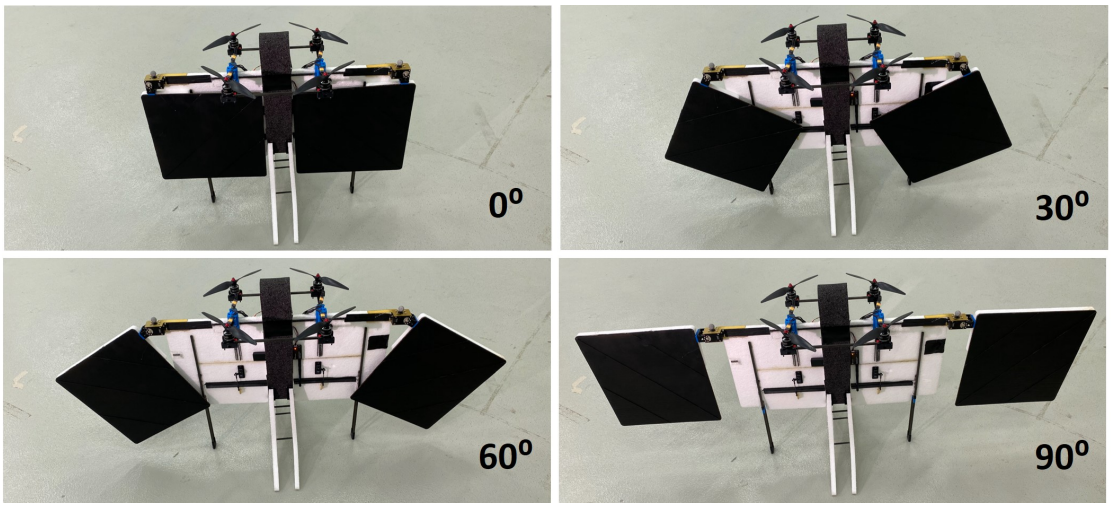

Figure 2.2: Symmetric wing configurations of the morphing VTOL tailsitter.

The drone in its extended and retracted wing configurations with detail in its sweeping wing servo mechanism. The drone's weight is 1.8 kg. The drone with wings unfolded has a wingspan of 1.45 m and a wing area of 0.44 m^2, while with the wings retracted, it has a wingspan of 0.79 m and a wing area of 0.29 m^2. The length of the fuselage is 0.62 m. The propulsion system consists of four propellers in tractor mode actuated by four Rctimer 2830 1000 KV brushless motors with a 45 A four-in-one Electronic Speed Controller (ESC). For the wing actuation, two Dynamixel XM430-W350-T servomotors are used. Elevons are only used for attitude control in forward flight. A lithium polymer battery of 2500 mAh in a four-cell configuration powers the drone. The fuselage and the wings are made from cardboard and Expanded PolyPropylene (EPP), a foam material with high mechanical resilience and flexibility. The center of gravity is

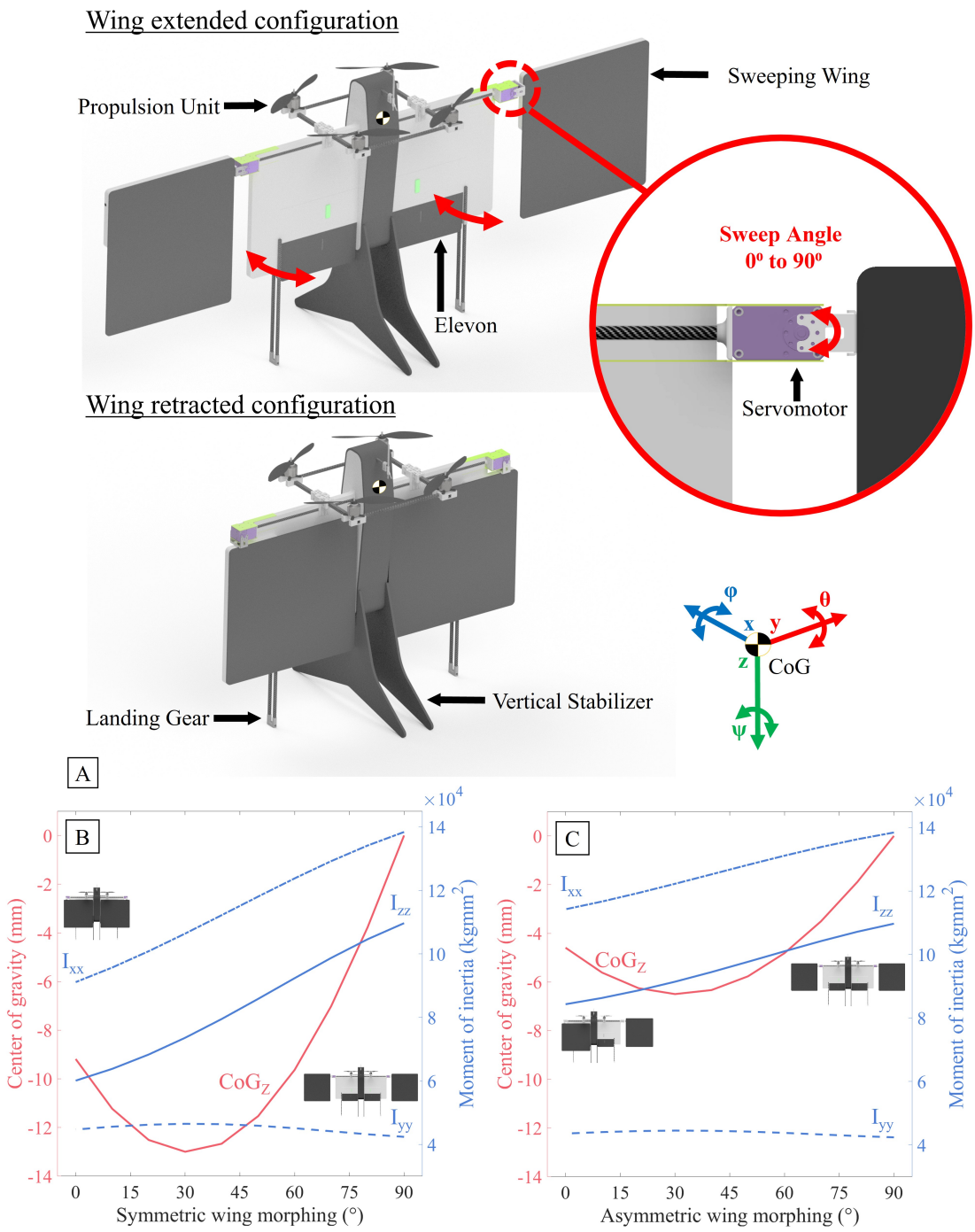

Figure 2.3: (A) A morphing VTOL tailsitter drone. (B) Change in the center of gravity (CoG) in the z-axis and moments of inertia (Ixx, Iyy, Izz) in symmetric wing morphing. (C) Change in the center of gravity (CoG) in the z-axis and moments of inertia (Ixx, Iyy, Izz) in asymmetric wing morphing.

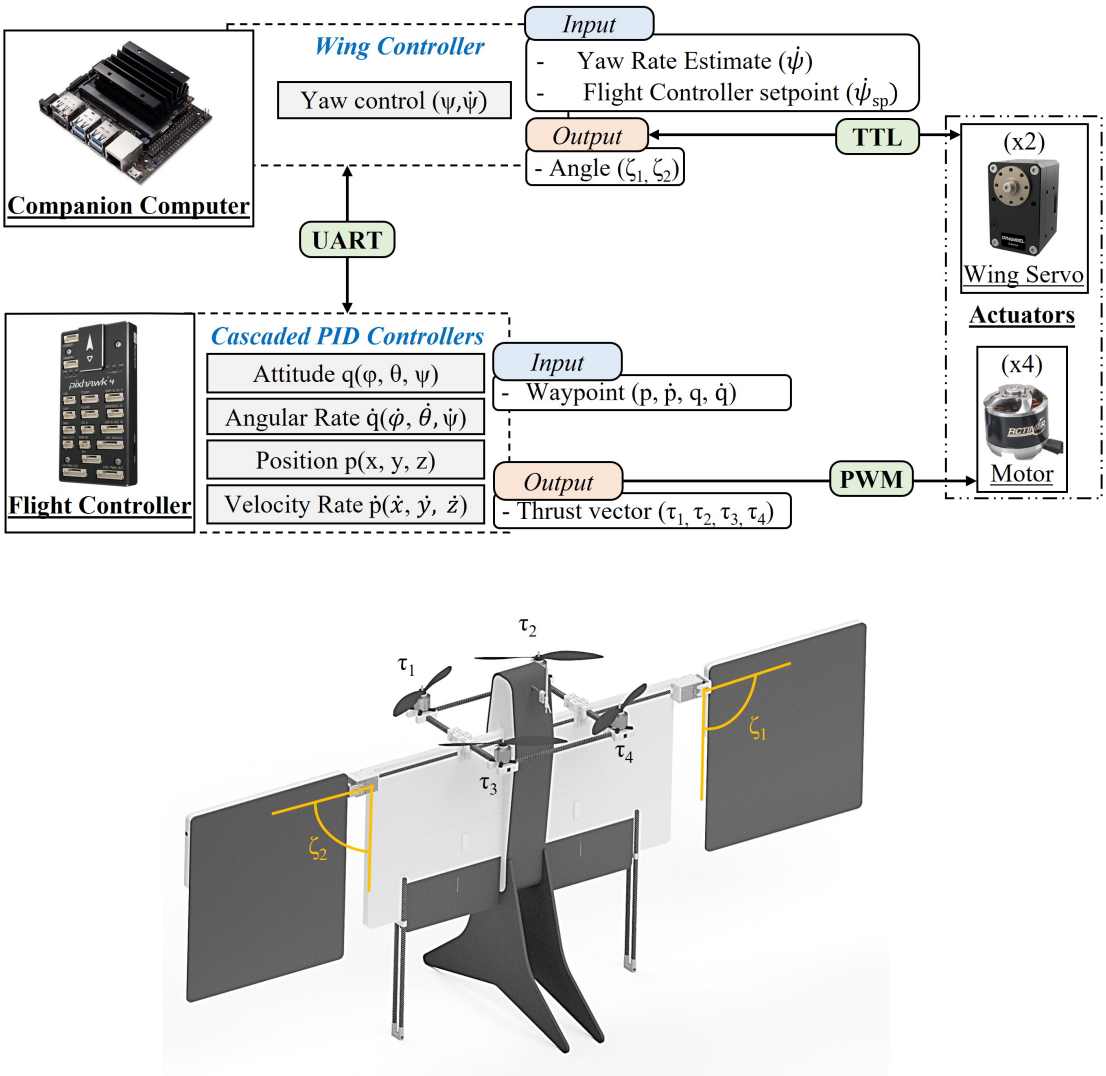

Figure 2.4: High-level controller architecture. A P controller is deployed for controlling the wing morphing state when the wings are used for actively stabilizing yaw. It takes as input the yaw rate error computed by the flight controller [20] and outputs the desired wing angle magnitude (ang_magn). According to the wind direction ($wind\_dir\_sign$) in the body frame, the commanded wings angle is: $[-wind\_dir\_sign \cdot ang\_magn, wind\_dir\_sign \cdot ang\_magn]$. This command is then clipped between $[0, pi/2]$ and sent to the servomotors, which track a trapezoidal velocity profile with an acceleration of 18.73 rad/s^2 and a top speed of 2.4 rad/s. The companion computer communicates with the autopilot through MAVROS, which is a ROS bridge for the MAVLink protocol.

depicted in both configurations. Carbon beams were used to reinforce the structure and to mount the two servo actuators (Dynamixel XM430-W350-T) used to fold the wing tips. The motor mounts, the servo actuator mounts, and the landing gear components were 3D printed with Acrylonitrile Butadiene Styrene (ABS) plastic.

The drone is utterly autonomous during flight (Figure2.4). For the autonomous flight experiments, a Pixhawk 4 autopilot is utilized in conjunction with a Jetson Nano companion computer on a carrier board modified for weight reduction. The companion computer is required to run the wing controller parallel to the autopilots' function. The companion computer receives information from the autopilot through MAVROS, a ROS bridge for the MAVLink protocol. It uses the state estimation and the trajectory setpoints from the autopilot to adaptively morph the wings. It does so by sending commands to the servo actuators through Dynamixel protocol 2.0 (Figure2.4). All the hardware components are connected serially. The wing servo controller's functionality is generalized and independent from the autopilot as it uses the calculated yaw rate error as input. Therefore, different autopilots could provide the yaw rate setpoint and state estimation.

While wind estimation in actual missions can be estimated either by a wind sensor or changes in the state estimate, the current prototype does not utilize a wind estimation method for simplification.

2.3 Aerodynamic characterization

Experiments were performed to investigate the aerodynamic properties of the different wing morphing configurations. A 6 DOF ATI Gamma loadcell was mounted to the bottom part of the drone at its center of gravity (Figure 2.5).

Through combinations of different wing morphing states, eight configurations were characterized. These correspond to both symmetric and asymmetric wing morphing configurations for wing sweep angles of 0° to 90° with increments of 30°. Similar to [60, 59], the drone was attached to a Stäubli robotic arm which was placed in an open-jet WindShape wind tunnel [19]. The robot was programmed to drive the robot through a commanded angle of attack. The angle of attack, defined as zero when the vehicle is hovering vertically, was varied between 40° and −50° starting from 0° and in increments of 4°.

The drone was positioned such that the fuselage of the drone is approximately 50 cm from the wind tunnel filter. Experiments were run at wind speeds of 1.7 m/s, 3.4 m/s, and 4.6 m/s measured at the beginning of the free stream, which corresponds to Reynolds numbers of 35898, 71796, 97135 as calculated with the reference length of the morphing wing when horizontal to the flow. Data samples were recorded at 120 Hz after the wing flow had reached a steady state. Recorded forces were rotated to the wind frame to calculate Lift, Drag, and Yawing Moments.

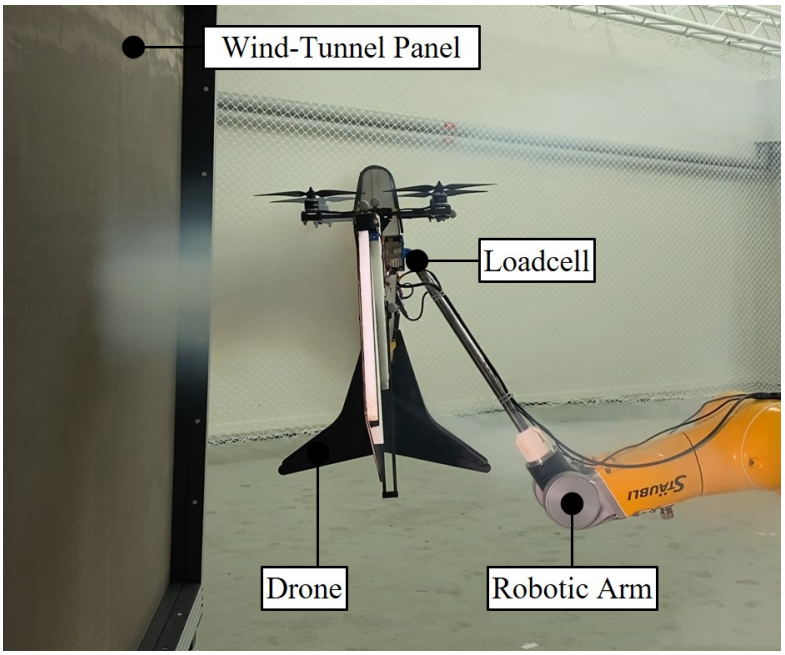

Figure 2.5: The aerodynamic experimental setup is composed of the drone, a Stäubli robotic arm, a WindShape wind tunnel, and an ATI Gamma F/T Sensor. The drone is at 0° angle of attack in this figure as it would be hovering.

The aerodynamic results, which are displayed in Figure 2.6, show an increase in lift and a decrease in drag as the plane shifts from the 0° position (A), (B), (C). Drag increases significantly in the open-wing configuration compared to the fully retracted wing configuration (Figure 2.6 (A)). The aerodynamic effects in both lift and drag intensify with the increase in wind speed. Yaw moments display a significant increase in the case of asymmetric morphing configurations of one wing fully extended, and one wing fully retracted at all angles, as shown in Figure 2.7 (A). The yaw moment varies from 0 Nm in the retracted wing configuration to approximately -0.8 Nm in the one-wing retracted and the one-wing extended configuration. In comparison, the maximum yaw moment which can be generated by the motors while maintaining the drone's altitude is -0.23 Nm. This shows that the wings can significantly contribute to controlling the yaw angular rate. From Figure 2.7 (A), a linear relationship can be identified between the wing angle and the yaw moment. In addition, it is also observed that the angle of attack generally does not have a significant impact on the generated yaw moment (Figure 2.7 (B)). The linearity in the wing angle - yaw moment relationship in most tested cases and near-constant moment suggest that an error rate P controller can be sufficient for active wing yaw stabilization.

2.4 Autonomous flight experiments

The proposed hypothesis's validation and the proposed controller's functionality require flight experiments. Each experiment was performed three times. These experiments aimed to clarify

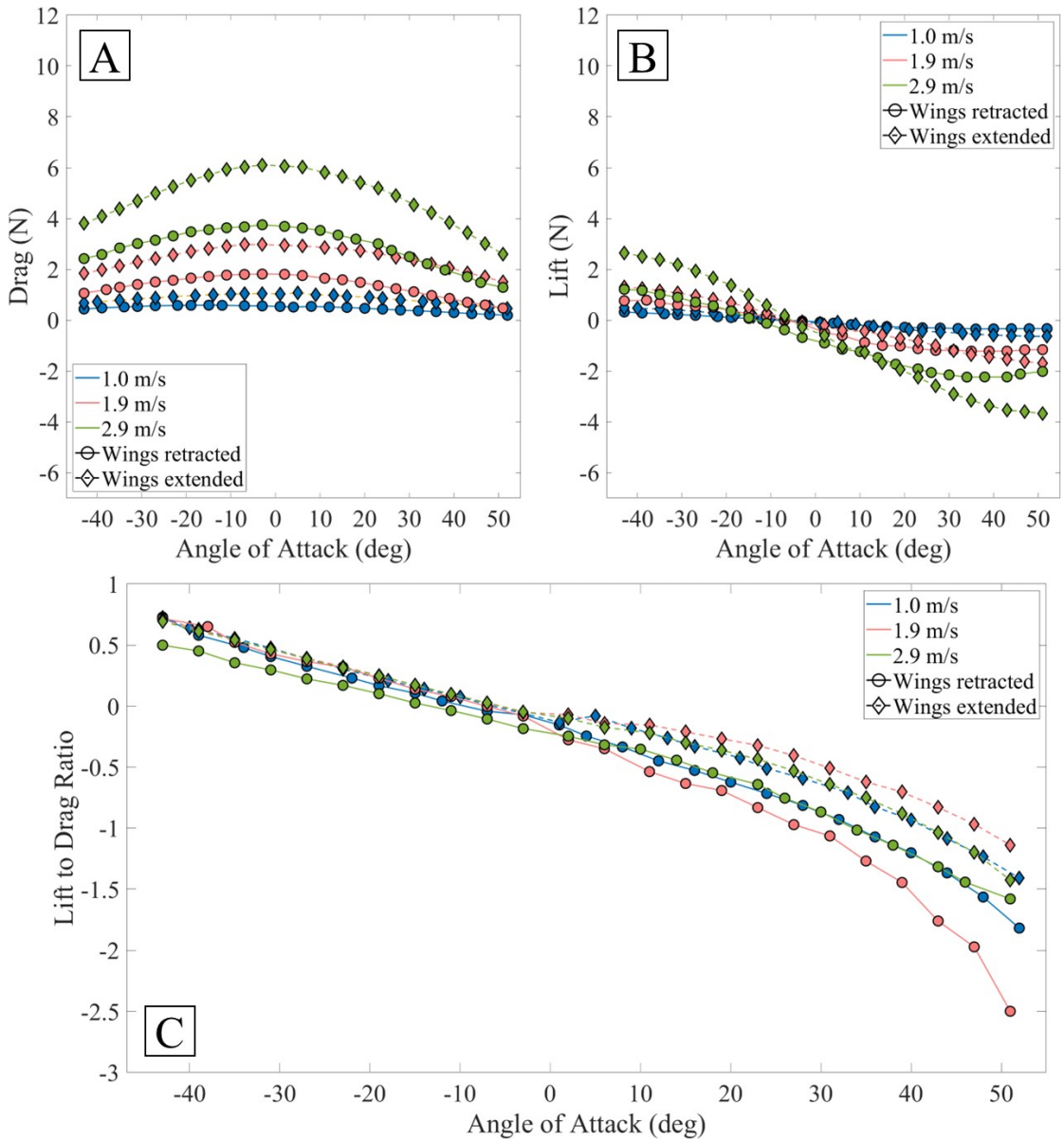

Figure 2.6: Aerodynamic experimental results of the different wing morphing symmetric and asymmetric configurations. (A) The drag force as a function of the angle of attack at different wind speeds for the extended and retracted configurations. (B) The lift force as a function of the angle of attack at different wind speeds for the extended and retracted wings configurations. (C) The lift-to-drag ratio is presented as a function of the angle of attack at different wind speeds for the extended and retracted wing configurations.

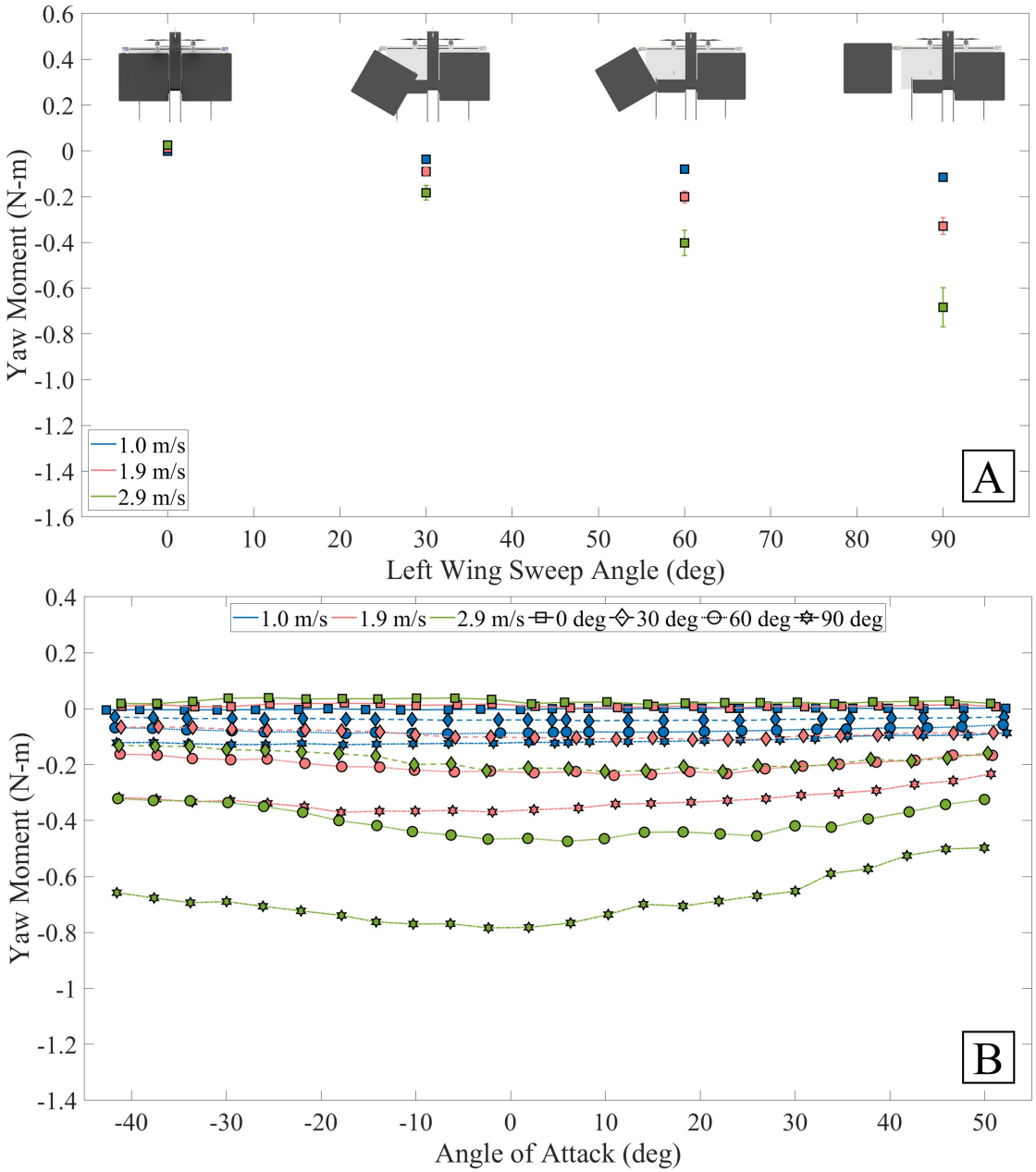

Figure 2.7: Aerodynamic experimental results of the different wing morphing symmetric and asymmetric configurations. (A) The yaw moment generated as a function of the left-wing sweep angle at different wind speeds. (B) The yaw moment is generated by the sweep of the left wing as a function of the angle of attack at different wind speeds and sweep angles.

the benefits of changing symmetrically or asymmetrically the wing area while performing different flight trajectories. Flight experiments were performed in an experimental facility composed of a motion capture system of 23 cameras and a wind stream generator capable of producing different wind velocities. The generic trajectory of a drone mission in a horizontal plane can be decomposed into three main trajectories, namely, linear trajectory, rotational trajectory, and mixed trajectory composed of both previous trajectories.

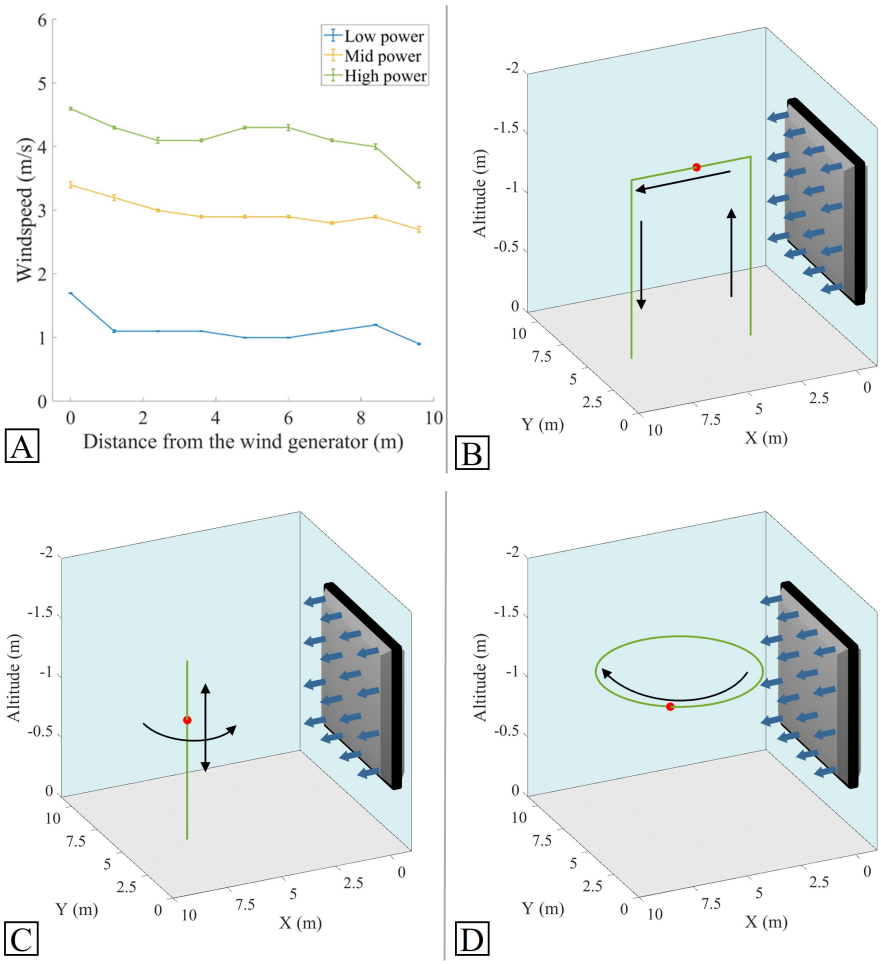

Figure 2.8: In this experimental setup, the wind direction is known, and the state estimation of the drone is provided by a motion capture system. The wind is generated by the Windshape and varies by the distance from the fan due to momentum loss in the flow field. (A) Diagram of wind speed to distance from the wind generator. (B) Linear trajectory. (C) Rotational trajectory. (D) Circular trajectory.

As a first step towards performing a mixed trajectory, hovering at a setpoint was commanded. The wings were continuously actuated based on the yaw rate error estimated from the autopilot. The wings activation was regulated by a custom P controller. Hovering at the setpoint with a fixed orientation parallel to the wind tunnel while exposed in a wind current, the drone with

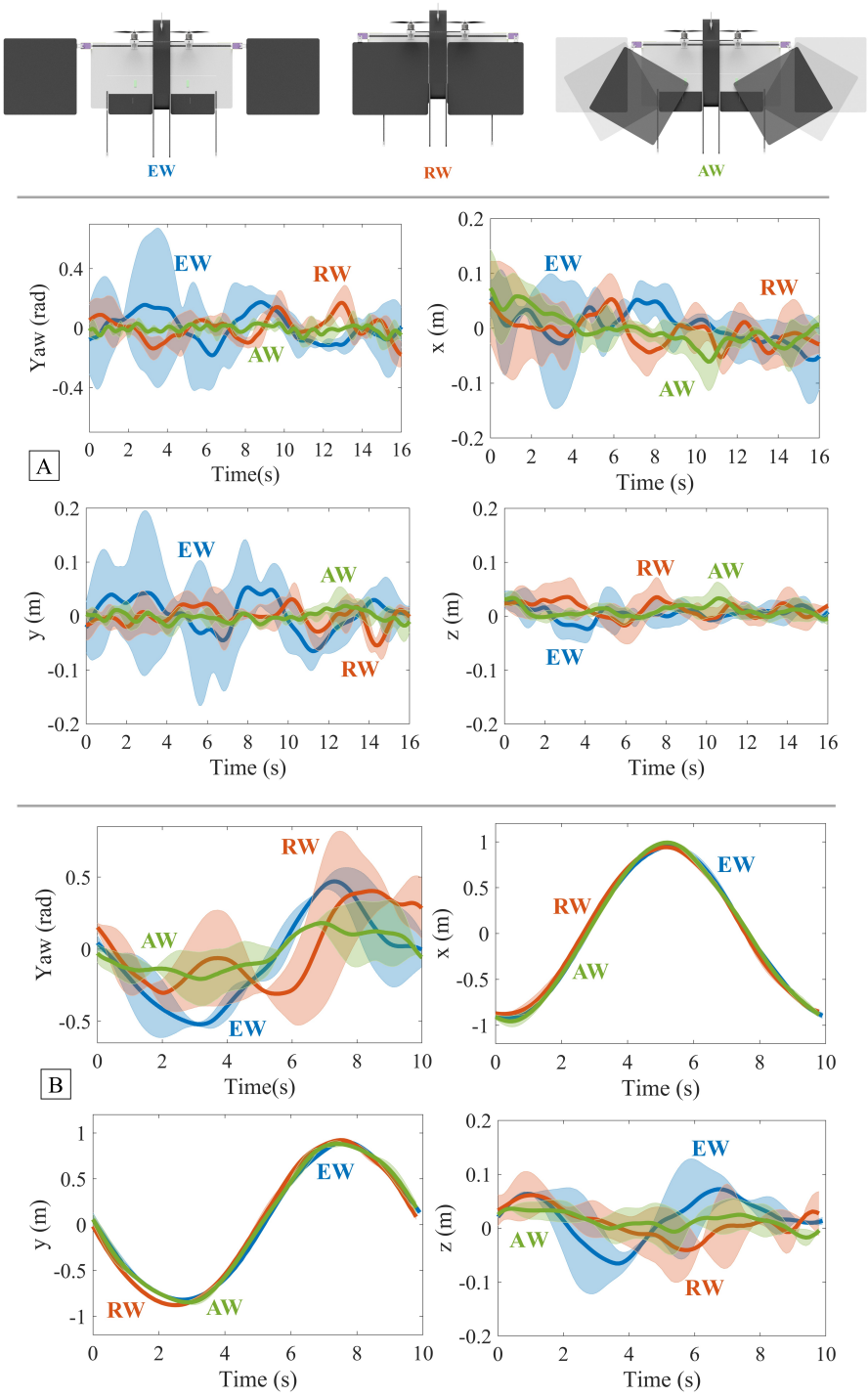

Figure 2.9: Flight experiments with active wing morphing for yaw stabilization and wind disturbance rejection. EW is for extended wings, RW is for retracted wings and AW is for wings that are continuously activated. (A) Hovering at a setpoint with a fixed orientation, (B) Hovering in circular trajectory (Figure 2.8 (D)). The experiments were performed at low to mid power of the wind generator at 1 to 3 m/s.

active wing stabilization exceeded the performance in yaw stabilization of both fully extended and fully retracted wings. In fact the standard deviation of the yaw error decreased by 76% and 69% respectively (Figure 2.9 (A)). In addition, the position error in X remained the same while in the Y and Z axis it was decreased for the active wing morphing by 72% and 11% compared to the extended configuration. When compared to the retracted configuration, an increase of 14% in the position error is observed for X, while a significant improvement is displayed in Y and Z with a decrease of 48% and 26% respectively (Figure 2.9 A)).

Continuing, testing the circular trajectory (Figure 2.8 (D)), where the plane performs a mix of linear and rotational trajectories, revealed similar results to the hovering at a setpoint experiment. The goal was to track the trajectory; the morphing wings were used for active stabilization and wind rejection. When tracking the trajectory with active wings, the standard deviation of the yaw error decreased by 58% and 49% compared to fully extended wings and fully retracted wings respectively. Therefore, the drone with active wing morphing displayed a performance increase in yaw stabilization and the ability to better resist wind currents compared to both the extended and retracted wing configurations (Figure 2.9 (B)). Although beneficial for increased stability and wind rejection, continuously morphing the wings might reduce the energy performance of the vehicle. Thus, in addition to the previous experiments, we investigated the impact of morphing to a fixed symmetric or asymmetric wing configuration in such a way that we use only the wings to change the drone's attitude or assist the motor's function. Linear and rotational trajectories were investigated.

At first, a linear trajectory was performed (Figure 2.8 (B)). The drone was commanded to take off, hover, and then fly, fending off the wind generator and to a given setpoint where it was commanded to land. A custom attitude controller allowed the drone to drift in the presence of wind current along the x-axis, while maintaining zero pitch (Figure 2.8 (A)). The goal of the linear trajectory was to assess the operation and performance of the drone while flying with different wing configurations in the generated wind stream. The drone was placed 2.5 m from the wind generator and was commanded to a setpoint 7.5 m away inside the wind stream. In this experiment, where there is no motor contribution to the horizontal displacement, it was observed that drifting with extended wings is faster than drifting with retracted wings due to the increased drag generated by the larger area of the extended wings (Figure 2.10 (A)). Moreover, it is able to travel faster while maintaining the same motor thrust. This means the aircraft is more controllable because it could use the motors to perform other attitude commands (Figure 2.10 (B)). In addition, extended wings can reduce the drone's normalized energy consumption by 4%, 28% and 2% for wind currents corresponding to 10%, 20% and 30% wind power respectively. The normalized energy consumption is calculated using the power consumption difference between the power consumed throughout the trajectory and the baseline, which is the average power required during one second in static hovering before performing the trajectory. The significant advantage is observed in middle wind current speeds. At low wind speeds, the added drag is smaller and, at high wind speeds, the drone controller tries to compensate for the generated pitching moment.

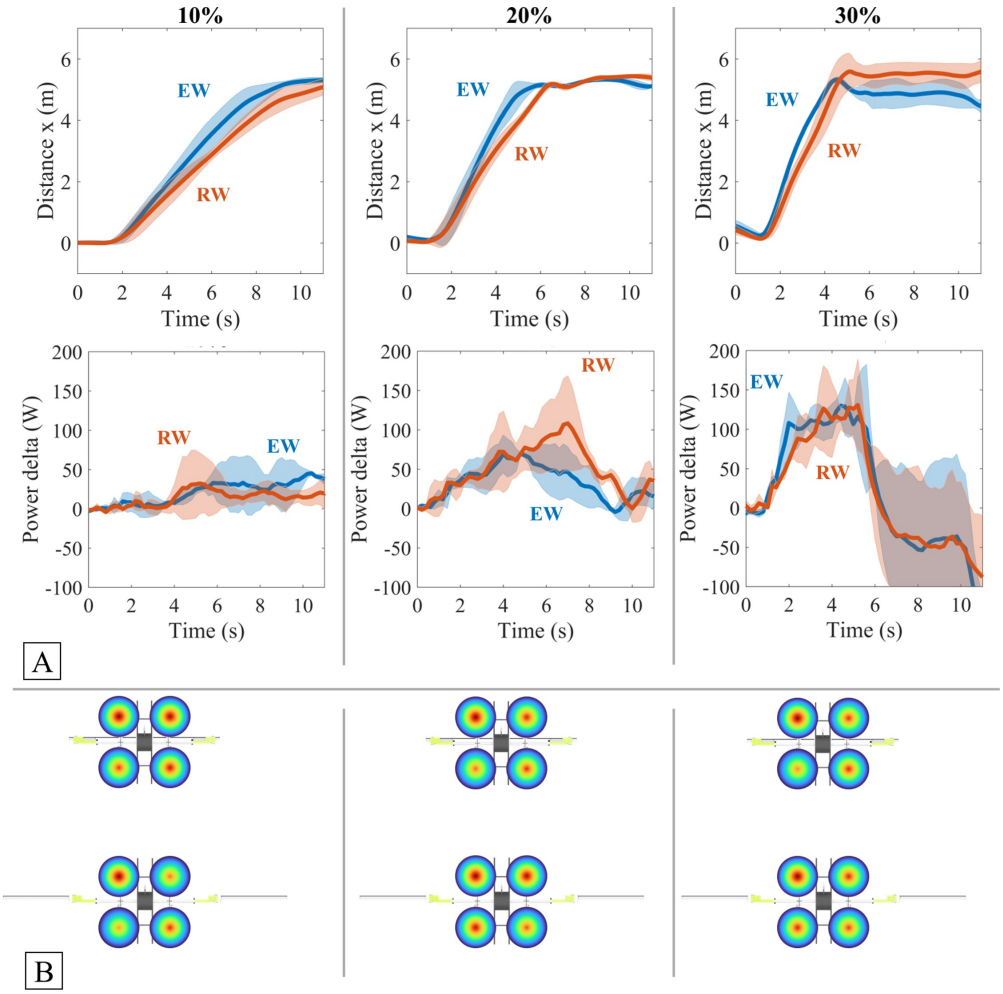

Figure 2.10: Drifting in linear trajectory (Figure 2.8 (B)) at different wind current intensities (%) and the motor saturation levels in different wind speeds while at the extended or retracted configuration. The colored circles represent the motor PWM signal and, thus, the motor saturation. A higher change in color means higher motor saturation. EW is for extended wings, and RW is for retracted wings. (A) The drone maneuvers without the motor contribution. (B) Saturation levels for maneuvering without the motors' contribution.

In addition to the drifting, where the motors do not actively contribute to flying throughout the commanded setpoints, experiments were performed where the drone was commanded to reach a waypoint at a speed that was set to be higher than the drifting speed with the motors contributing in extended and retracted wing configurations. The results are similar to the previous set of experiments. Extended wings always lead to lower motor saturation levels by a few percent. On the other hand, the energy depends on the wind speed. Extended wings are beneficial in the case of 20% for an 10% decrease in the normalized energy consumption. Although in the other cases, the motors consume more power to accelerate the drone when at 10% or when they try to compensate for the adverse pitching moment generated at 30% wind power (Figure 2.11 (A, B)).

The yaw authority of the drone at different wind speeds was also tested by performing rotational trajectories. This experiment aimed to determine the effect of crosswind on the performance of the drone when commanded to achieve a specific angle using pure yaw motion in hovering flight. The drone was commanded to take off, hover, rotate to an angular setpoint, and finally land. The drone was placed 2.5 m from the wind generator. First, a custom attitude controller allowed the drone to rotate freely while hovering at a commanded setpoint 2.5 m from the wind generator (Figure 2.8 (C)). At first, the drone is tested in yaw motion with one wing fully extended, thus rotating due to only the yawing moment generated by the wing. To continue, the drone is commanded to match the rotational speed of the one-wing fully extended configuration with both wings extended and both wings retracted. For the one-wing extended configuration, it is observed a decrease in the energy consumption of up to 98% compared to the other configurations as shown in Figure 2.12 (A). At 30% of wind current, the fully extended wings cannot perform the commanded trajectory and get destabilized by the wind current. Furthermore, the motor saturation levels for the single-wing extended experiment remained lower when compared to the other configurations in most of the wind current speed tests, thus enabling better maneuverability (Figure 2.12 (B)).

In addition to the yaw experiments where the motors do not actively contribute to the yaw motion, experiments were performed where the drone was commanded to reach an angular waypoint at the highest possible speed, with the motors contributing in all wing configurations. Though, the results are similar to the previous set of experiments. The experiments were conducted with extended wings, retracted wings, and one wing extended and one retracted Figure 2.13 (A). It is observed that when commanding the asymmetrical extension of one wing in synchronicity with the motors yaw command, the drone severely outperformed both the extended wing and the retracted wing configurations in terms of normalized energy efficiency by 75% and 77% for the extended wing configuration and by 20% and 51% respectively at wind current speed of 10% and 20%. At the same time, it is observed that at the wind current speeds of 20% and 30%, the drone reaches the angular setpoint faster and with less overshoot compared to the other wing configurations Figure 2.13 (A). The maximum yaw rate is increased up to 200%. Motor saturation levels had a similar indication to the experiments without yaw contribution due to the impact of the asymmetric wing in the yaw maneuver Figure 2.13 (B).

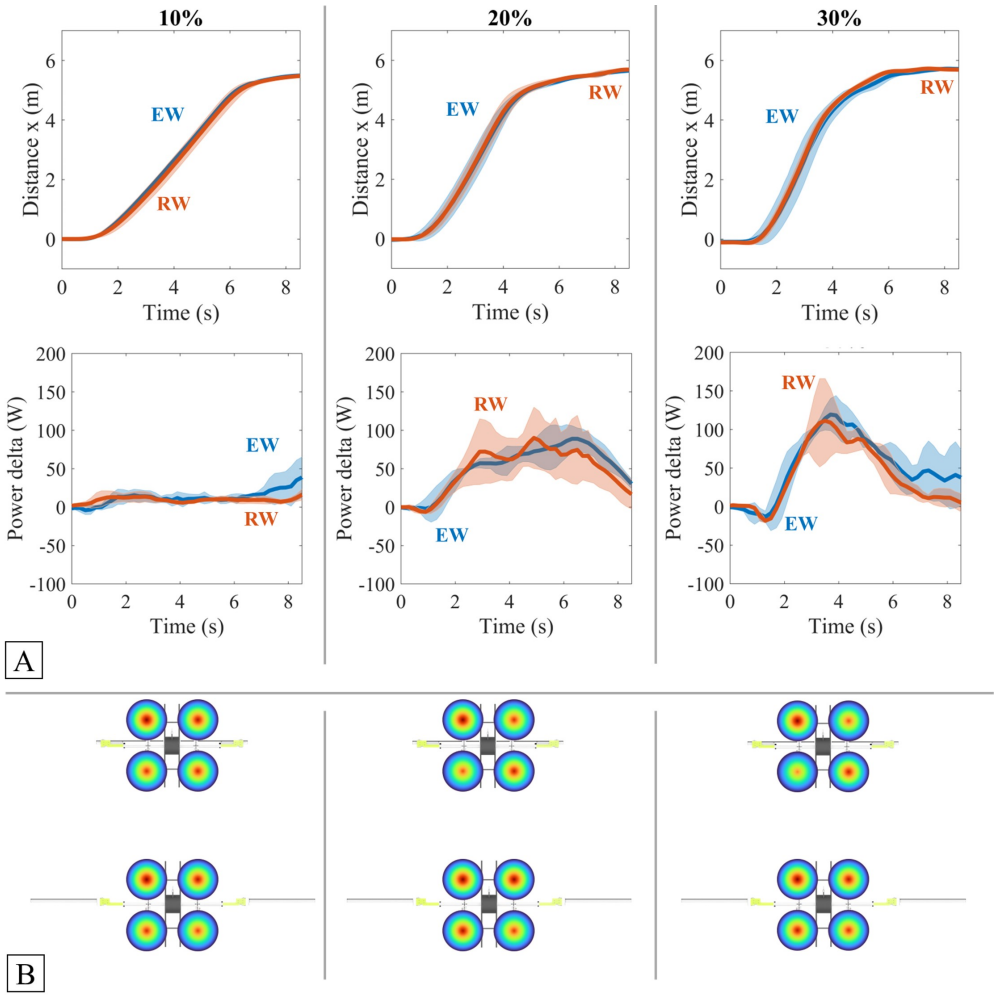

Figure 2.11: Drifting in linear trajectory (Figure 2.8 (B)) at different wind current intensities (%) and the motor saturation levels in different wind speeds while at the extended or retracted configuration. The colored circles represent the motor PWM signal and, thus, the motor saturation. A higher change in color means higher motor saturation. EW is for extended wings, and RW is for retracted wings. (A) The drone maneuvers with the motors' contribution. (B) Saturation levels for drone maneuvering with the contribution of the motor.

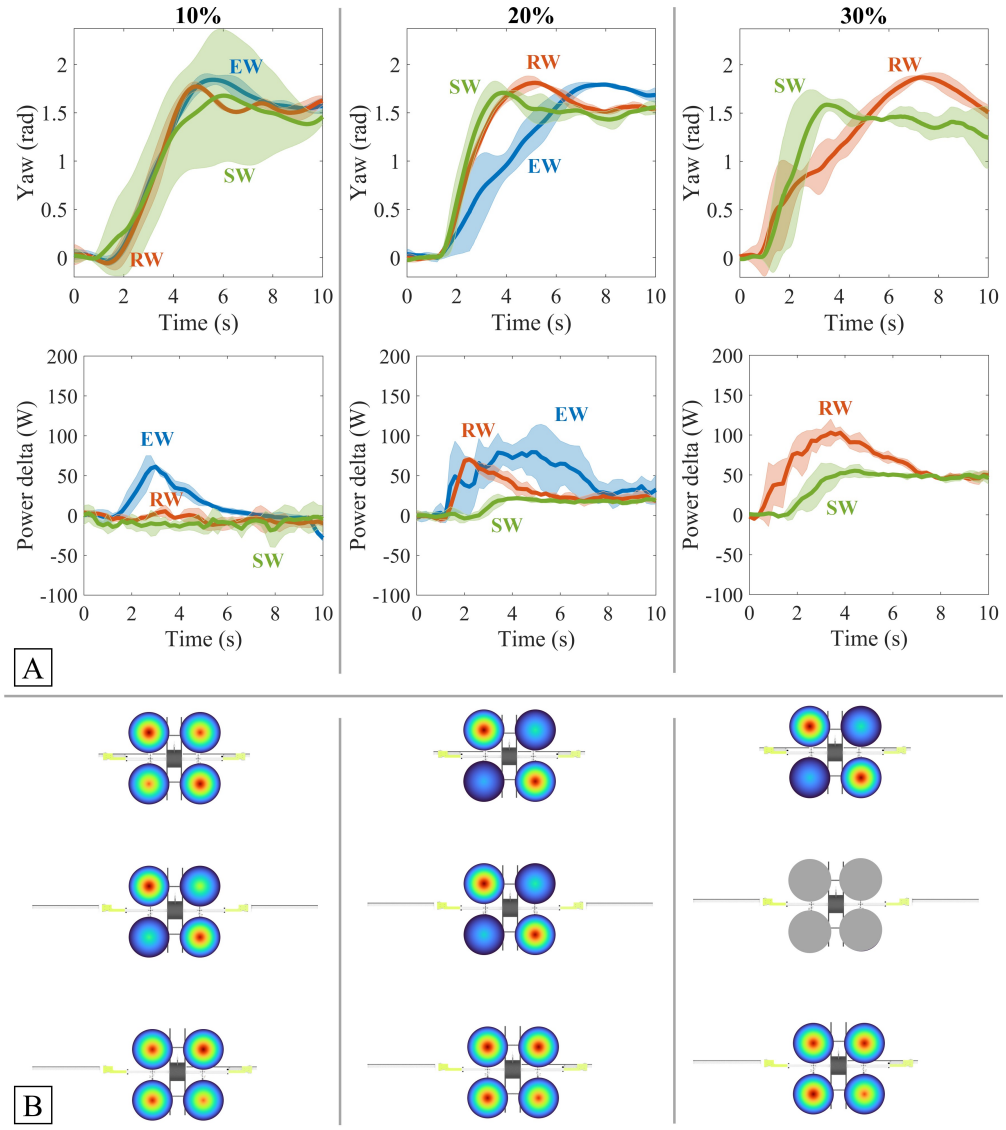

Figure 2.12: Yaw in rotational trajectory (Figure 2.8 (C)) at different wind current intensities (%) and the motor saturation levels in different wind speeds while at the wings extended, wings retracted or single wing extended configuration. The colored circles represent the motor PWM signal and thus the motor saturation, a greater change in color means higher motor saturation. EW is for extended wings, RW is for retracted wings, and SW is for a single wing extended. (A) The drone maneuvers without the motor contribution. (B) Saturation levels for maneuvering without the motors' contribution.

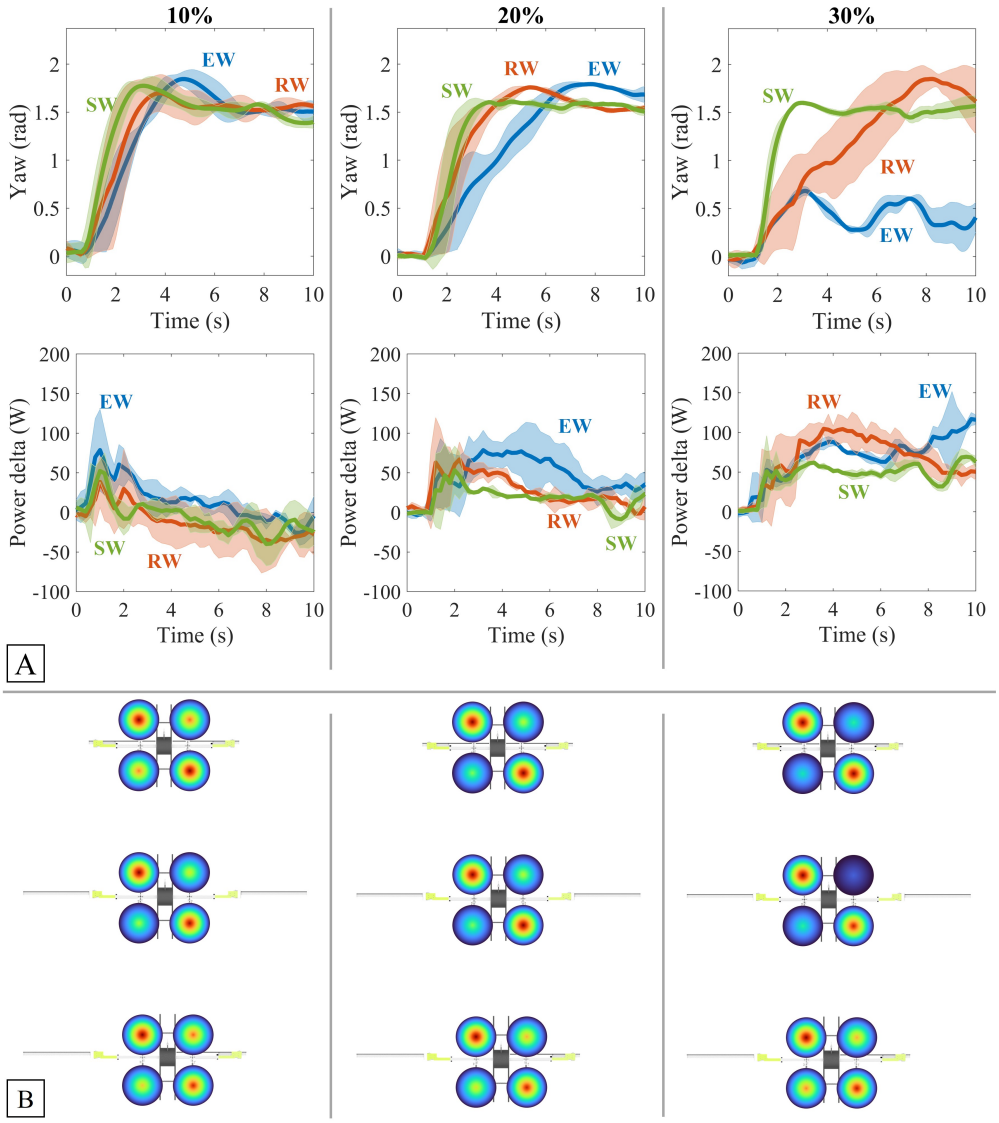

Figure 2.13: Yaw in rotational trajectory (Figure 2.8 (C)) at different wind current intensities (%) and the motor saturation levels in different wind speeds while at the wings extended, wings retracted or single wing extended configuration. The colored circles represent the motor PWM signal and thus the motor saturation, a greater change in color means higher motor saturation. EW is for extended wings, RW is for retracted wings, and SW is for a single wing extended. (A) The drone maneuvers with the motors' contribution. (B) Saturation levels for drone maneuvering with the contribution of the motor. For visualization purposes, we plot yaw from 0 to 2 rad.

2.5 Discussion

The results show that continuous morphing can assist stability and wind rejection while morphing to a fixed configuration can help exploit wind currents to increase the yaw rate or increase the normalized energy efficiency significantly. Despite performing the experiments in the Micro Aerial Vehicle scale, we expect similar behavior for larger vehicles at higher Reynolds numbers within the low Reynolds number regime of up to 150000 [26]. The same aerodynamic effects are expected to be observed because of the same behavior of flat surfaces in the low Reynolds number regime. Meaning that when in the deep stall, the angle of attack increases drag and decreases lift [77]. For this study, the vehicle's shape was kept to the simplest possible as flat plates were used for the morphing wings and fuselage. Shape optimization can increase the aerodynamic benefits of continuous and noncontinuous morphing while sustaining larger wind currents. In addition, exploring the integration of another degree of freedom might be significantly beneficial for further demonstrating energetic benefits. During hovering operations, the wings could adjust their angle of incidence to generate lift during static hovering and thus increasing the time of flight operations. In the transition from horizontal to vertical flight and vice versa, many VTOLs are required to operate in high degrees of angle of attack while maintaining high throttle values to enable the transition. Adjusting the angle of incidence of the wings could enable slower transition speeds by ensuring that the flow stays attached during the operation and that the wings generate adequate lift. Furthermore, concerning the previous discussion on the shape, structure, and actuation, morphing wings also have the side benefit of increasing the agility and efficiency of the drone in horizontal flight [14, 68]. Moreover, during horizontal flight mode, extending the wings and moving the center of gravity to the front and further away from the aerodynamic center can increase the longitudinal stability of the aircraft and thus increase the energy consumption benefits [78]. On the other hand, forward flight with retracted wings can lead to reduced drag, higher flight speeds, and locomotion through narrow passages where fixed wingspan drones would not be able to pass.

Regarding limitations, to apply the method in a real flight mission, the drone must have an accurate estimate of the wind direction and magnitude. This is because wind direction and wind force tend to change unpredictably in a natural environment. As stated before, in the experiments presented here, the wind direction is known as the drone always flies in front of the wind generator. Therefore, additional sensors or software estimators are needed for a real flight mission. At present, this type of sensor can be difficult to integrate into small vehicles. Currently, existing flight controllers for VTOL platforms are being used [79]. Further research could investigate integrating the wing morphing methodology developed at an end-to-end flight controller. Moreover, as a next step, a controller that automatically chooses between fixed or continuous wing actuation should be implemented to exploit the current method's full potential in a real flight mission. An automatic wing morphing controller would select the way of morphing depending on the mission trajectory, the effective velocity, and the wind direction changes.

2.6 Conclusion

This work has shown the stability, maneuverability, and energetic benefits of a morphing wing tailsitter UAV compared to a conventional fixed-wing configuration of the same weight. Similar results are expected to be applicable throughout the low Reynolds number regime. Additionally, the findings presented here are a promising solution for various types of drones with vertical wing surfaces, such as multi-modal terrestrial and marine winged robots. Finally, the proposed method's applicability is highlighted by the fact that it can be adapted to different avionic setups or morphing wing designs as there are no specific hardware requirements. These findings indicate the potential for future aerial robotics systems not just to reject wind gusts but actively exploit them to increase range and endurance, improve agility and maneuverability, and expand the weather conditions in which UAVs can operate.

3 Ultra Wind Defiant Morphing Drones

In the previous chapter, the benefits of morphing wings in VTOL drones were demonstrated. Namely, they could be used to reduce the normalized energy consumption and increase the attitude and positional stability of a tailsitter VTOL drone. Despite the experimental outcomes, it was also observed that the proposed design suffered from limitations on the amount of wind force it could sustain (Level 3, (Annex C)) due to the exposed surface of the fuselage. In this chapter, a new design is proposed that can sustain a wind force of Level 5 (Annex C) while operating in hovering mode. The drone's design is inspired by the insect order Odonata*, which includes the* Zygoptera*, which are commonly known as Damselflies, and the* Anisoptera*, which are commonly known as Dragonflies. Similar to these types of insects, the vehicle features four independently actuated morphing wings that allow different amounts of wing surface exposure to the perpendicular wind during hovering or horizontal flight.*

3.1 Introduction

In the previous section, it was shown that exposed wings are a major drawback for a VTOL aircraft in hovering flights due to their exposed surface in side winds. In addition, a morphing methodology, which mitigates adverse wind effects in hovering flights or exploits them so that they assist in increasing the maneuverability, stability and energy efficiency of the drone, was described. A limitation that was observed throughout the experimental phase was that despite utilizing morphing to decrease the surface area of the wings and the fuselage, the wind resistance of the plane remained at the lower levels of the wind force scale (Level 3) (Annex C). The limitations in wind force were observed due to several factors like the rectangular flat plate design of the fuselage that remained exposed even after fully retracting the main wings, the rectangular airfoil profile of the aircraft that induced tip turbulence and increased drag, and the roughness of the aircraft's foam surfaces that substantially increased parasitic drag. Modern industrial VTOLs of weight below 5 kg, feature wind resistance slightly above wind force level 4 in hovering flight, which is approximately 8m/s.

In this section, the design of a morphing VTOL is presented. It has the capability to sustain wind force similar to industrial VTOL drones while retaining the ability to use its wings to maneuver with similar agility to the drone Morpho presented in the previous section. Designing such a vehicle is required to address the shortcoming of Morpho. In fact, the surface folding ratio of Morpho in folded and unfolded configurations was 0.66. This means that approximately two-thirds of the surface remained exposed after wing folding. Another challenge for designing the next generation of wind-defiant drones is the requirement to rapidly decrease or increase their folding wing area in order to retain the ability to exploit wind currents to increase the aircraft's agility and energy efficiency.

There are several examples of folding patterns in nature that allow up to 85% reduction in surface area. However, high surface and volume changes usually come with complex multistage folding patterns that are challenging to replicate in engineering applications. Nevertheless, there is one order of insects that significantly decreases its wing surface without complex wing folding methods: the *Zygoptera* species of the order *Odonata*. Insects of the *Odonata* order are composed of four independently actuated wings, as seen in the dragonfly presented in Figure 3.1 (A). During the flight, the wings are unfolded, and they work synergistically to provide thrust by flapping. However, dragonflies, during rest, have their wings remain unfolded. On the contrary, in the damselfly, when the insect is landed, its wings are rested, folded on each other as seen in Figure 3.1 (B).

3.2 The wind defiant morphing VTOL drone

The Morpho^2 design was inspired by the *Odonata* insects. Morpho^2 is a quad morphing biplane tailsitter that features four identical and independently actuated wings that are folded during hovering flight and unfolded for efficient horizontal flight. Different morphing configu-

Figure 3.1: Species of the *Odonata* order. (A) *Anisoptera* commonly known as dragonflies. Figure adapted from [21, 22]. (B) *Zygoptera* commonly known as damselflies.

rations of the wings are presented in Figure 3.2. Currently, similar to Morpho, the independent wing actuation is used to improve the drone's energy efficiency and maneuverability in hovering flight. The drone is autonomous during flight. For the autonomous flight control, a similar setup to Morpho was deployed, which includes the Pixhawk 6 autopilot and a Jetson Nano companion computer for running the wing controller. Similar to Morpho, Morpho^2 uses the state estimation and the trajectory setpoints from the autopilot to adaptively morph the wings.

3.3 Live wind estimation

Another limitation of the first drone version was that there was no wind estimation during the flight experiments, which limited the drone's potential for actual missions. Several wind estimation methods include sensor integration. However, for weight reduction purposes, a software method was chosen to be integrated for estimating the wind force and direction through changes in the state estimation [80]. In this version of the wing controller, the wing surface morphing is adjusted to the estimated wind magnitude. For example, if the drone senses no wind, the morphing function gets deactivated, and it operates with retracted wings in hovering flight. Moreover, if the wind estimation affects the plane backward, the morphing wing function is mirrored to compensate for the wind currents acting on the back of the plane. The integrated wind estimation function and the adjustment of the wing controller enable the drone to morph its wings for compensating in any estimated wind direction and thus allowing for real missions.

3.4 Geometric characterizations

Morpho^2 is 3.8 Kg with four 500 W motors and 12x5.5 inch propellers. The estimated hovering time is 17 min. The drone's morphing configurations, along with their effects on the center

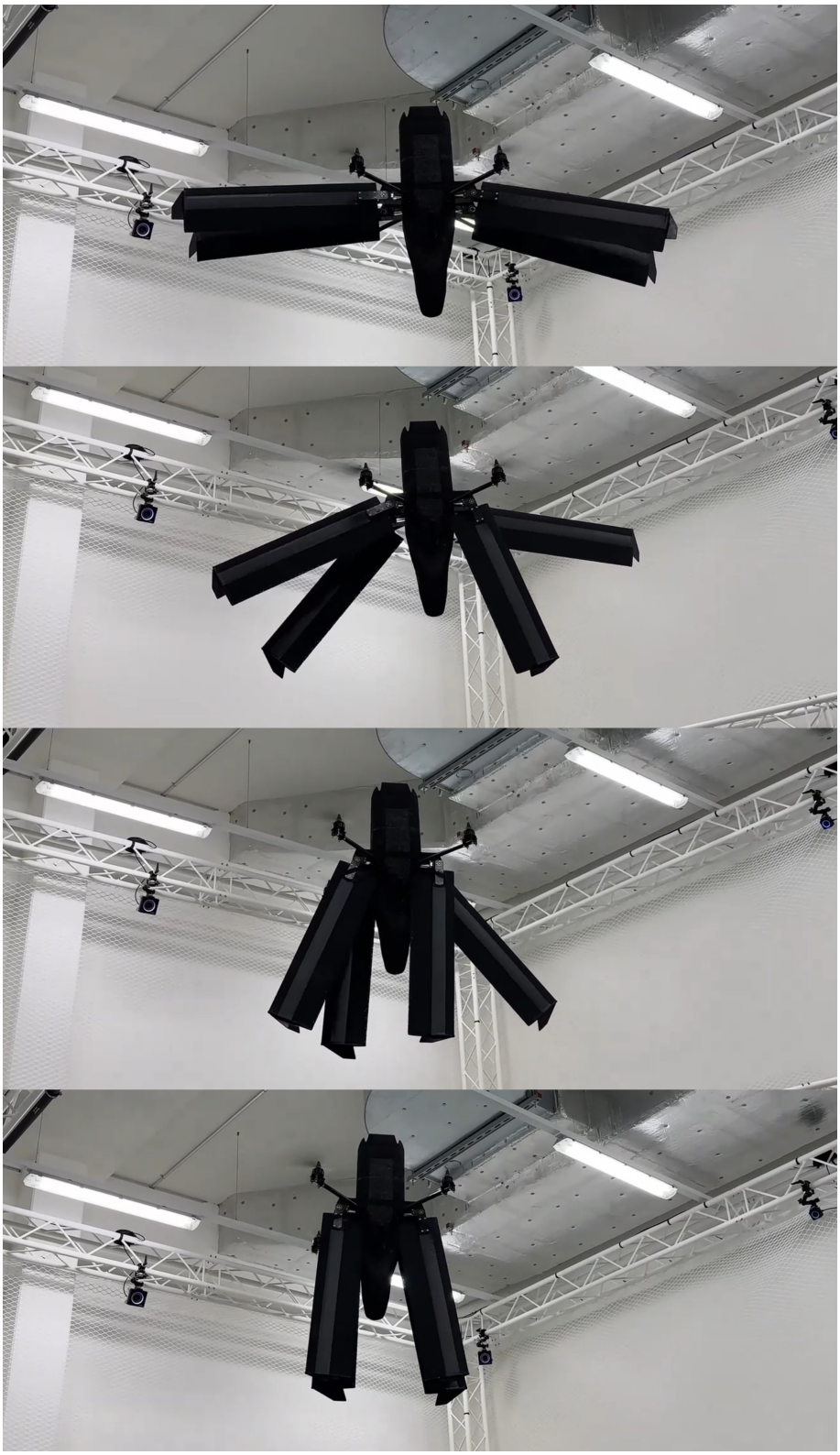

Figure 3.2: Morpho^2 in hovering flight with different wing configurations.

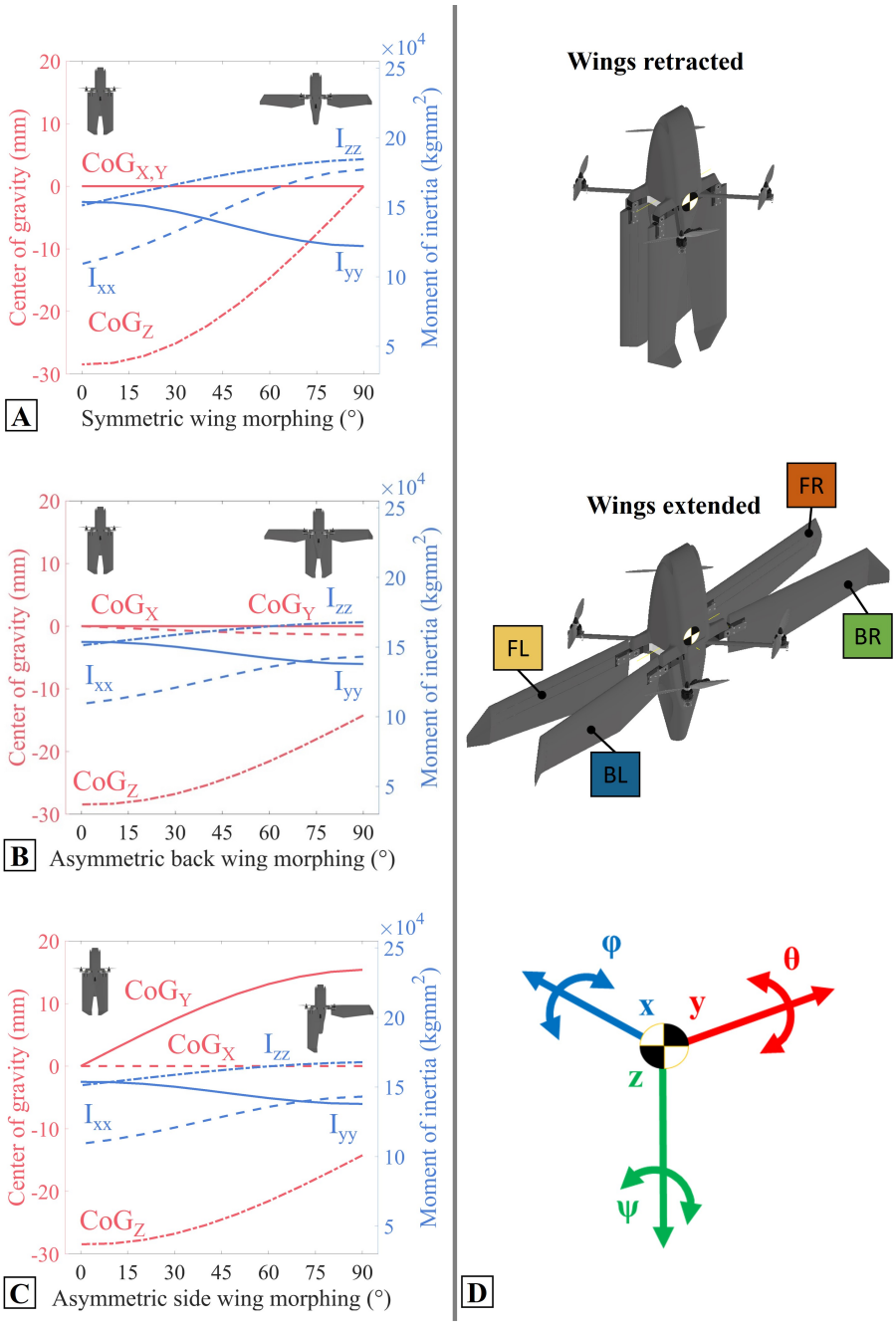

Figure 3.3: Morpho^2 geometric characteristics. (A) The maximum displacement of the center of gravity in the z-axis is 2.8 cm when at full wing retraction. (B) The maximum displacement of the center of gravity on the x-axis is 0.13 cm when the front or back wings are fully extended. (C) The maximum displacement of the center of gravity in the y-axis is 1.4 cm when both wings on one side are fully extended and wings on the other fully retracted. (D) Morpho^2 in retracted and extended wing configurations. Front Left, Front Right, Back Left, and Back Right wings are indicated with the respective initials. A reference coordinate system is also displayed.

of gravity of the plane and the moment of inertia, are presented in Figure 3.3. Each of the wings weighs approximately 140 gr and is attached to a servo motor which can move the wing within a range of 0° to 90°. Center of gravity adjustment is beneficial both for hovering and horizontal flight. In hovering flight, the center of gravity is close to the motor plane, which improves the stability of the aircraft by minimizing adverse torque effects related to the mass distribution outside of the motor plane. In addition, the reduction of moments of inertia around the hovering axis is another factor that increases the stability of the plane. In fact, the yaw axis is the one that has less controllability for quadcopters since the differential of the motors' counteracting torque is used – contrary to the roll and pitch axes which use thrust differential multiplied by the lever arm. Moreover, in horizontal flight, the wings assist in adjusting the center of gravity in front of the aerodynamic center, which is beneficial for the longitudinal stability of the plane. The ability to adjust the center of gravity in forward flight also assists in adopting more or less agile configurations. Wing morphing in forward flight can also be used for roll and pitch control.

3.5 Flight experiments

Similar to Morpho, Morpho^2 was placed in front of the Windshape wind generator [19], which generated the needed wind current to test the vehicle.

The main goals that needed to be validated for the new design were the following:

- Integrate the wing controller developed in Morpho updated with the wind estimation method
- Show that morphing the wings in Morpho^2 can demonstrate performance benefits similar to Morpho
- Demonstrate wind resilience similar to industrial drones

To demonstrate the updated wing controller with the integrated wind estimation algorithm, the following experiment was performed. Morpho^2 took off, and after a few seconds, a wind current of approximately 3 m/s was applied. After applying the wind current, Morpho^2 performed a 360° yaw maneuver. In Figure 3.4 (A) and (B), it is presented that the drone tracks the yaw and yaw rate successfully without being destabilized by the wind currents. The first and second picks in both graphs demonstrate the 180 ° yaw maneuver. In Figure 3.4 (C) and (D), the wing actuation angles are presented with different colored tags. In Figure 3.4 (B) and (D), the two picks in the wing angle graphs show the back right and front left wings to be actuated to assist with the yaw maneuver. The reason why different wings are actuated for each yaw setpoint is that the wing controller mirrors the wing outputs so that it can support the drone while the wind currents are applied in the back of the drone.

To confirm that Morpho^2 has a similar maneuvering performance to Morpho, the active yaw experiment was conducted. In this experiment, the drone was commanded to reach an angular waypoint at the highest possible speed, with the motors contributing to achieving the yaw

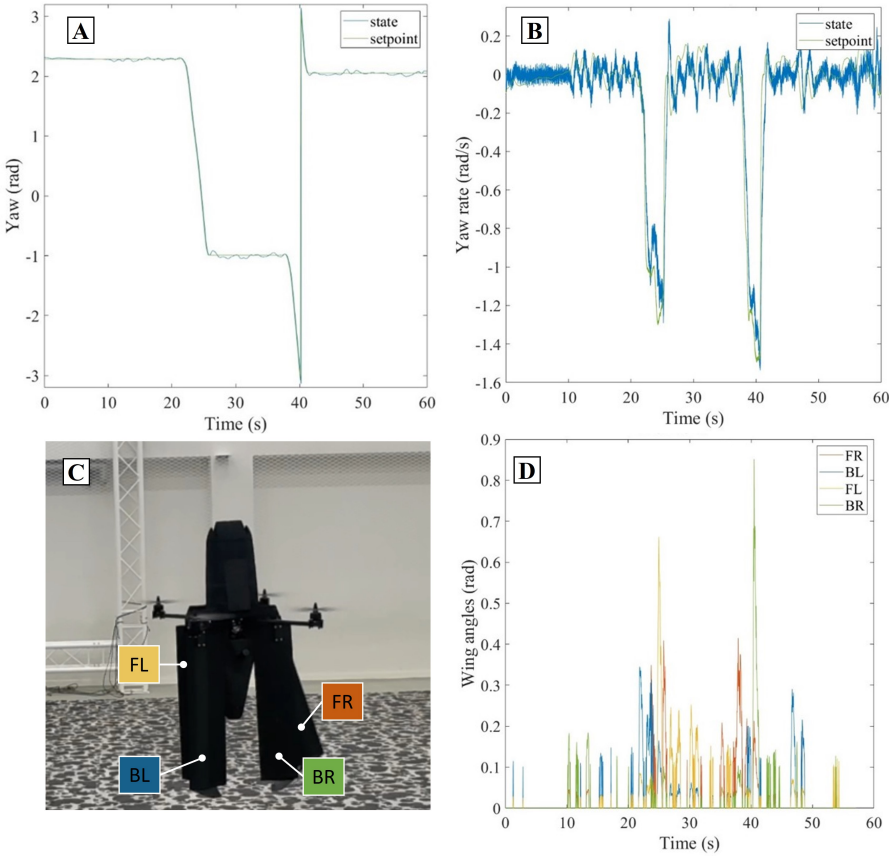

Figure 3.4: The updated wing controller. (A) Yaw state estimate and setpoint. (B) Yaw rate state estimate and setpoint. (C) A caption of Morpho[2] during the hovering experiment (D) Wing angles over time for FR-Front Right, FL-Front Left, BR-Back Right, BL-Back Left.

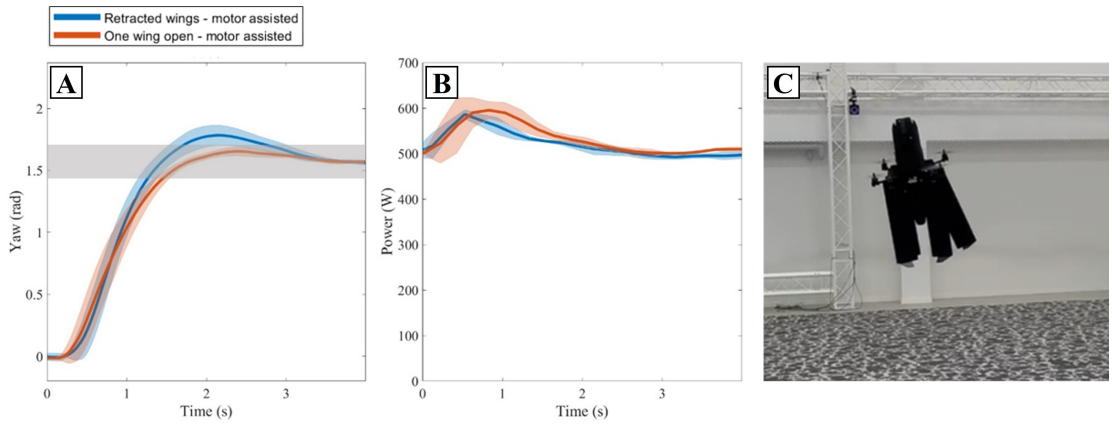

Figure 3.5: Maneuvering in rotational trajectory when wings retracted or single wing extended configuration. The drone rotates with the motors' contribution. (A) The yaw in the rotational trajectory. The grey area represents the 5% position error. (B) The power consumption. (C) Morpho[2] while performing the rotational trajectory with one wing extended.

setpoint. Once take-off in front of the wind generator, the wind speed is set at around 5 m/s. After a few seconds, the drone is commanded to reach a waypoint at 90° as fast as possible. To achieve that, the motors' differential is commanded to a maximum while sustaining enough thrust for hovering. The experiment is conducted three times with all the wings retracted and three times with one of the wings opened at 15°. As depicted in Figure 3.5 (A), similar results to Morpho are observed. The drone with one wing open in 15° reaches the commanded yaw setpoint faster and with less overshoot. The normalized energy consumption of the drone shows that the drone with one wing open consumes 14.33% less than the drone with both wings closed to reach the setpoint within a +-5% error band.

To demonstrate the wind resilience of Morpho^2, the drone was placed in front of the wind generator and after taking off a gradual increase of the wind speed took place from approximately 3 m/s to 9 m/s with a step of 1 m/s. In Figure 3.6 (A), the pitch angle is observed, which starts from 0° and reaches approximately 45° at the 9 m/s speed (Figure 3.6 (C)). An interesting observation from Figure 3.6 (B) is that as the wind speed increases, the power draw decreases due to the fact that the fuselage and the exposed wings start generating lift while the drone starts generating less drag than when completely vertical.

3.6 Discussion

The results from the experimentation of Morpho^2 validate the hypotheses presented in the previous section. As expected, morphing the wings of Morpho^2, which is a larger vehicle operating in higher Reynolds numbers, demonstrated similar behavior to Morpho. The main differences in the geometric design of the vehicles were in the wings and the fuselage. In Morpho, the wings were based on rectangular flat airfoil profiles, which significantly increased drag. In Morpho^2, the fuselage and the wings were based on conventional airfoil profiles for an optimized lift-to-drag ratio. The goal of the Morpho was to be a generic and easy-to-manufacture platform. On the contrary, in the second version of the drone, the focus was on achieving the highest possible folding ratio with the minimum surface exposure to side winds in hovering flights.

Further optimization of the surface distribution could increase the drone's stability in hovering flight. In addition, a better manufacturing method could be deployed to decrease the roughness of the fuselage and wing surface and thus significantly decrease the surface-generated drag of the foam components. It is anticipated that with further aerodynamic optimization, the vehicle would be able to sustain winds of Level 6 and above. Moreover, the wind estimation algorithm integration will be a useful and necessary tool for calculating the magnitude and direction of the wind in real flight missions with dynamic wind conditions (Figure 3.4). Concluding the discussion, similar to Morpho, Morpho^2 used existing flight controllers for VTOL platforms[79]. Since morphing the wings can have a significant contribution to the passive and active stability of the drone both in horizontal and hovering flight, an end-to-end model-based flight controller for actively integrating morphing with the required flight mode

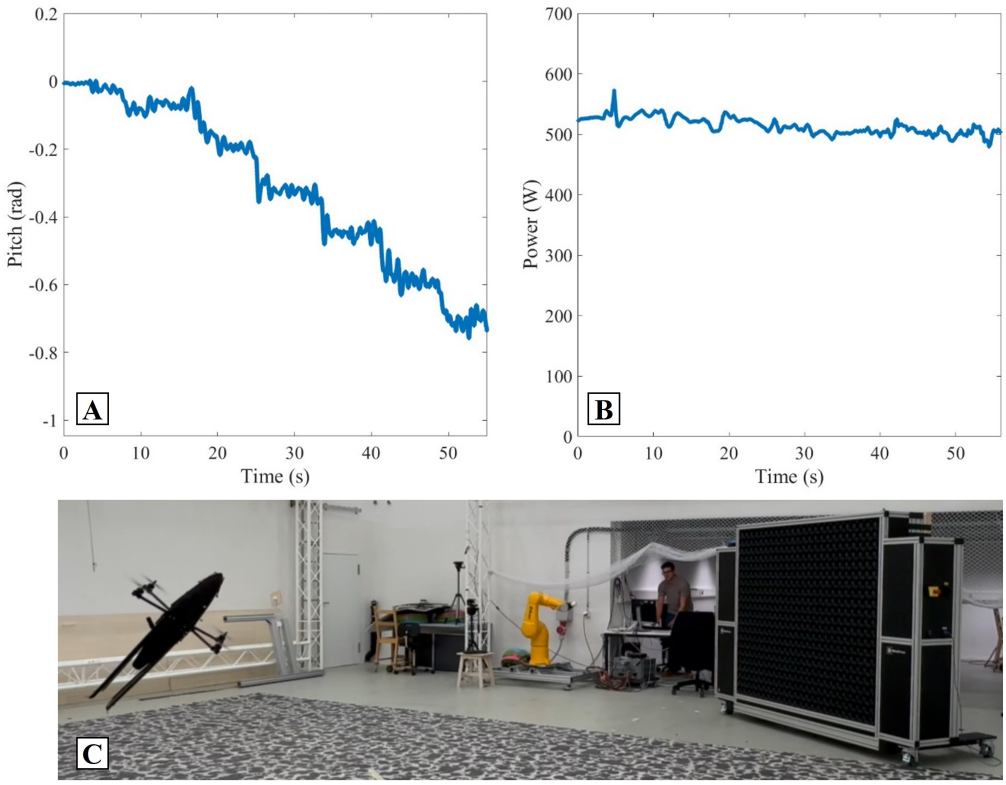

Figure 3.6: Morpho^2 during the Level 5 wind hovering. (A) The pitch angle change during the airspeed ramp-up from 0 to 9 m/s. (B) The energy consumption of Morpho^2 as a function of the time of the experiment. (C) Morpho^2 hovering at 9 m/s wind in front of the Windshape wind-tunnel.

could demonstrate higher performance and increased robustness compared to the current setup.

3.7 Conclusion

In this chapter, a new version of Morpho, Morpho^2, was presented. Morpho^2 demonstrated several improvements and advantages over the first version of the drone, with the most significant being the wind resistance which was more than double of its predecessor. The morphing capabilities of the drone and its ability to significantly vary its aerodynamic and inertia profile through adjusting the wings suggest promising future research venues in the exploration of morphing for different flight modes. It is foreseen that utilizing the wings in the VTOL transitioning phase or during the horizontal flight phase could significantly reduce the energy consumption of the drone and provide energetic benefits compared to vehicles of similar sizing.

4 Robotic *Elytra*: Insect-Inspired Protective Wings

What happens, though, when drones are required to operate both in the air and on the ground? Winged drones that fly in close proximity to obstacles or that are capable of aerial and terrestrial locomotion can benefit from protective systems that prevent damage to delicate aerial structures. Existing protective solutions focus on multi-copter drones and consist of adding structures, such as cages, mechanisms, and instruments that add weight and drag. Here, a protective strategy is described for winged drones that mitigate the added weight and drag by means of increased lift generation and stall delay at high angles of attack. The proposed structure is inspired by the wing system found in beetles and consists of adding an additional set of retractable wings, named elytra, *which can rapidly encapsulate the main folding wings when protection is needed.*

- The work presented in this chapter is adapted from [59]:
  C. Vourtsis, W. Stewart and D. Floreano, "Robotic Elytra: Insect-Inspired Protective Wings for Resilient and Multi-Modal Drones," in *IEEE Robotics and Automation Letters*, vol. 7, no. 1, pp. 223-230, Jan. 2022.

- Supportive video material can be found at:
  https://www.youtube.com/watch?v=ARuuxTFpuHI&ab_channel=EPFLLIS

- Supportive material can be found at:
  https://doi.org/10.21227/jvch-0g88

4.1 Introduction

Protection from collisions has been extensively studied for multi-rotor drones and terrestrial robots. Among the most common protective strategies is to completely enclose the vehicle in a cage [81, 82, 83, 84, 85], or partially surround it in protective bumper structures [86, 87]. However, these solutions are not practical for fixed-wing drones as the enclosing structure would interfere with the lift generating capabilities of the wings. As a result, alternative strategies are required for winged drones. The most common strategy consists of fabricating the robot out of impact-resilient foam materials (such as Expanded Polypropylene-EPP, e.g.). These foams can sustain high impact loads, but remain susceptible to puncture. Simply using impact resilient materials in this manner also leaves the extended wing structure exposed to damage from contact with the environment [88]. Passively folding wings can be retracted to avoid collisions, but in the event of a collision with sharp surfaces they are still vulnerable to being torn [89]. State of the art, sub-gram micro-aerial robots display collision resilience properties although their constantly exposed wings and fuselage allow for continuous structural degradation with each collision [90]. Multi-modal locomotion drones such as DALER [91] can even use their shape-shifting mechanisms to absorb impact energy at contact, but they too remain vulnerable to damage from penetration by spicular surfaces. Despite increased resilience, folding wing solutions remain vulnerable to damage because even when folded, their wings are exposed to contact.

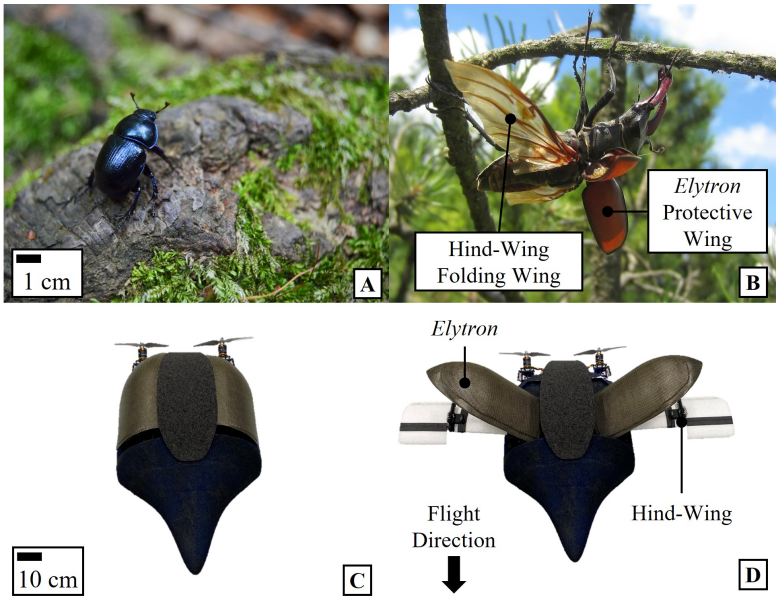

Figure 4.1: (A) A *Scarabaeidae* beetle in its natural habitat, perching on a branch, in protective configuration with the hind-wings folded under the protective *elytra* [23]. (B) Wing anatomy of a *Scarabaeidae* beetle. The figure displays the system of the hind-wings and the *elytra* in a *Scarabaeidae* beetle [24, 25]. (C) HercuLIS, the drone described in this article, with retracted wings. Hybrid carbon-Kevlar *elytra* encapsulate the fragile folding wings. (D) HercuLIS with deployed wings for horizontal flight.

Inspired by the protective structure of beetles, here we describe a novel protective mechanism for winged drones that protects folded wings from puncture by enclosing them in a protective shell, which also generates lift during flight to offset its added weight. *Coleoptera* (beetles) are insects that have exhibited resilience for more than 60 million years to the point that today they represent approximately 40% of all living insects [45] (Figure 4.1 (A)). Anatomically, flying beetles are characterized by a protective exoskeleton and a dual-wing system; hind-wings and the *elytra* (Figure 4.1 (B)). The hind-wings are the primary source of lift generation and are soft, foldable, membrane structures. The *elytra* are multi-functional hardened shells that can fully encapsulate the folding wings when not in flight and provide collision and penetration resilience [92]. When in flight, the *elytra* work in synergy with the hind-wings to generate additional lift to support their weight [44] and delay stall [93].

In this chapter, we show that a dual-wing system, (hind-wings and *elytra*), can be used for small winged drones to provide protection from puncture while mitigating the added drag and weight costs that other protective solutions, such as cages, suffer from. In our solution, the *elytra* completely encompass the folded hind-wings, protecting them from spicular surfaces or obstacles in the vicinity of the aircraft. Specifically, our approach (i) generates additional lift to partially offset the *elytra* weight in cruise flight (ii) improves the lift to drag ratio at high angles of attack compared to single wing configurations and (iii) delays stall. To investigate these benefits, we performed aerodynamic experiments on a simplified test article composed of a fixed wing and *elytra* that could change their dihedral and angle of incidence. As beetles are of small size and weight (NAV scale shown in Figure 4.2) compared with most commercial UAVs (MAV scale in Figure 4.2), we scaled up the geometric parameters of the insect to fit the size of a common MAV (Figure 4.2)[45]. This scale of vehicle is useful for roboticists as it is small enough to be cheap and easy to manufacture robots, while large enough for the robots to be capable of carrying payloads. The proposed hind-wings and *elytra* system resemble a biplane configuration, so we also examined how well the existing biplane model can describe the lift and drag generation of our dual-wing system. Finally, we validated the proposed design with a free-flying, multi-modal, winged drone code named HercuLIS that can fly and locomote on the ground using wheels. On the ground, the *elytra* cover the folded wings and electronics to protect them. During flight, the *elytra* and the hind-wings unfold to produce lift.

The rest of the chapter is organized as follows. In the second section, we explain the rationale behind the geometric design of the hind-wings and the *elytra* while we discuss the aerodynamic modeling and the aerodynamic experiments in the wind tunnel. Then in the third section, we describe the integration of the hind wings and *elytra* system into HercuLIS, and outdoor experiments. Finally, in the fourth and final section, we discuss possible applications and extensions of the proposed system.

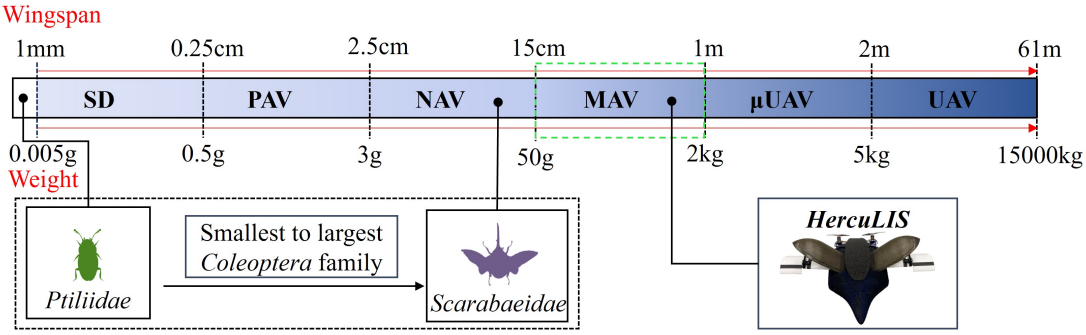

Figure 4.2: The morphology and size of *Coleoptera*. Wingspan and weight comparison of existing drone sizes (SD Smart-Dust, PAV-Pico Aerial Vehicle, NAV-Nano Aerial Vehicle, MAV-Micro Aerial Vehicle, UAV-Micro Unmanned Aerial Vehicle, UAV-Unmanned Aerial Vehicle) with the smallest and the largest size of *Coleoptera* families. The drone scale was adapted from [26]. The green box indicates the weight and size category (MAV) that HercuLIS belongs to.

4.2 Aerodynamic characterization

To investigate whether the aerodynamic advantages of the beetle hind-wing and *elytra* system can be translated to a drone, we performed experiments in an open wind tunnel using a simplified test article. As the insect flies, it varies its *elytra* dihedral and *elytra* angle of incidence, thus, we examined how these angles could affect lift and drag forces for a given wing configuration. The test article consists of a dual-wing system that captures the relevant geometric parameters of the beetle. We scaled the beetle wing geometric ratios (length and chord) such that they fit the dimensions of a standard MAV platform (Figure 4.2), [45]. These scaled parameters were used for the chord and wing length of the *elytra* and the hind wings. The relative distances between the hind-wings and the *elytra* (parameters x,z in Table 4.1 and Figure 4.3) were designed in CAD for achieving the different configurations of *elytra* angle of incidence and dihedral angle that we chose to investigate while reducing structural weight (Figure 4.3(B, C)). For clarity, the angle of incidence refers to the angle between the hind-wing and *elytra* (α_e in figure 4.3), while the angle of attack refers to the angle between the hind-wing and the incident airflow (α in figure 4.3).

The main wings of the test article consisted of hot-wire cut polystyrene foam reinforced with a rectangular carbon fiber beam. The main wings had a total span of 1 m and chord of 15 cm. The *elytra*, as well as the interface between the test article and the load sensor were fabricated from polyamide (PA) and acrylonitrile butadiene styrene (ABS) respectively. The *elytra* were 3D printed by a EOSINT P-395 printer (ABS) and the interface between the test article and the load sensor by a Stratasys Dimension Elite printer (PA). The *elytra* were mounted to two 2-axis servo actuators (Robotis Dynamixel 2XL430-W250-T). The servo motors were communicated with through serial (TTL) protocol and controlled by a laptop using custom python scripts.

We performed wind tunnel experiments in an open-jet wind tunnel (WindShape [19], [68]).

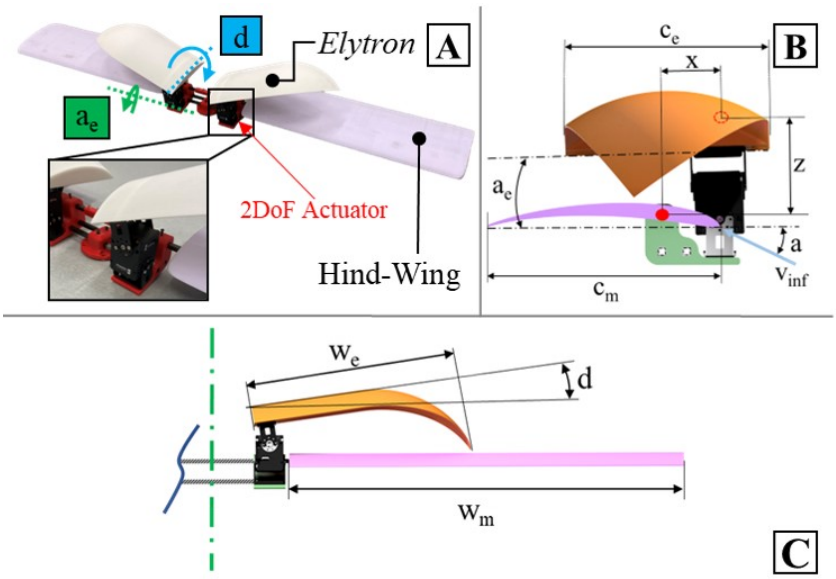

Figure 4.3: The aerodynamic test article. (A) A simplification of the hind-wings, *elytra* wing system to investigate the aerodynamic performance at different angle configurations. The test article is composed of a fixed-wing and *elytra* that are mounted on 2 DoF (Degrees of Freedom) actuators. (B - C) The relative positioning of the *elytra* and the hind-wings in the x and z axis was dictated by the insect geometry and physical geometric limitations e.g. actuator size.

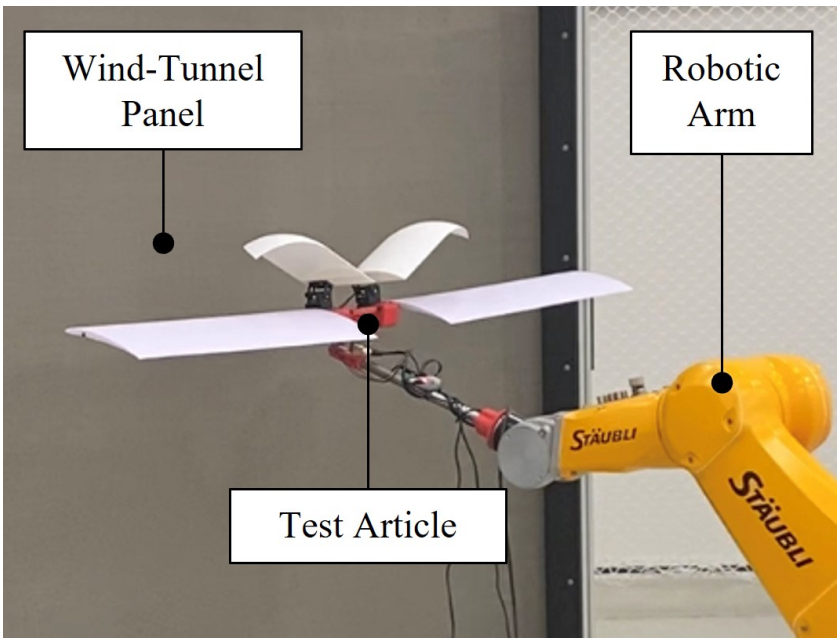

Figure 4.4: Aerodynamics experimental setup. In the figure is depicted the test article with the hind-wings and the *elytra*, the robotic arm used to change the tested angle of attack and the front of the open wind-tunnel section.

The flow speed was measured with a one dimension (1D) flow meter which was used to tune the wind tunnel to mean airspeed of 8 m/s. Turbulence was measured to be less than 2%. The wind tunnel testing cross-section was 1.7 m wide 1.5 m tall for a total test section area of 2.55 m^2. The angle of attack was measured by the robotic arm, while the angle of incidence and the dihedral angle were measured by the position feedback of the servo motors. The uncertainty in angle of attack was estimated to be < 0.2° while in the servo motor angles < 0.5°. The indicated airspeed corresponds to Reynolds numbers (Re) of 95,727 for the hind-wings and 84,465 for the *elytra* as calculated from [94]. The test article was mounted at its center of gravity to an ATI Gamma load-cell. The load-cell was in turn mounted to the end of a STAUBLI TX2-90 robotic arm for automatic positioning of the test samples at the correct attitude (Figure 4.4). For data logging, we used a National Instruments NI-DAQmx 9.5.1. Before each measurement sequence, the load-cell was zeroed at 0m/s airspeed. Then, we set the tunnel to a mean wind speed of 8 m/s. We incremented the angle of attack from -4° to 20° in 2° steps. The angle of incidence was varied between -20° and 20° with a step of 10° and the dihedral was varied between 12° and 27° with a step of 7°. At each step, the loads were measured for 6 seconds at 1000Hz. We used the combined area of the hind-wings and *elytra* (0.22 m^2) to calculate the aerodynamic coefficients. The wind tunnel raw data and the data analysis are provided as supplementary material.

Table 4.1: Experimental constants and variables adjusted from beetles to robots

Environment Constants and Variables	**Symbol**	**Range / Value**
Angle of Attack	a	$-4° \leq a \leq 20°$
Wind-Speed	v_{inf}	8 m/s
Hind-Wings Constants and Variables	**Symbol**	**Range / Value**
Hind-Wing Length	w_m	0.5 m
Hind-Wing Chord	c_m	0.17 m
Hind-Wing Airfoil	af_h	E63
***Elytra* Constants and Variables**	**Symbol**	**Range / Value**
Elytron Wing Length	w_e	0.28 m
Elytron Chord	c_e	0.15 m
Elytron Airfoil	af_e	Cambered Plate
Elytra Hind-Wings Vertical Distance	z	0.05 m
Elytra Hind-Wings Horizontal Distance	x	0.04 m
Elytron Angle of Incidence	a_e	$-20° \leq a_e \leq 20°$
Elytron Dihedral Angle	d	$12° \leq d \leq 27°$

The experiments indicated that there is not one single configuration that is optimal for all angles of attack of the hind-wings with *elytra* system (Figure 4.5 (A, B)). We observed that at a given angle of incidence, at high angles of attack, higher dihedral can perform better in terms of lift-to-drag ratio compared to lower dihedral, while this effect is reversed for lower angles of attack (Figure 4.5 (B)). We also see that the highest efficiency configuration is achieved at 6°

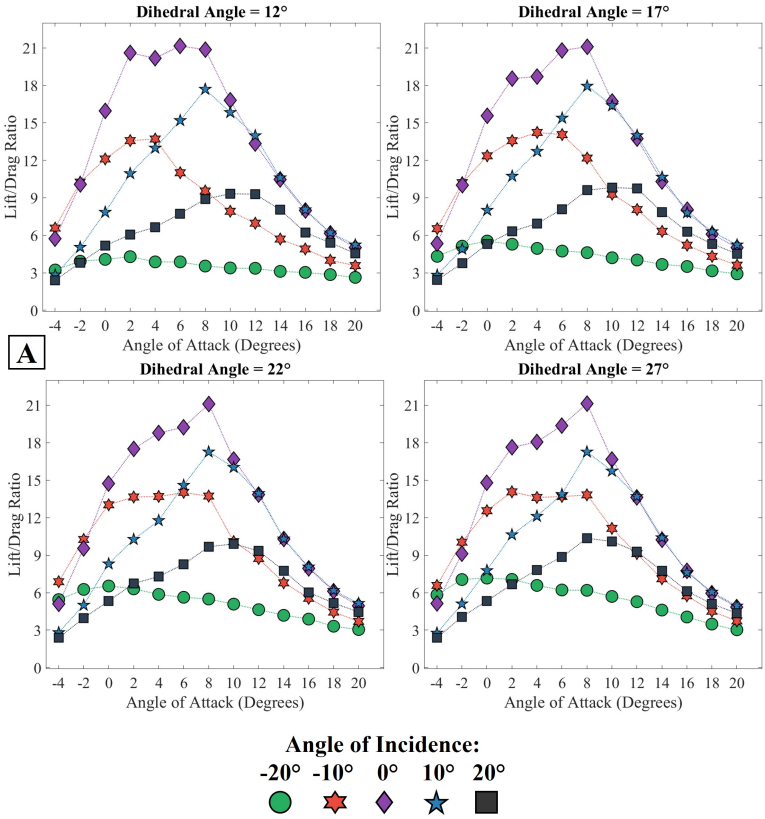

B

Angle of Attack (Degrees)	Dihedral (Degrees)	Angle of Incidence (Degrees)	Efficiency (Dimensionless)
-4	22	-10	6.87
-2	12	-10	10.25
0	12	0	15.97
2	12	0	20.59
4	12	0	20.18
6	12	0	21.15
8	27	0	21.11
10	12	0	16.79
12	17	10	13.98
14	17	10	10.65
16	17	0	8.06
18	17	10	6.28
20	12	10	5.22

Figure 4.5: (A) The angle of incidence and dihedral were varied during the experiments as shown in Table 4.1. In this graph, we plot the angle of attack and the lift-to-drag ratio for each dihedral angle and each angle of incidence. (B) The integrated table presents the most efficient configuration for each angle of attack that was studied in the aerodynamic experiments. With the red rectangle, we highlight the highest efficiency achieved and with the blue rectangle we highlight the lowest efficiency achieved.

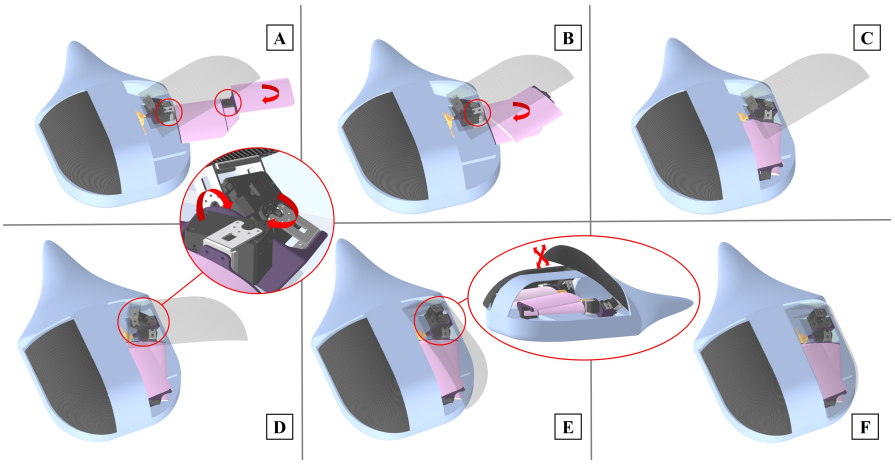

Figure 4.6: Folding and unfolding of the hind-wings - *elytra* system. (A) The outer section of the hind wing starts folding on top of the inner hind wing section by enabling one DoF actuator. (B) In less than 0.2 seconds, the one DoF actuator in the root of the hind wing initiates the folding of the whole wing section on top of the fuselage compartment. (C) Before the completion of the hind-wing folding, the 2 DoF actuators of the *elytron*, operate simultaneously. (D) The *elytron* starts approaching the fuselage. The actuators move with rotations presented in the zoom-in detail. (E) The *elytron* folds on top of the hind wing and thus fully encloses it within the compartment that the concave *elytron* surface and the fuselage create. The red arrows in the perspective view, indicate the direction of the *elytron* motion. (F) Similar to the beetles, the hind wing now is completely enclosed and geometrically isolated from its surroundings and thus ready for ground locomotion [27]. The reverse procedure describes the unfolding of the wing system to its flight configuration.

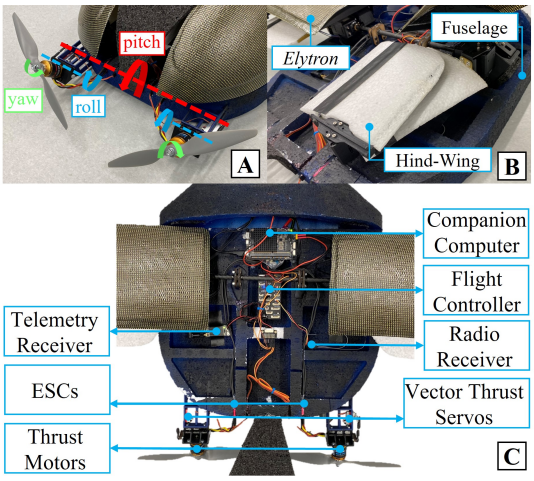

Figure 4.7: (A) The vectored thrust motors control pitch when moving symmetrically, roll when moving asymmetrically, and yaw with differential thrust. (B) Detail of folded hind-wing on top of the fuselage with the *elytra* on extended position. (C) HercuLIS consists of a blended body fuselage manufactured from Expanded Polypropylene (EPP) foam, dual vectored thrust motor propulsion system, an autopilot with data logging, and a companion computer for controlling the hind-wings and *elytra* servos.

angle of attack, with 0° angle of incidence and 12° dihedral angle, while the lowest is achieved for 20° angle of attack, with 10° angle of incidence and 12° dihedral.

We selected the highest efficiency configuration for the hind-wings and *elytra* system to illustrate the performance of the hind-wings and *elytra* both individually and in synergy. For the beetles, it has been shown that one of the *elytra* benefits is delaying stall by interacting with the hind wings [95]. For this configuration of hind-wings and *elytra* at dihedral of 12° and 0°angle of incidence, and as presented in Figure 4.8 we found that the *elytra* not only increase lift over the hind-wing on its own but also delay the stall of the system from 14 ° without *elytra* to 20° with *elytra*.

The data collected as part of this experiment can be used to calculate a hypothetical cruise power required. We estimate the power required of a fixed-wing UAV given by [96],

$$P_{CRUISE} = D_{CRUISE} * V_{CRUISE} \tag{4.1}$$

where D_{CRUISE} and V_{CRUISE} are the total drag and velocity in cruise flight, respectively. Given a cruise angle of attack of 6 degrees, we found that with the elytra the power required is 2.65 W, while without it is 0.75 W (Figure 4.8). This is an estimated 2.5 times increase in power requirement, however, state-of-the-art caged structures would have a power required of 56.95 W (hind-wing drag plus caged structure drag in Figure 4.8) which is around 20 times more than our solution.

The hind-wings and *elytra* system resemble a biplane configured aircraft, so we modeled the aerodynamics of test article with a standard biplane model. A good match between the biplane model and our experimental results would indicate that there is an existing aerodynamic model that could be applied to hind-wings and *elytra* systems rather than necessitate the development of a new one. We used the model presented by Jones et al. [97] where lift and drag coefficients are respectively modeled as,

$$C_{L_{total}} = \frac{A_{HW} C_{L_{HW}} + A_E C_{L_E}}{A_{HW} + A_E} \tag{4.2}$$

$$C_{D_{total}} = \frac{A_{HW} C_{D_{HW}} + A_E C_{D_E}}{A_{HW} + A_E} \tag{4.3}$$

where A_{HW} is the aerodynamic reference area of the hind-wings, A_E is the reference area of the *elytra*, $C_{L_{HW}}$ and $C_{D_{HW}}$ correspond to the lift and drag coefficients of the hind-wings and C_{L_E} and C_{D_E}correspond to the lift and drag coefficients of the *elytra*.

The experimental results show good agreement with the biplane model (Purple line in Figure 4.8 (A). The root mean squared error of the theoretical model for the lift coefficients is 0.0013 and for the drag coefficients is 0.0005. In addition, Figure 4.8 (A) also presents measured

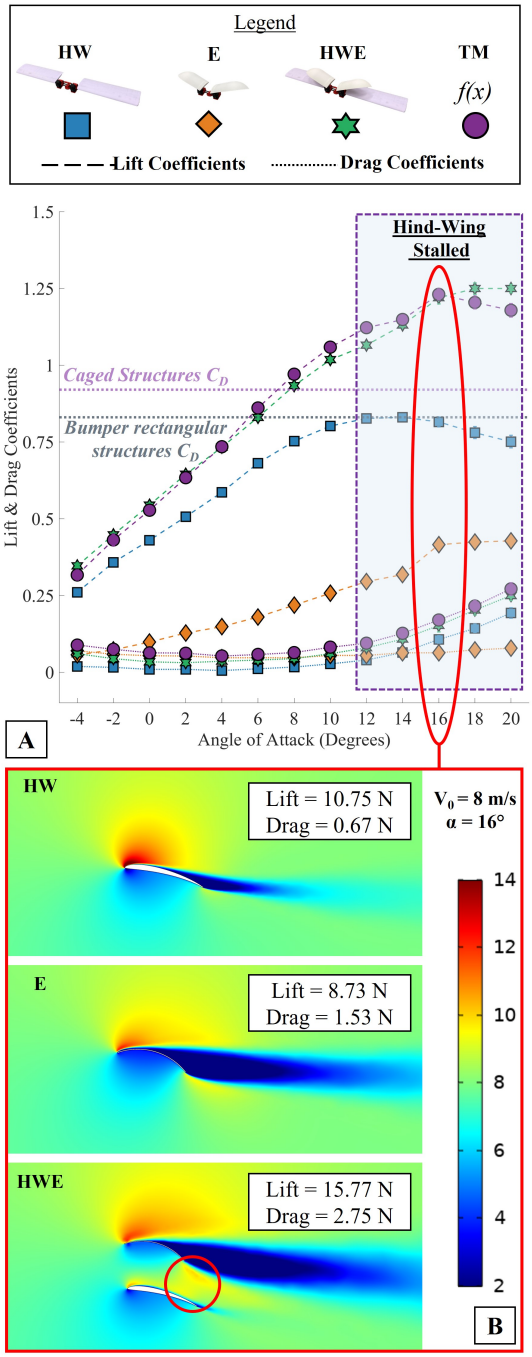

Figure 4.8: (A) Experimental results and the theoretical model prediction as a graph of the aerodynamic coefficients and the angle of attack. Wind-tunnel experiments performed show the added lift that *elytra* generate. The shaded area displays the hind-wings post-stall domain. In the legend, HW for Hind-Wings, E for *Elytra*, HWE for Hind-Wings *Elytra*, and TM for the Theoretical Model. The horizontal lines represent the drag coefficients of existing protective solutions [28, 29]. (B) CFD experiments for the hind-wing, *elytron* and the hind-wing - *elytron* in the post-stall angle of attack of 16°. The red circle indicates the region where the airflow over the hind wing gets re-energized.

and estimated drag coefficients of existing protective solutions. To further investigate the aerodynamics between the hind wing and the *elytra* system and possible interactions between the two wings in the post-stall region, we performed Computation Fluid Dynamic (CFD) experiments using COMSOL 5.5. We applied a Reynolds-averaged Navier–Stokes k-ϵ model in the 2D domain of the hind-wing, the *elytron*, and the hind-wing - *elytron* [98]. The geometrical model was meshed into approximately 12000 polygons. The inlet flow speed was set at 8 m/s. We varied the angle of attack between 12, 16, and 20 degrees. Figure 4.8 shows the results for the experiment at 16 degrees. At all the measured angles, we observed that there is a reduction of the low-velocity area of the hind wing in the trailing edge region, an increase in the velocity region, and a re-energization of the flow between the trailing edge of the hind wing and the trailing edge of the *elytron* (red circle in Figure 4.8). The proposed model from [97] assumes that interactions between the wings are negligible. Thus, we hypothesize that the observed interactions between the hind wing and the *elytron* in the CFD results justify the deviations from the proposed model that appear to be sovereign in the post-stall region.

To understand the relative importance of the experimental variables of the angle of attack, angle of incidence, and dihedral affects overall system performance, we study their individual effect in the lift and drag coefficients using a linear regression model. With this analysis, we can highlight the parameter that has the most significant impact on the flight efficiency, which in turn will inform future designers of such systems on the importance of each parameter. We performed two linear regression fits on the experimental results to study the linear effects of the variables. One regression was performed between the three angles and the lift coefficient and the other regression was performed between the same angles and the drag coefficient. Assuming that statistical significance exist with pValue less than 0.05, the first regression results (Table 4.2), displayed a statistically significant effect of all of the angles on the lift coefficient. The most significant factor is the angle of attack, followed by the angle of incidence, and finally, the dihedral. The second linear regression results (Table 4.3), display a significant effect of both angle of attack and angle of incidence, but not the dihedral. The order of importance for the drag coefficient is first the angle of attack, then the angle of incidence.

4.3 Design, fabrication and experimentation with HercuLIS

In order to illustrate the value of the proposed protective concept, we fabricated the drone demonstrator, HercuLIS. The drone has the ability to fold its wings rapidly (less than half a second) and thus, during the approach to a dangerous environment, encapsulate the folding wings beneath the *elytra* to protect them. When locomoting on the ground, the hind wings are folded and protected by the *elytra*. When the vehicle is clear of obstacles and on the appropriate ground for take-off, it unfolds the wings and is ready to fly.

The hind wings were sized to fit underneath the *elytra* and have a folding ratio (planform area of the wing closed to wing open) of about 39%. The wing length of the hind wing was reduced to 0.35m to allow full encapsulation with the current folding method. The length of

Figure 4.9: HercuLIS in field tests.

the *elytron* was increased from 0.28m to 0.33m so that the surface area of the *elytra* that was in the airflow is the same as the amount of surface area of the *elytra* that was in the wind-tunnel. The concave compartment that the elliptical shape of the *elytra* and the fuselage forms is used to completely encapsulate the folding hind-wings (Figure 4.6). The geometry of the *elytra* was derived as a geometric abstraction of the beetle's *elytra*. We scaled by a factor of ten the chord and length dimension of the animal's *elytra* to the size range of a MAV [45, 26]. The shape of the curve was derived as a section of an ellipsoid defined by a linear and a circular part. The 3D model of the *elytron* is shared as supplementary material. The *elytra* are mounted on two, 2 DoF servomotors that reorient their position to cover the folded hind-wings on the back of the fuselage. HercuLIS electronic components are labeled in Figure 4.7. The communication between the components is achieved through a ROS node in the ROS network that receives the user inputs and commands the *elytra* and the hind-wings servos to fold or unfold.

Table 4.2: Linear regression for the lift coefficients

Coefficients	**Estimate**	**pValue**
Angle of Attack	0.031	**4.157e-103**
Dihedral	0.002	**0.012**
Angle of Incidence	-0.003	**2.717e-15**

Table 4.3: Linear regression for the drag coefficients

Coefficients	**Estimate**	**pValue**
Angle of Attack	0.007	**4.486e-50**
Dihedral	3.456e-11	0.350
Angle of Incidence	-0.001	**2.149e-19**

For the fabrication of the main wings of the demonstrator, we used EPP foam due to the ease of manufacturability and robustness. The two 2 DoF actuators were mounted in such an orientation that upon actuation the *elytra* were completely encapsulating the hind-wings (Red arrows in Figure 4.6). The desired angle of incidence was achieved with a fixed 3D printed interface fabricated with the material and methods used for the test article, while the folding of the *elytra* and the regulation of the dihedral angle, was achieved with two XC-430-W250-T servos. For reducing the structural weight of the demonstrator, we fabricated the *elytra* from hybrid carbon Kevlar fabric with a 3mm honeycomb core for added stiffness. For the fuselage of the demonstrator, we used EPP foam that was machined with a Modela Pro II MDX-540S 3D milling machine in six parts that were attached together with UHU POR glue. For the propulsion system, two commercially available electric motors, AXI 2217/12 GOLD LINE V2 were used with 9x4.5 APC propellers and a 60 A electronic speed controller from Hobbywing. The vector thrust components were fabricated from plywood and 3D-printed ABS components. The motors' thrust vector was adjusted in pitch by two X08H V5.0 digital

high-voltage servos from KST. The pusher configuration was chosen in order to avoid the flow interaction of the wings and the propeller. We used a Futaba R2000SBM receiver and a Futaba 12K transmitter for the manual control of the drone. For powering the system we used a 3-cell Hacker lithium polymer battery pack with a 3800 mAh capacity. An overview of the electrical setup can be found in Figure 4.7 (C). In the HercuLIS vehicle, the folding and unfolding were manually controlled. The pilot deployed or retracted the wings depending on the mode of locomotion. In future iterations of the vehicle the folding, unfolding, and in-flight wing configuration will be controlled by the autopilot. The goal of the demonstrator was to show that despite the mechanical complexity, a folding hind-wing *elytra* system can be integrated into a working multimodal platform while displaying basic operational capabilities. The platform would need further optimization such as weight and volume reduction and aerodynamic optimization such that the blended fuselage design does not interfere with the aerodynamics of the hind-wing *elytra*. Field experiments of HercuLIS were conducted with the goal of demonstrating the dual-wing protective system in ground locomotion with the hind-wings folded below the *elytra* for protection and hind-wings and *elytra* deployed for flight (Figure 4.9). The two flight test flights were conducted in calm wind conditions of approximately 1.5 m/s. The vehicle was hand launched as there was no adequate runway to take off, and it performed given manual inputs from the pilot. The experiments showed that the vehicle is capable of flying and locomoting on the ground by means of four foam wheels. The propellers produce the necessary thrust for forward motion, while the differential thrust from the propellers allows the vehicle to steer. Although in the current implementation, the vehicle's clearance to the ground is 10 cm, it could successfully locomote over uneven terrain with 5-7 cm high grass.

4.4 Conclusion

In this chapter, we described a novel insect-inspired approach for protecting winged drones in challenging environments. Similar to beetles, we used a secondary set of wings akin to *elytra*, that, when swept back, encapsulate a set of hind-wings that are folded into the fuselage. We validated the feasibility of the proposed solution in a flying platform named HercuLIS. During the field experiments, we validated the capabilities of the platform for folding its hind-wings and *elytra* during on uneven and unstructured ground, and thus protecting the hind-wings surfaces and actuators from external damage, namely spicular surfaces or ground collisions. The experiments provided insights on the *elytra* lift and drag generation, and in the future, the system's geometry can be optimized to achieve better performance.

The solution proposed here could fit as a design choice for vehicles with different mission profiles. The current work and our previous work on the hind-wings and *elytra* systems validated the benefits of such systems compared to existing solutions [60]. In both studies, we found that the biplane model provides an adequate approximation for the aerodynamic forces in the regions of Re 68000 and Re 90000 [60]. Multi-modal locomotion drones could benefit when using *elytra* to protect their main wings when locomoting on challenging terrain.

Morphing wing drones could benefit by using *elytra* wings to protect their fragile wing surfaces and morphing mechanisms. Further work can explore integrating different *elytra* shapes to maximize performance or hind-wings with higher folding ratios. Moreover, a third degree of freedom in the *elytra* actuation could increase the possible geometric adaptations of the *elytra* during flight and might be a sustainable way of achieving greater performance in a wider flight regime. Moreover, different elytra configurations could be explored for high-speed forward flight, where no additional lift is needed and the drone is not in a stall condition. Then, for example, the elytra could retract on the back of the plane and thus reduce drag, increasing flight efficiency and operational time. In nature, beetles use their *elytra* to achieve multiple goals beyond collision resilience. For example, camouflage [99], thermoregulation [92], humidity control [92], control through passive flight stability [100], and radiation control [101] according to the physical or chemical properties of the *elytra*. We also believe that with structural and chemical adaptation, it is possible to integrate further capabilities in the *elytra* to enable future robots to perform multiple other functionalities that are similar to what the *Coleoptera* have utilized to survive for millions of years in challenging and hazardous environments.

4.5 Acknowledgements

The authors are grateful for the engineering help provided by Simon Honigmann, Nathan Müller, Olexandr Gudozhnik, and Angelika Romanou.

5 Insect Inspired Self-Righting for Fixed-Wing Drones

It is evident now that winged drones can be required to perform in different types of environments. While in the air or on the ground thought, an overturn can compromise an operation. Micro Aerial Vehicles (MAVs) are being used in a wide range of applications such as surveillance, reconnaissance, inspection and search and rescue. However, due to their small size and complex mission profile, they are prone to tipping over, jeopardizing their operation. Self-righting is an open challenge for fixed-wing drones since existing research focuses on terrestrial and multicopter flying robots with solutions that increase drag and structural weight. Until now, solutions for winged drones remained largely unexplored. Inspired by beetles, a robust and elegant solution is proposed. In the previous chapter, it was presented that when retrofitting a drone with elytra, they can be used to protect it during ground locomotion. In this work, a fixed-wing drone is retrofitted with elytra to assist it in self-righting during an overturn incident. It is shown that artificial elytra provide additional lift during flight to mitigate their structural weight while also being able to self-right the MAV when it has been flipped over. Simulations were performed along with dynamic and aerodynamic experiments to validate our results.

- The work presented in this chapter is adapted from [60]:
  C. Vourtsis, V. C. Rochel, F. R. Serrano, W. Stewart and D. Floreano, "Insect Inspired Self-Righting for Fixed-Wing Drones," in *IEEE Robotics and Automation Letters*, vol. 6, no. 4, pp. 6805-6812, Oct. 2021.

- Supportive video material can be found at:
  https://www.youtube.com/watch?v=15DdVN97A38&ab_channel=EPFLLIS

- Supportive material can be found at:
  https://doi.org/10.21227/vvjg-yw40

5.1 Introduction

Over the past few years, drones have displayed great potential for operating in difficult environments across a great span of applications and mission profiles [41]. These include being deployed in arduous weather conditions, confined spaces, or areas cluttered with debris. During these missions drones are prone to being tipped over. To takeoff again and continue their mission, robots must be able to self-right. To date, studies on self-righting robots have been limited to terrestrial robots and multi-rotor drones, but have not considered winged aircraft. In this work we present the first self-righting winged drone.

We accomplished this by taking inspiration from the *coleoptera* order, commonly known as beetles. Beetles have shown a remarkable ability to self-right after falling to the ground by using an outer set of hardened wings called elytra, (singular: elytron) displayed in Figure 5.1 (A)[102, 103]. These elytra serve to provide the insect with self-righting capacity as well as producing auxiliary lift during flight. In this way, the added weight and complexity of the second set of wings is offset by the additional lift they produces [45]. Similarly, we incorporated a set of artificial elytra made from a hybrid carbon fiber and Kevlar composite fabric onto a fixed-wing MAV (Figure 5.1 (B)). The elytra are attached through two sets of two servos allowing them to be swept back and pitched 180° forward. By first sweeping the wings backward and then pitching them forward, the aircraft can flip itself over.

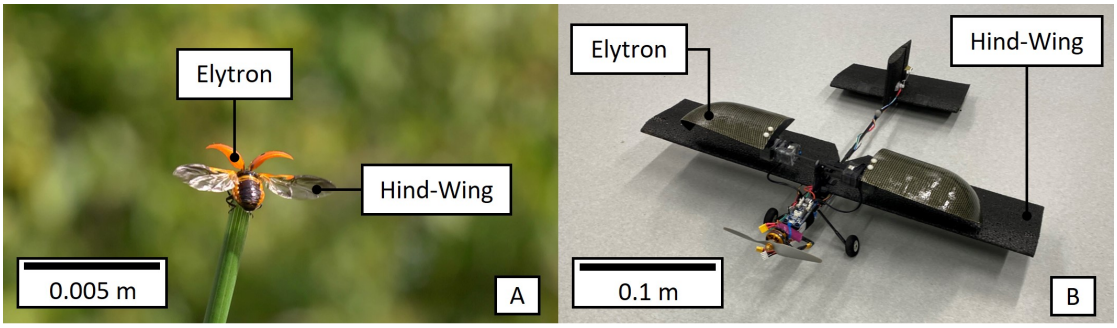

Figure 5.1: (A) Ladybug (*Coccinellidae*) with spread wings (Adapted from [30]). Ladybugs, like all flying beetles, have two sets of wings: the hind wings and the elytra. (B) Ely has a set of fixed wings akin to the beetle's hind wings and a set of artificial elytra.

We characterized the performance of the artificial elytra both in terms of self-righting and aerodynamics. Our experiments showed that there is no trade-off in performance between self-righting and aerodynamic efficiency. Namely, larger span elytra produce faster self-righting than shorter span elytra, without an appreciable difference in aerodynamic performance. Further, we demonstrate that a simple biplane model is adequate to predict aerodynamic performance in cruise conditions.

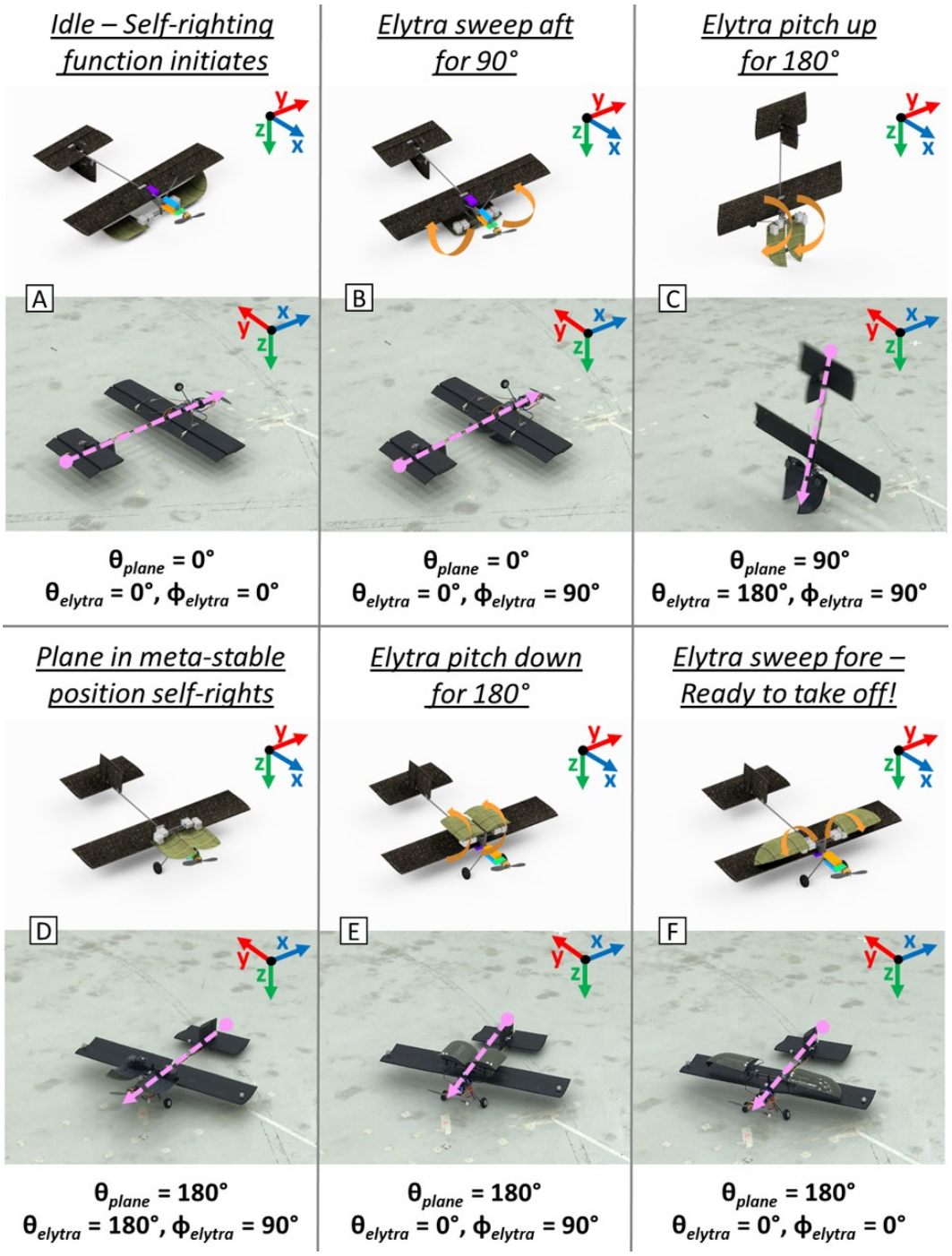

Figure 5.2: (A) The self-righting maneuver is triggered as the drone is tipped over. (B), The elytra sweep 90° around their vertical axis. (ϕ_{elytra} from 0° to 90°). (C) Next, the elytra pitch for 180° (θ_{elytra} from 0° to 180°) to rotate the plane around its lateral axis (θ_{plane} from 0° to 180°). (D) The plane is now uprighted. (E) After the uprighting (θ_{plane}=180°), the elytra move back to their flight position (θ_{elytra}=0° ϕ_{elytra}=0°). (F) The plane is ready to take off again with the elytra extended in their initial configuration.

5.2 Related work

Self-righting techniques have been extensively investigated both on terrestrial and flying robots. In terrestrial robots, a common strategy is to integrate a separate mechanism that assists with the self-righting. These mechanisms are usually elongated protrusions that use actuators to generate the torque required to self-right the robot[104, 105, 106, 107, 108]. For example, Casarez and Fearing used a carbon fiber beam to self-right their VelociRoACH robot [109]. In addition to self-righting, Zhang et al. added a mass to their beam and were able to re-orient a jumping robot [107]. However, these protrusions and actuators add mechanical complexity and weight. Legged robots have avoided additional weight and complexity by utilizing controllers that allow them to use their legs for self-righting[110, 111]. Some terrestrial robots have used reconfigurable treads or reconfigurable bodies to enable self-righting [112, 113]. Despite their effectiveness, these solutions would require the integration of complex mechanical systems into flying robots, which would increase design and manufacturing complexity as well as energy consumption. Another work explored the principles of cockroaches and used actuated shell structures resembling cockroach wings for self-righting [114, 108]. Despite its effectiveness for self-righting, this strategy also has limitations. The shell configuration in that work would not perform in flight as the chosen self-righting mechanism is not able to extend the wings and generate lift.

Self-righting in flying robots has been limited to integration in multi-copter vehicles. Engineers have utilized multi-actuated protrusions that generate torque to reorient drones into their upright position similar to the ones used on terrestrial robots[115, 116, 117]. These suffer from performance reduction due to aerodynamic deficiencies and added weight. Prevention of the tipping over of multi-copters was also achieved by combining a caged multi-copter with a gimbal system. After the robot has tipped beyond a given angle, the gimbal assists in reorientation and self-righting [81]. Other researchers optimized the design of the cage, resulting in an ogive shape that allowed passive self-righting when tipped over [118, 119]. However, integrating cages in multi-copters has been found to significantly reduce aerodynamic performance and increase structural weight [28].

Cages, legs, treads, reconfigurable bodies or protrusions would allow fixed-wing drones to self-right, although by substantially decreasing aerodynamic performance, adding weight or increasing mechanical complexity. Our method, inspired from beetles, exploits recent advances in materials and electronics, to allow the integration of an additional set of wings akin to elytra for self-righting while mitigating the performance cost of the added mechanism by generating lift during forward flight.

5.3 The self-righting operating principle

In this section, we describe the design principles inspired from the beetles as well as the self-righting performance of a fixed-wing vehicle retrofitted with elytra. Some beetle species utilise

their elytra to self-right. In particular, ladybugs, beetles of the family *Coccinellidae*, position their elytra on the ground to stabilize their bodies and self-right using the force generated by their legs or their hind-wings to pitch over their heads [102]. Similar to the animal, we use the drone's elytra to stabilize the fuselage but instead of providing torque using legs, we use actuators connected to the elytra that enable the drone to pitch itself into an unstable position and tip over its nose as presented in Figure 5.2. The artificial elytra are installed on a conventional fixed-wing platform code-named Ely. The length of the elytra play a critical role in the self-righting maneuver, as the torque generated on the ground by the elytra, is directly associated with the distance of the applied force.

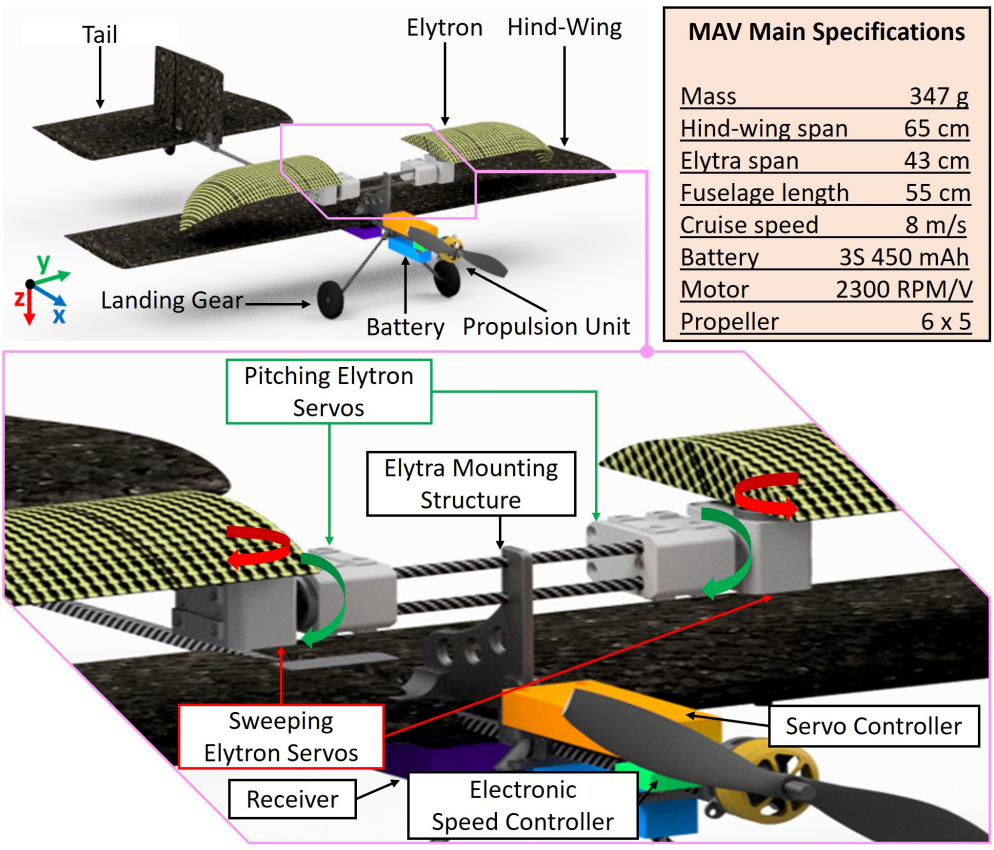

MAV Main Specifications	
Mass	347 g
Hind-wing span	65 cm
Elytra span	43 cm
Fuselage length	55 cm
Cruise speed	8 m/s
Battery	3S 450 mAh
Motor	2300 RPM/V
Propeller	6 x 5

Figure 5.3: The winged drone, code-named Ely, with detail of the self-righting mechanism composed of elytra that rotate in pitch and sweep through a pair of servos controlled by an on-board micro-controller. Specifications are summarized in the inset table.

Beetles feature three degrees of freedom (DOF) in each wing to facilitate flapping and folding in addition to self-righting [24, 102]. Because this study is focused only on self-righting and not on flapping or folding, we use only the required two out of the three DOFs, which keeps weight and structural complexity low. When the self-righting maneuver is triggered (Figure 5.2 (A)), each elytron is swept (DOF 1) 90° around its vertical axis (ϕ_{elytra} from 0° to 90°) by the sweeping servomotor (Figure 5.2 (B)). Next, the pitching servomotor pitches (DOF 2) the

elytron 180° (θ_{elytra} from 0° to 180°) to rotate the plane about its lateral axis (θ_{plane} from 0° to 180°) (Figure 5.2 (C)). After the uprighting (θ_{plane}=180°), the elytra move back to their flight position (θ_{elytra}=0°, ϕ_{elytra}=0°) (Figure 5.2 (D - E)). After the self-righting maneuver, the drone is ready to take off again (Figure 5.2 (F)).

5.4 The self-righting MAV

Ely is a conventional fixed-wing MAV with a single electric motor in tractor configuration (Figure 5.3). The hind-wings were made from Expanded Poly Propylene (EPP); a resilient and highly flexible foam material. The elytra were 3D printed with Acrylonitrile Butadiene Styrene (ABS) plastic and were re-enforced with carbon-Kevlar composite fabric and epoxy adhesive for added resilience. The fuselage was fabricated from a carbon fiber rectangular beam and the hind-wings and elytra were attached with 3D printed ABS mounts. We used a low Reynolds number airfoil for Ely's hind-wings, namely Eppler E168. The elytron geometry was modeled with a simplified ogive shell representation where the main dimensions were obtained by scaling up those of the insect. For the hind-wings and the elytra, the spans and chords were respectively scaled so as to correspond to standard Micro Aerial Vehicle wing proportions [26]. The vertical separation distance between the hind-wings and elytra was optimised in computer-aided design (CAD) for reducing structural weight. On a beetle, the elytra are positioned forward of the hind-wings (positive stagger), as both pairs of wings require space for flapping. On Ely, the thrust is generated by the propeller and the wings are fixed; therefore, for simplicity, the hind-wings and elytra are aligned at the quarter chord (aerodynamic center).

5.5 Self-righting elytra - mechanical characterization

5.5.1 Simulation of the self-righting

To validate the self-righting principle, and characterize design parameters such as the amplitude of the sweeping and pitching motions, a simulation of the self-righting maneuver was developed. The simulator was built using Simscape Multibody in a Simulink environment [120]. Simscape simulates interactions between multiple bodies for 3D mechanical systems. The Simscape model includes two solid bodies for the elytra, two for the sweeping servos, one for the propeller and one body for the rest of the plane (including the pitching servos). Finally, a spatial contact force block connects each solid block of the aircraft to the ground to simulate their interaction. In our model (Figure 5.4), each elytron is connected to the sweeping servo by the yaw revolute joint, which models the sweeping motion. That servo is connected to the aircraft solid body by the pitch revolute joint which models the pitching of the elytra. Since the propeller is in contact with the ground while self-righting and is free to rotate, the propeller solid body is connected to the aircraft solid body by the propeller revolute joint.

In each solid block (except the ground which is fixed), the mass, the position of the Center of

Gravity (COG), and the moments and products of inertia are specified. These values were taken from the CAD model of Ely. Each revolute joint requires a torque, a damping factor and a spring stiffness factor. These factors characterize the behaviour of the revolute joint and they are set to match their respective components on Ely. The simulation begins with the elytra already swept back, so torque values were only applied to the revolute joints responsible for pitching the elytra on the ground. This joint is additionally bounded with an upper and lower limit on rotation so that the elytra do not exceed 180° of rotation during self-righting. Similarly to the revolute joints, there are factors to characterize the spatial contact force between the aircraft and the ground. The static and dynamic friction coefficients were measured on Ely. Each parameter of the spatial contact force and revolute joint blocks are given in the Supplementary Material - Supplementary_Table.

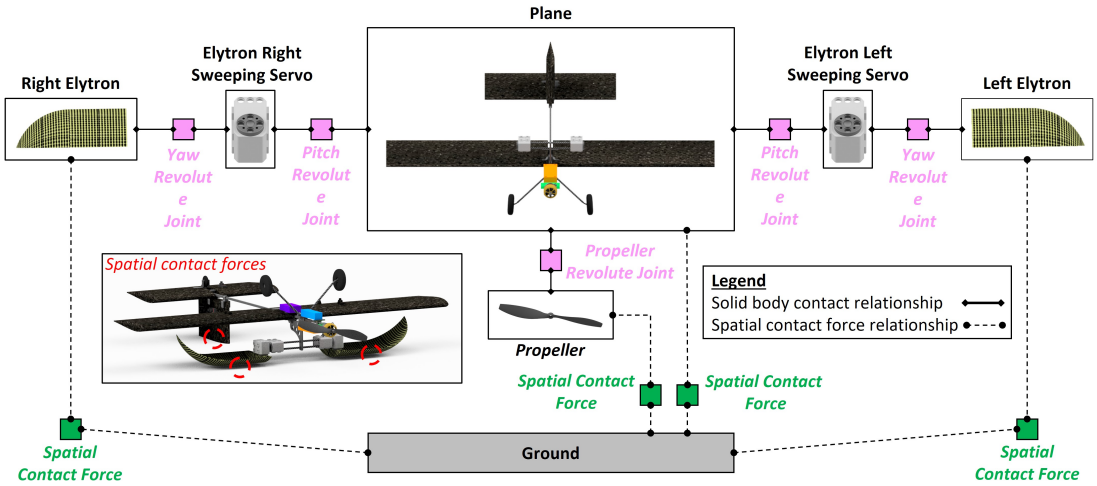

Figure 5.4: The simplified Simulink - Simscape model of Ely highlights the main blocks (solid body, 1 DOF revolute joint, spatial contact force) and their relationships.

The self-righting simulation assumes that the solid bodies such as the elytra and fuselage are perfectly rigid, and hence neglects aerodynamic effects and deformations during the self-righting maneuver. Two different torques (0.31 and 0.39 Nm) and three different elytron lengths (11, 14, and 17 cm) were simulated. The simulations showed that for the elytron measuring 11 cm, the aircraft was not able to self-right, regardless of the torque (Figure 5.5 (B)). The simulations of the plane equipped with 14 cm elytra was capable of self-righting only when the highest torque was applied. Finally, the simulations of 17 cm long elytra were successful at self-righting no matter the torque. These simulations indicate that larger elytron lengths have better self-righting performance. The simulations were also used to predict the time required for the robot to self-right. They indicated that when successful, the vehicle could right itself in less than a second, but that there was some variation with elytron length. That is, longer elytra will self-right the vehicle faster than shorter elytra.

To have a better understanding of why longer elytra are more successful at self-righting, we

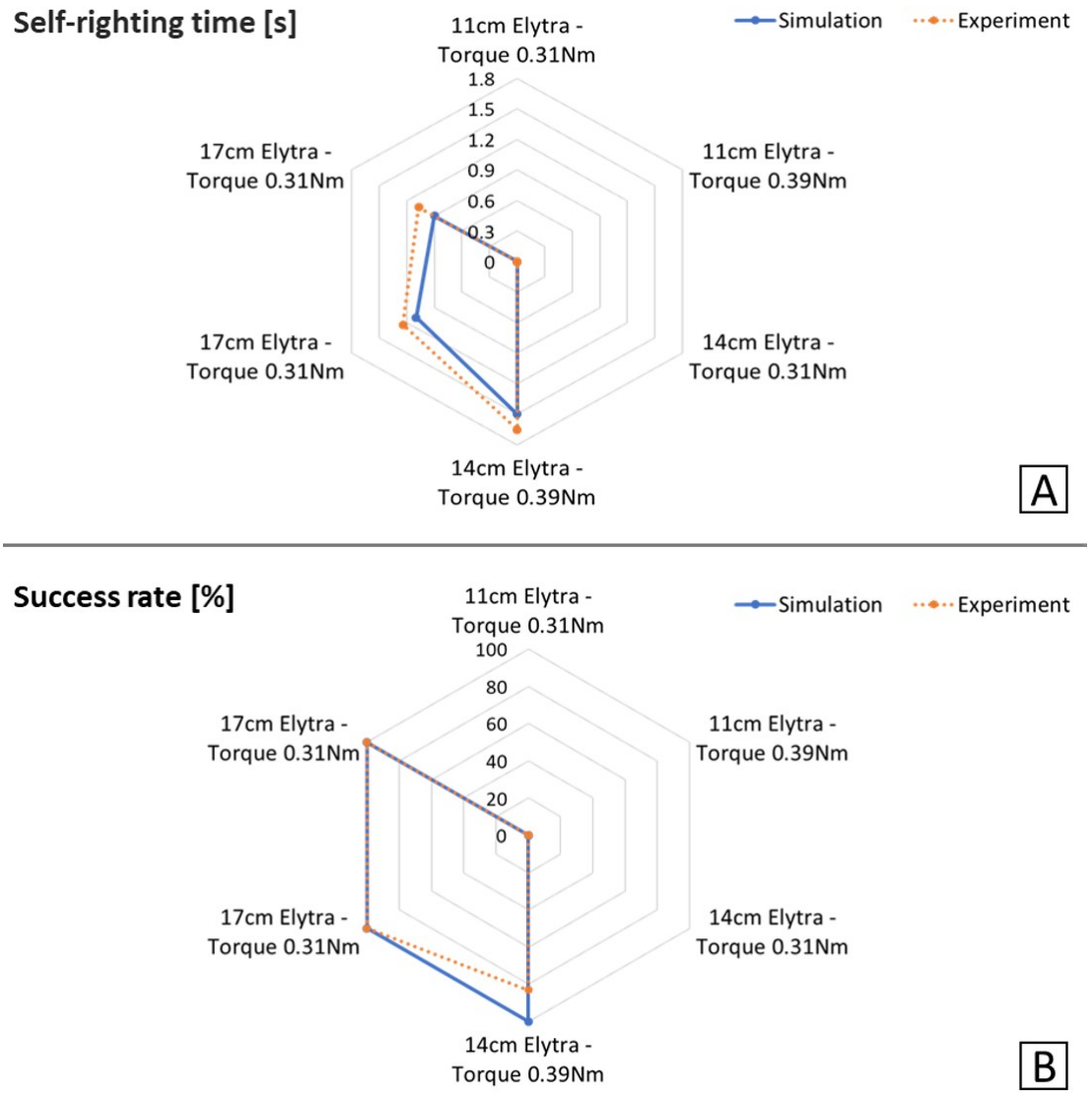

Figure 5.5: (A) Simulated and experimentally measure self-righting time. (B) Simulated and experimentally measure self-righting success.

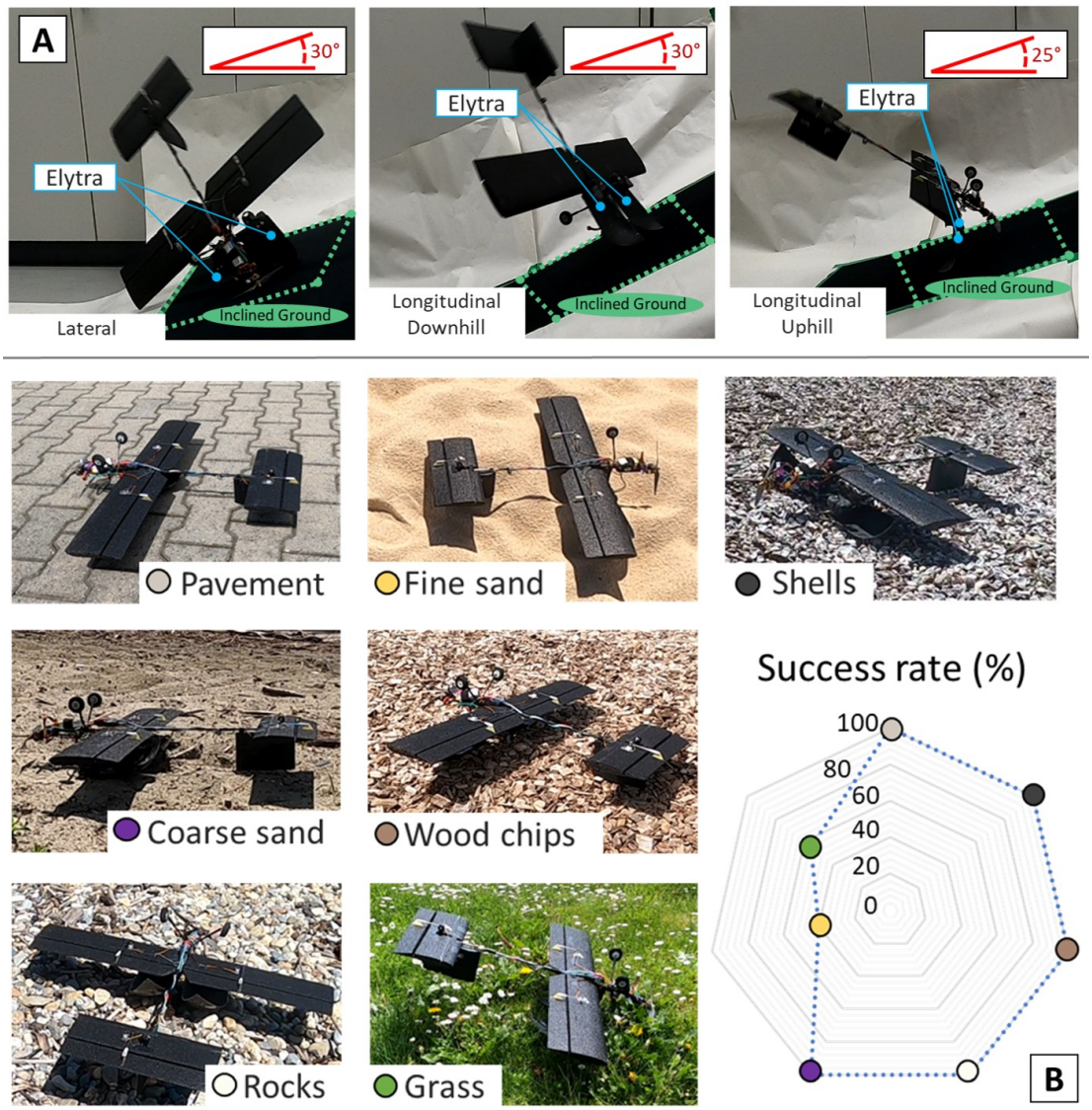

Figure 5.6: (A) Experimental robustness validation of the mechanism in inclined terrain of lateral vehicle position of 30° to −30°, longitudinal downhill of 0° to 30° and longitudinal uphill of 0° to 25°. (B) Experimental robustness validation of the mechanism in seven types of uneven terrain.The decrease in self-righting success rate on sand and grass results from the loss of grip between the surface of the elytra and the surface of the ground due to the lower friction coefficients of these surfaces.

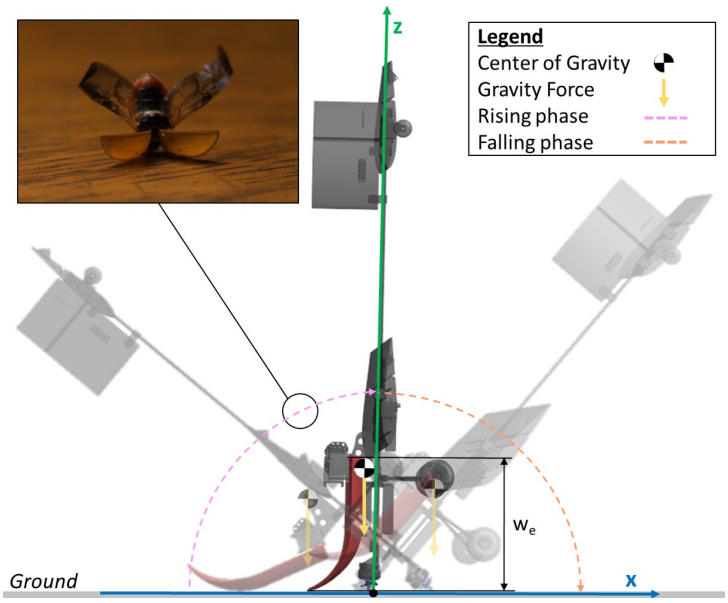

Figure 5.7: Specific Elytron length that pushes on the ground during the entire rising phase and completes its pitching revolution (θ_{elytra}=180°) at the moment the plane enters in the falling phase ((θ_{plane}=90°)). The specific elytron length corresponds to the distance between the nose of the aircraft and the point of rotation of the elytron. Insect picture adapted from [31].

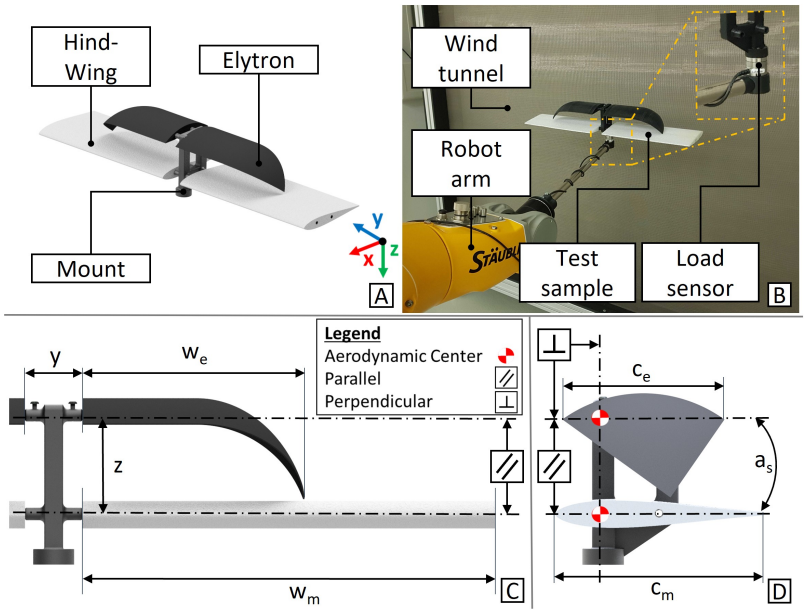

Figure 5.8: (A) Isometric view of the test sample. (B) Experimental setup composed of the aerodynamic test article, Stäubli robot arm, WindShape wind tunnel and ATI Nano25 F/T Sensor. The test article is composed of a mount, hind-wings and elytra of 17 cm wingspan. (C) Front view of the test article (D) Side view of the test article.

split the self-righting maneuver into two phases. The rising phase takes place when θ_{plane} is between 0° to 90° (Figure 5.2 from (B) to (C)) and the falling phase happens from 90° to 180° (Figure 5.2 from (C) to (D)). If the COG passes through 90° (Figure 5.2 (C)), then the force of gravity will cause the plane to fall. Once the elytra have completed their 180° pitch rotation, they cannot contribute to rotating the plane anymore. If the elytra are long enough that the COG has reached 90° before the elytra have completed their 180° rotation, then the plane is guaranteed to transition to the falling phase. Therefore, with elytra length at or beyond the specific elytron length (Figure 5.7), the only factor determining if the plane can self-right is whether there is enough torque to lift the COG up to 90° or not. In our case, the simulations of the 17 cm elytra correspond to this scenario, as the specific elytron length of Ely is 16 cm. Conversely, elytra shorter than the specific elytron length will finish their pitching revolution within the rising phase. This will result in one of two different scenarios. The first scenario is if the torque is high enough that when the elytra reach 180°, the plane has enough momentum to reach the falling phase. Consequently, the first scenario implies that the self-righting maneuver is successful. This corresponds to the simulations of 14 cm elytra and a torque of 0.39 Nm. The second scenario is if the torque is not high enough to generate enough momentum to carry the plane to the falling phase, resulting in an unsuccessful self-righting maneuver. This also corresponds to the case of 14 cm elytra, but this time at a torque of 0.31 Nm.

5.5.2 Experimental validation of self-righting simulation

To validate the results of the simulation, experiments were conducted which consisted of the airplane attempting the self-righting maneuver for each of the configurations simulated, namely, three different elytron lengths (11, 14, 17 cm) and two different torques (0.31 and 0.39 Nm). For each configuration (Elytron length - torque), the experiments were repeated four times. The experiments took place in an Optitrack motion capture hall. Five tracking markers were glued to specific locations (Figure 5.9) on the plane. In the motion capture system's software, these markers comprised a rigid body, whose motion was recorded during the self-righting maneuver.

The self-righting success rates and times in simulations and experiments are shown in Figure 5.5 (A), (B). The results of the experiments were found by computing the mean of the trials for each configuration. The experiments showed that when the plane is equipped with short elytra (measuring 11 cm in span), it cannot self-right (0 % success) no matter the torque. This matches the results from the simulations. The medium elytra (14 cm) were also not able to self-right when using the lowest tested torque and were 83% successful with higher torque (0.39 Nm), closely matching the simulation which predicted 100% success for this case. Finally, the elytra measuring 17 cm were 100% successful regardless of the torque, which also matched the simulation results. In Figure 5.5 (A), for the same elytron length and torque, the simulation shows a maximum of 10% difference in self-righting time compared with the experiments. This indicates good agreement between the simulation and physical vehicle.

These experiments have characterized the self-righting performance on flat and even terrain. However, in many applications, the robot will be required to self-right on more rugged terrain. We therefore conducted a validation of the self-righting mechanism on seven different terrain as well as inclined ground (Figure 5.6 (A) and (B)). For this experiment, the 17 cm elytra were used with 0.31 Nm torque. For each ground type and inclination, the self-righting maneuver was conducted five times. The inclinations tested were 10°, 20°, and 30°. Above 30°, the vehicle could no longer self-right at all because the vehicle would slide down the inclination. For each inclination angle, we tested three different vehicle orientations, longitudinal uphill, longitudinal downhill, and lateral. With only one exception, we found that the vehicle self-rights with a 100% success rate for each tested inclination angle in all headings. The exception was longitudinal uphill, which was not able to self-right at 30°, so for this case we also tested 25°, at which inclination it achieved a 100% success rate. The mechanism was also tested on flat ground, but with varying terrain types. In these tests, the mechanism displayed a 100% self-righting success in five out of the seven tested terrains and thus enabling self-righting for vehicles with versatile range of operational environments. The two terrains which did not have a 100% success rate were in grass and fine sand.

5.6 Self-righting elytra - aerodynamic characterization

An aerodynamic test article was built to investigate the aerodynamic properties of the proposed self-righting mechanism (Figure 5.8), namely the lift and drag coefficients as well as the lift-to-drag ratios of the dual-wing system as compared with a mono-wing system. The test article consists of a central wing mount with bonded hind-wings and slots for swapping elytra in and out (Figure 5.8(A)). Each elytron is equipped with two carbon fiber rods that slide into the mount slots. Set screws were used to prevent the elytra from slipping in the spanwise direction (Figure 5.8(C-D)). A 6 DOF ATI Nano25 loadcell was mounted to the base of the test article at its aerodynamic center. Through combinations of different elytra, seven test article configurations were aerodynamically tested. These configurations were the three different elytra lengths corresponding to the lengths characterized for self-righting with hind-wings, those same three elytra without hind-wings, and the hind-wings without elytra (Figure 5.10).

The test article was attached to a Stäubli robotic arm, which in turn was placed in an open-jet WindShape wind tunnel [19] (Figure 5.8 (B)). The robot was programmed to set the test article at a commanded angle of attack. Throughout the experiments, the angle of attack range was varied between $-4°$ and $17°$ in increments of $3°$. The uncertainty in angle of attack was estimated to be $< 0.2°$. To ensure the air flow was smooth, the test sample was positioned such that the leading-edge of the hind-wings was 18 cm from the wind tunnel filter. Tests were run at a wind speed of 8.3 m/s which corresponds to a Reynolds number of about 68,000. At each angle of attack, 500 data samples were recorded at 100 Hz after waiting a few seconds to let the wings reach steady-state. The measured forces were then projected to obtain lift and drag measurements, from which lift and drag coefficients can be calculated.

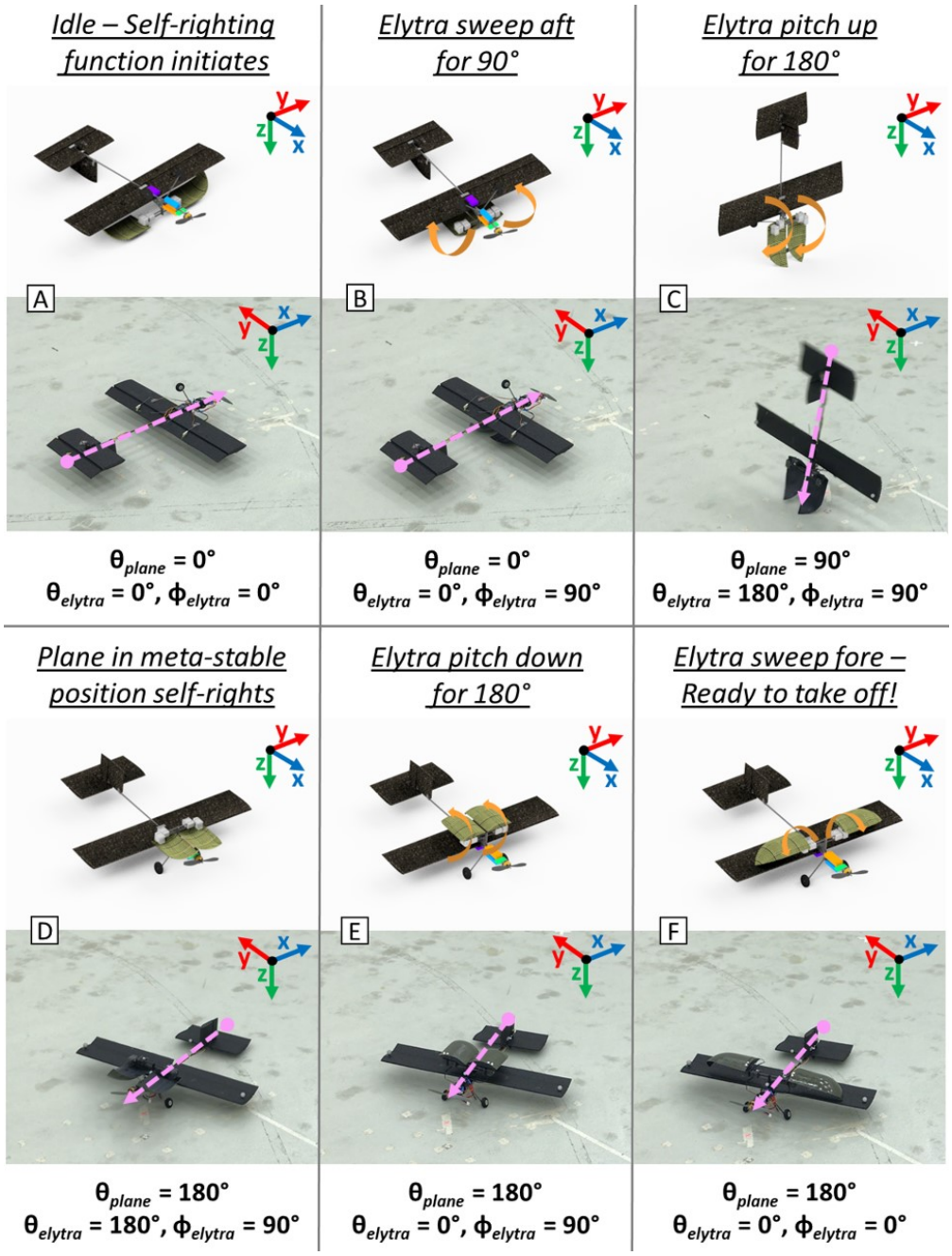

Figure 5.9: Sample of the experimental self-righting characterization. A motion capture system was used to record the motion during the self-righting process in real time. Five passive tracking markers were attached to the plane and tracked in the 3D space. Pitching angle and self-righting time was characterized for different elytra configurations and torques. The graph shows a sample diagram for the configuration of the vehicle with the 17 cm elytra and 0.39 Nm.

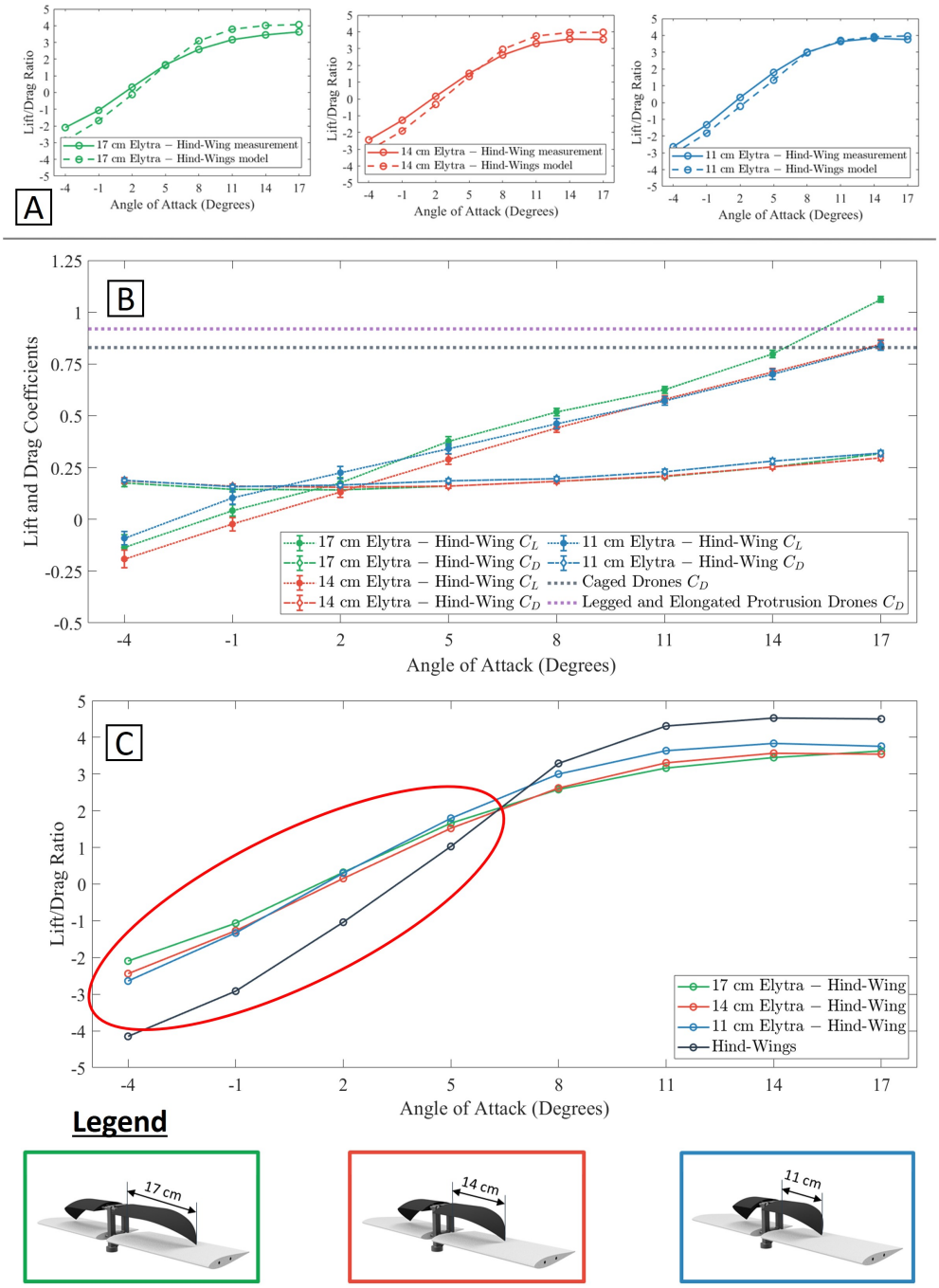

Figure 5.10: Aerodynamic characterization of hind-wings with different elytra configurations. (A) Lift/Drag ratio for the aerodynamic test sample mounted with hind-wings and different elytra lengths in comparison with their theoretical model. (B) Lift and drag coefficients of the test sample mounted with elytra of different lengths and in comparison with existing self-righting solutions in the state of the art. (C) Lift/Drag ratio of the hind-wings and of hind-wings with different elytra configurations.

5.6.1 Aerodynamic experimental results

Figure 5.10 shows that elytra generate non-negligible lift which mitigates the weight penalty they incur from an angle of attack of 2° to 17° (Figure 5.10 (C)). For angles of attack from −4° to about 6°, the elytra hind-wings system, increases the aerodynamic efficiency by displaying a higher lift-to-drag ratio than that of hind-wings (Figure 5.10 (B)). At higher angles of attack the performance of the elytra and hind-wings system deteriorates due to the elytra hind-wings aerodynamic interactions. However, for most UAV applications, this is a minor effect as wing systems usually fly at angles of attack between 2° and 5°. The additional lift production is the reason that elytra as self-righting mechanisms outperform other systems in the state of the art. Self-righting systems with similar weight, such as gimbal-cages, legs or elongated protrusion mechanisms, show approximately a consistent 70% higher drag without having the lift generation benefits of the elytra [28, 29] (Figure 5.10 (B)). There is no consistent trend between elytra of different lengths (Figure 5.10 (B)). For instance, below an angle of attack of about 3° the shortest elytra have the highest lift coefficient, but above 3°, the longest elytra have the highest lift coefficient (Figure 5.10 (B)).

To estimate the aerodynamic effects of the elytra on the hind-wings, we applied the biplane model. Figure 5.10 (A) displays the aerodynamic performance of the hind-wing and elytra system alongside the predictions from the biplane model. The total lift coefficient for a biplane can be defined as [97]:

$$C_{L_{total}} = \frac{A_{HW} C_{L_{HW}} + A_E C_{L_E}}{A_{HW} + A_E} \tag{5.1}$$

$$C_{D_{total}} = \frac{A_{HW} C_{D_{HW}} + A_E C_{D_E}}{A_{HW} + A_E} \tag{5.2}$$

Where $C_{L_{total}}$ and $C_{D_{total}}$ are the total lift and drag coefficients based on total planform area ($A_{HW} + A_E$). A_{HW}, A_E are the Hind-wing and Elytra wing areas respectively, and $C_{L_{HW}}$, C_{L_E}, $C_{D_{HW}}$, C_{D_E} are respectively, the independent lift and drag coefficients of the hind-wings and elytra. Figure 5.10 (A) presents the measured lift-to-drag ratios of the hind-wing and elytra of different spans as well as the lift-to-drag predicted by the biplane model. The biplane model is able to most accurately predict the measurements for small angles of attack, with the highest precision being achieved at 5° for the 14 and 17 cm elytra and at 8° for the 11 cm elytra. This corresponds closely to Ely's cruise angle of attack of about 5°. Differences between measurements and the biplane model are likely due to interactions between the elytra wing tips and airflow over the upper surface of the hind-wings. While short elytra achieve the highest aerodynamic performance at cruising angles, they are unable to self-right with the selected motors. At the cruise angle of attack of about 5°, all three elytra lengths perform similarly. Thus, the selection of elytra lengths for Ely should be 17 cm as they achieved a 100% self-righting success rate. Alternative design objectives, such as increased compactness could

favor shorter span elytra, in cases such as this, a trade-off is made with self-rightability over aerodynamic performance.

5.7 Free flight test

The flight tests consisted of first dropping Ely onto the ground such that it landed in an inverted position. At impact, the elytra absorbed the landing loads and immobilized the drone. Then, the self-righting function was manually triggered. The pre-programmed self-righting function autonomously began after 5 seconds. As described in previous sections, the elytra are first swept back 90° and then pitched forward 180° to flip the plane into its upright position. After uprighting, the elytra move back to their flight position. Next, the pilot engages full throttle and the plane takes off. Ely flew steadily, given manual inputs from the pilot, at an approximate speed of 8 m/s (Figure 5.11). The flight test was carried out in calm wind conditions of less than 2 km/h. The plane successfully flew for 45 seconds before landing in short grass. The flight test can be viewed in Supplementary Material - Supplementary_Video.

Figure 5.11: Image from the flight experiments of Ely.

5.8 Conclusion

In this work, we present an insect-inspired, self-righting solution for small-winged drones. We integrated a set of artificial elytra that are utilized for self-righting and providing additional lift, mitigating the extra energy use incurred by the self-righting mechanism. We characterized the self-righting capabilities and the aerodynamic performance of a flight-worthy drone and studied the trade-off between self-righting mechanics and aerodynamic performance.

The proposed solution is suitable for fixed-wing drones at the Micro Aerial Vehicle scale [26]. In this study, we used widely available materials. Elytra materials with different mechanical properties could be used to enable self-righting in a variety of challenging environments with diverse surface compositions in terms of temperature, humidity, and friction coefficients. Elytra geometries with differing levels of camber or airfoil shapes could be employed depending on the aerodynamic performance required. Moreover, the simple yet robust mechanical design of the self-righting mechanism makes the system fit for use not only in aerial vehicles but also in terrestrial and marine robots that require self-righting capabilities.

6 Beyond

In this thesis, various methodologies were investigated for developing the next generation of resilient, autonomous flying robots capable of operating in challenging, diverse environments. These methodologies focused on developing solutions for applications in routine industrial missions, namely inspection, monitoring, reconnaissance, and search and rescue missions. The presented methodologies feature a wide range of applicability from conventional fixed-wings planes to morphing VTOL platforms.
In this chapter, the main achievements of the work presented in this thesis are summarized, along with the limitations of the technologies and methodologies described in the previous chapters. Concluding, an outlook for possible industrial applications is presented along with potential avenues for future research avenues.

6.1 This is not a conclusion

Several methodologies for increasing the resilience of winged drones were explored throughout the work of this thesis. The first two chapters, Chapter 2 and Chapter 3, focused on developing and validating methodologies for increasing the resilience of wing drones in the air during flight operations in adverse wind conditions. The work of these two chapters discussed the limitations of current winged VTOL drones and presented a methodology for rejecting adverse wind effects or exploiting them to increase the maneuverability and energy efficiency of the vehicle. In the first of these chapters, the methodology was applied in a simplified lab prototype drone with morphing wings, while in the second chapter, the methodology was applied in an optimized prototype drone inspired by the *odonata* insects, which also displayed Level 5 (Annex C) wind force resilience.

The other two chapters, Chapter 4 and Chapter 5, focused on increasing the resilience of winged drones on the ground. At first, inspiration from the beetles was used to abstract from their protective wing design to develop a strategy for shielding a drone during ground locomotion. The developed methodology gave inspiration for integrating a set of protective wings that would enclose the set of main wings and the electronics of the drone and thus protect them. The added value of the solution was that, compared to the state-of-the-art solutions, the protective structure could offset its weight by generating lift. In the second of these chapters, the work focused on the vehicle's recovery after a tip-over. Studying the protective properties of the beetles' *elytra* revealed that they could be used not only for passive protection but also for self-righting. The beetles' protective principle inspired a self-righting methodology for fixed-wing drones.

The hypothesis in this work is that, similar to nature, morphing wing concepts can be used to improve energy efficiency, demonstrate gains in flight performance, and advancements in out-of-flight resilience properties. While each chapter investigated these aspects individually, future operations will require combining these features in a single solution to meet the challenge of future missions. Despite the fact that the solutions are demonstrated in different drones with different sizes and characteristics, it is possible to envision and develop a platform that combines the investigated concepts in a single drone. In the work presented, the most prominent drone for integrating all features is the drone HercuLIS, developed and discussed in Chapter 4. HercuLIS featured sweeping wings and elytra wings with 2 degrees of freedom. Upon further structural optimization and integrating a third degree of freedom, elytra could enable self-righting of the platform during overturn as discussed in Chapter 5. Furthermore, simultaneous actuation of the elytra and the wings would allow the integration of the wind harvesting technologies developed in Chapter 2 and Chapter 3. In addition, fitting the propulsion system within the fuselage would reduce the exposed components during ground locomotion and enable safe ground locomotion without risking accidental collisions. The open challenges to developing a vehicle with all these features are the extended mechanic, aerodynamic and electronic design, and manufacturing optimization.

6.2 Limitations of current methodologies

Despite the several operational advantages demonstrated through the methodologies and technologies developed in this thesis, some limitations have to be discussed.
As mentioned in the previous chapters, adaptive morphology, both in natural and man-made applications, come with the integration of one or more degrees of freedom. Usually, these added degrees of freedom require additional actuators and support structures for their effective operation. These design adaptations required for increasing the degrees of freedom also increase the complexity of the electromechanical structure of the vehicle and its production cost. Systems with a lower number of components are usually easier to maintain and display fewer failure points during operation. These are critical factors for future operations requiring robust and maintenance-free vehicles.

In addition, another considerable limitation for further integrating adaptive morphology and multiple actuators is the weight penalty. As the energy benefits in aerodynamics from shape-shifting cannot offset the cost of added weight, there is still a trade-off in operational capability and resilience to mission range and operational time.

Another limitation can be the methodology to integrate morphing in current established designs. All the presented methodologies were applied in non-optimized lab prototypes that deviated from standard aircraft design. As the design and development of aerial vehicles can be both time demanding and expensive, an obvious challenge would be integrating the developed technologies into current drones.

Nevertheless, despite the identified limitations, adaptive morphology can be the key to unlocking resilient drones capable of fully autonomous operations. The accelerating advancement in materials and electronics will soon allow for integrating multiple degrees of freedom and multi-functional mechanisms in future drones. Similar to flying animals, future drones will be able to operate in the air, ground, or water simply by adapting their shape.

6.3 Possible directions for future work

This thesis presented several methodologies for resilient winged drones. These methodologies presented integration principles and experiments for validating the design hypotheses. However, there are still possibilities for exploring research avenues when considering a possible transition from a lab prototype to an industrial product.

A possible direction could be the optimization of the current prototypes for better performance. Weight reduction and aerodynamic optimization could transform the research prototypes presented in this work into useful tools for real operations in the domains of search, rescue, inspection, and monitoring.

Furthermore, in the current work, existing open-source VTOL controllers were used for

demonstrating the developed methodologies [79]. Future work might focus on the integration of end-to-end, model-based controllers that would increase the performance of the developed systems and allow them to perform with robustness in challenging environments.

Moreover, another future research direction might be the integration of all of the technologies and methodologies presented in this work into a single drone, as discussed in the previous section. Currently, the limitations of efficiency in energy storage devices and the low power-to-weight ratio of state-of-the-art actuators limit the probability of a one-for-all solution. Although it might be significantly challenging to integrate multiple functionalities in a single platform, a possible solution could be to integrate a set of different functions in each of the members of a flying swarm. Each swarm member could have the ability to operate autonomously while sharing operational data with the other swarm members. After evaluating the environment, the swarm could decide autonomously which drone of the swarm will be deployed for a specific operation. For example, in a reconnaissance operation, a number of wind-defiant drones could be deployed to rapidly evaluate the weather conditions in a location while a set of multi-modal drones approach the area from land to gather ground information.

6.4 Outlook

After exploring further possible research avenues, it would be worth investigating if the current technologies developed in this thesis could demonstrate the potential of being applied with little to no modification to current industrial products. During investigating the state-of-the-art solutions deployed for search, rescue, inspection and monitoring, a gap was identified when a mission required a solution with precise, safe hovering and long-range flight.

Figure 6.1: Examples of linear infrastructure. Photos adapted from [32, 33, 34, 35, 36].

As an example, the case of linear infrastructure inspection and monitoring will be examined. Linear infrastructure refers to infrastructure that spans linearly for a substantial distance, such as roads, highways, electric powerlines, telephone lines, railway lines, pipelines, bridges, etc. Linear infrastructures consist of constructs that span through wide-open areas and form complex confined space hubs every few distance units (Figure 6.1). Examples can be electric powerlines and bridges that, every few kilometers, are composed of a pylon or a supportive tower. Currently, the geometric characteristics of these structures require the separate deployment of inspection and monitoring tools that are either specialized for long-range, wide-open areas or for being safe in complex confined spaces while operating close to the infrastructure.

Modern inspection and monitoring solutions involve the deployment of drones, such as copters and fixed wings. As discussed in previous chapters, copters resemble helicopters with one or more propellers capable of vertical flight missions. On the other hand, fixed wings resemble planes capable of horizontal flight missions. However, when monitoring and inspecting linear infrastructure, current drones have design limitations that reduce their operational autonomy, increase cost, and restrict the quality of data they can collect. These limitations are associated with their design which limits the drone's ability to adapt to both open-wide and confined environments, and their lack of autonomous functionality, which requires constant human intervention.

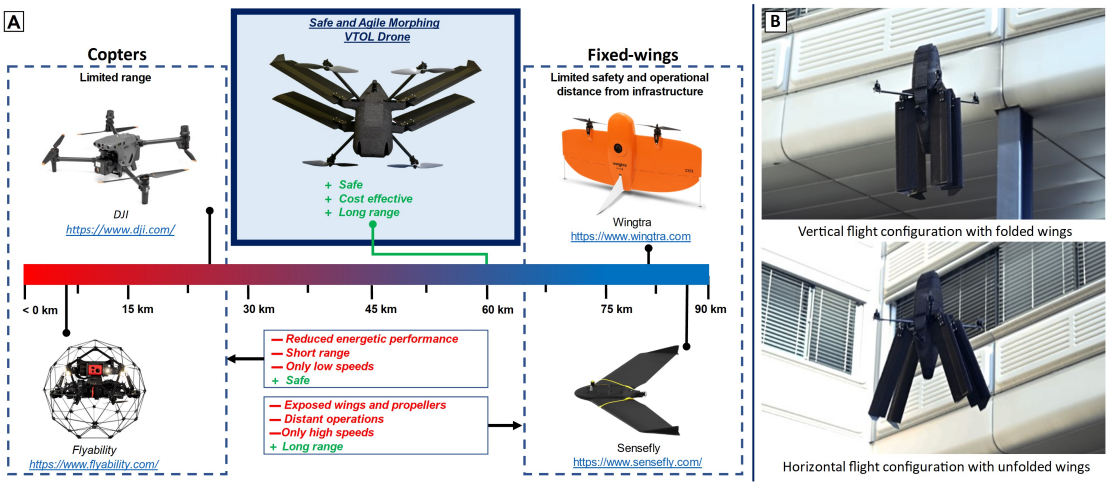

Figure 6.2: (A) Limitations of state of art. Copter and fixed-wing figures adapted from [37, 38, 39, 40]. Morpho^2 combines the best features of copters and fixed-wings in a morphing platform that can adapt its shape depending on if it is required to operate in open-wide or confined spaces (B) Two flight configurations. The folded, vertical flight configuration with fully retracted wings and the horizontal flight configuration with wings extended at 45 degrees.

Drones for inspection and monitoring of linear infrastructure are required to fly in the targeted construct's proximity at low speeds to record high-quality data and avoid collisions. At the same time, they must retain their ability to fly for long ranges to cover the entire length of the infrastructure without frequent recharging so that they do not compromise critical time

missions and increase operational costs. Modern solutions for inspection and monitoring use either multicopters or fixed wings. Multicopters display high precision but reduced energetic performance, while their limited range do not allow them to cover the length of linear infrastructure. On the other hand, fixed-wing drones fly for longer distances. However, their lack of protective configuration, namely exposed wings and high operation speed do not allow for operating close to the infrastructure (Figure 6.2 (A)).

As discussed in Chapter 3, Morpho^2 combines the advantages of copters and fixed wings by changing her shape according to the stage of the operation. In fact, Morpho^2 can transform into a stable and safe configuration with folded wings that will allow her to operate in proximity to humans and infrastructure when in vertical flight. In horizontal flight, Morpho^2 transforms into an efficient aerodynamic shape that will enable it to travel several kilometers. Morpho^2, by shaping her wings, can reject adverse wind effects and utilize wind currents while in vertical flight to save energy and increase its maneuverability, thus substantially expanding the time it can operate in vertical mode (20% compared to VTOL alternatives of similar weight). This can be crucial for close inspection missions due to the time the vehicle has to spend in vertical flight mode. A sample inspection and monitoring operation in the power sector is depicted in 6.3.

The identified potential for further exploring the industrial benefits of wind-defiant morphing drones as a solution for the inspection and monitoring of infrastructure led to the submission of a patent application related to [58] with the reference:

C. Vourtsis, V. C. Rochel, N. S. Müller, W. Stewart, and D. Floreano, “Method for wind harvesting and wind rejection in flying drones”, Patent Pending, Sep. 2022.

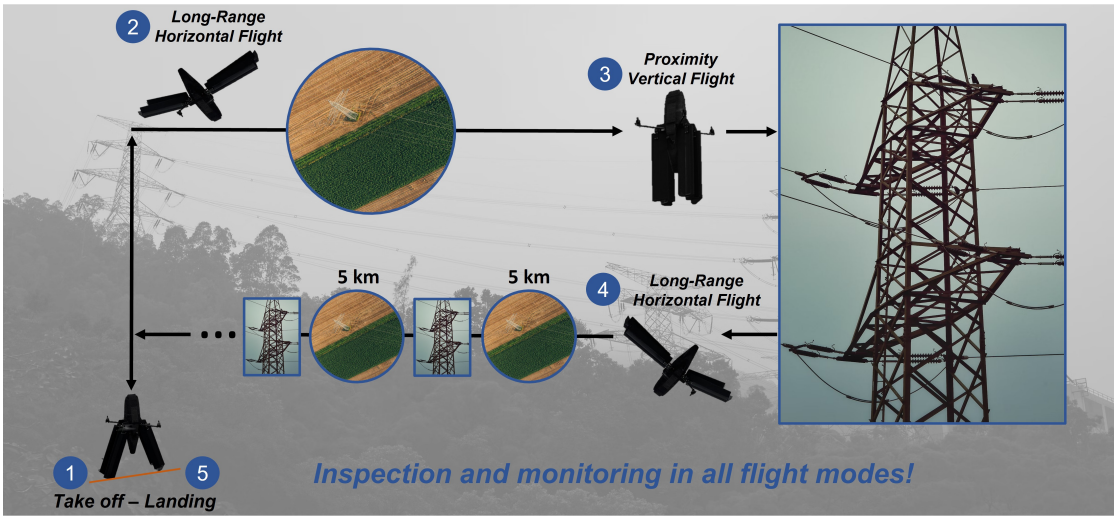

Figure 6.3: Sample monitoring and inspection mission. 1. The drone takes off in vertical mode with retracted wings and transitions to horizontal flight. 2. The drone travels in horizontal flight mode while inspecting and monitoring the infrastructure. 3. The drone arrives at a focus point and transitions to vertical flight mode to inspect it in proximity. 4. The drone moves away from the inspection area in vertical mode and transitions to horizontal flight while monitoring the infrastructure and approaching the next inspection points. 5. The drone continues the mission and then transitions again to vertical flight mode and lands. Wing morphing is automatic throughout the whole flight envelope.

A Publications

Articles published in peer-reviewed journals:

- C. Vourtsis, V. C. Rochel, N. S. Müller, W. Stewart, and Dario Floreano, "Wind Defiant Morphing Drones," in *Advanced Intelligent Systems*, 2200297, Jan. 2023, [58].
- C. Vourtsis, W. Stewart, and D. Floreano, "Robotic Elytra: Insect-Inspired Protective Wings for Resilient and Multi-Modal Drones," in *IEEE Robotics and Automation Letters (RA-L)*, vol. 7, no. 1, pp. 223-230, Jan. 2022, [59].
- C. Vourtsis, V. C. Rochel, F. R. Serrano, W. Stewart, and D. Floreano, "Insect Inspired Self-Righting for Fixed-Wing Drones," in *IEEE Access*, in *IEEE Robotics and Automation Letters (RA-L)*, vol. 6, no. 4, pp. 6805-6812, Oct. 2021, [60].
- C. Vourtsis, V. C. Rochel, N. S. Müller, W. Stewart, and Dario Floreano, "Method for wind harvesting and wind rejection in flying drones", *Patent Pending*, Sep. 2022.

B Drone Autonomy Levels

The drone autonomy levels are used to characterize the independence from external control and the levels of self-governance of a flying vehicle. The autonomy levels are presented on a scale from 0 to 5, where 0 represents the level of "No autonomy" and 5 represents the level of "Full autonomy". The drone autonomy levels are described in detail and with examples in [121] and are summarized below.

Level 0 - No autonomy
This level represents vehicles with no autonomy. The pilot has to be in full control of the vehicle all the time.

Level 1 - Pilot assistance
At this level, the pilot remains in control of the vehicle and is responsible for the overall operation and safety of the flight mission. The vehicle provides support for navigation and/or keeping altitude and position. The vehicle is not controlled in position and speed simultaneously.

Level 2 - Partial autonomy
This level represents some type of partial autonomy where the drone has the ability to control its heading, speed and altitude. The pilot is still fully responsible for the overall operation and safety of the drone although the drone can take over and assist in navigation.

Level 3 - Conditional autonomy
In this level, the pilot remains responsible for the overall operation and safety of the drone. The drone can perform autonomous flights and it can alert the pilot if intervention is needed.

Level 4 - High autonomy
In Level 4, the drone can be controlled by the pilot but it is not necessary. The drone can fly autonomously during the whole mission. The drone is also expected to feature backup systems. Although, the drone still depends on a fixed set of rules and predefined system behaviors for its operation.

Level 5 - Full autonomy
Level 5 represents fully autonomous operations. The drone can fly itself under all conditions with no expected pilot intervention. The drone utilizes artificial intelligence and learning methods to alter its operational behavior without human intervention and adjust to increase its mission success. There are no examples of Level 5 autonomous drones in academia or the industry.

C Wind Force Levels: The Beaufort Scale

The Beaufort wind force scale is an empirically developed scale that correlates wind speed to observed conditions on land and sea. In drone-related applications, the Beaufort scale is used to characterize the wind force a flying vehicle can safely operate [122, 123].

Beaufort wind scale	**Mean wind speed (m/s)**	**Wind speed limits (m/s)**	**Wind description**	**Probable wave height (m)**	**Probable max wave height (m)**	**Seastate**	**Sea description**
0	0	<1	Calm	-	-	0	Calm (glassy)
1	1	1-2	Light air	0.1	0.1	1	Calm (rippled)
2	3	2-3	Light breeze	0.2	0.3	2	Smooth (wavelets)
3	5	4-5	Gentle breeze	0.6	1	3	Slight
4	7	6-8	Moderate breeze	1.0	1.5	3-4	Slight - Moderate
5	10	9-11	Fresh breeze	2.0	2.5	4	Moderate
6	12	11-14	Strong breeze	3.0	4	5	Rough
7	15	14-17	Near gale	4.0	5.5	5-6	Rough- Very rough
8	19	17-21	Gale	5.5	7.5	6-7	Very rough - High
9	23	21-24	Strong gale	7.0	10.0	7	High
10	27	25-28	Storm	9.0	12.5	8	Very High
11	31	29-32	Violent storm	11.5	16.0	8	Very High
12	-	33+	Hurricane	14+	-	9	Pheno-menal

Table C.1: The Beaufort wind force scale.

Bibliography

[1] M. Adams, "Photo by Martin Adams on Unsplash," Feb. 2019. [Online]. Available: https://unsplash.com/photos/V-BPZ6r4sVA

[2] I. Benhesed, "Photo by Isaac Benhesed on Unsplash," May 2019. [Online]. Available: https://unsplash.com/photos/nCm8AOjM_zE

[3] "Krossblade Aerospace Systems." [Online]. Available: https://www.krossblade.com

[4] J. Haseltine, "A U.S. V-22 Osprey tiltrotor aircraft flies a test mission. U.S." Aug. 2003. [Online]. Available: https://commons.wikimedia.org/wiki/File:V-22_Osprey_tiltrotor_aircraft.jpg

[5] "HADA, the helicopter capable of flying in helicopter and airplane modes." [Online]. Available: https://www.embention.com/projects/hada-helicopter-adaptive-aircraft/

[6] R. Lee, "Photo by Richard Lee on Unsplash," Jan. 2018. [Online]. Available: https://unsplash.com/photos/xWQcud4Xtr4

[7] Y. H, "Photo by Yannis H on Unsplash," Jan. 2020. [Online]. Available: https://unsplash.com/photos/V3HpOznbJl4

[8] D. Dennis, "Photo by Dan Dennis on Unsplash," Apr. 2020. [Online]. Available: https://unsplash.com/photos/jqAFeujFetI

[9] D. Li, S. Zhao, A. Da Ronch, J. Xiang, J. Drofelnik, Y. Li, L. Zhang, Y. Wu, M. Kintscher, H. P. Monner, A. Rudenko, S. Guo, W. Yin, J. Kirn, S. Storm, and R. D. Breuker, "A review of modelling and analysis of morphing wings," *Progress in Aerospace Sciences*, Jun. 2018. [Online]. Available: https://linkinghub.elsevier.com/retrieve/pii/S0376042117301835

[10] S. Barbarino, R. Pecora, L. Lecce, A. Concilio, S. Ameduri, and E. Calvi, "A Novel SMA-based Concept for Airfoil Structural Morphing," *Journal of Materials Engineering and Performance*, vol. 18, no. 5-6, pp. 696–705, Aug. 2009. [Online]. Available: http://link.springer.com/10.1007/s11665-009-9356-3

[11] R. Siddall, A. Ortega Ancel, and M. Kovac, "Wind and water tunnel testing of a morphing aquatic micro air vehicle," *Interface Focus*, vol. 7, no. 1, p. 20160085, Feb. 2017. [Online]. Available: http://rsfs.royalsocietypublishing.org/lookup/doi/10.1098/rsfs.2016.0085

[12] J. Flanagan, R. Strutzenberg, R. Myers, and J. Rodrian, "Development and Flight Testing of a Morphing Aircraft, the NextGen MFX-1." American Institute of Aeronautics and Astronautics, Apr. 2007. [Online]. Available: http://arc.aiaa.org/doi/10.2514/6.2007-1707

[13] "RoboSwift." [Online]. Available: https://www.roboswift.nl/

[14] M. Di Luca, S. Mintchev, G. Heitz, F. Noca, and D. Floreano, "Bioinspired morphing wings for extended flight envelope and roll control of small drones," *Interface Focus*, vol. 7, no. 1, p. 20160092, Feb. 2017. [Online]. Available: http://rsfs.royalsocietypublishing.org/lookup/doi/10.1098/rsfs.2016.0092

[15] P. Santos, J. Sousa, and P. Gamboa, "Variable-span wing development for improved flight performance," *Journal of Intelligent Material Systems and Structures*, vol. 28, no. 8, pp. 961–978, May 2017. [Online]. Available: http://journals.sagepub.com/doi/10.1177/1045389X15595719

[16] D. T. Grant, M. Abdulrahim, and R. Lind, "Design and analysis of biomimetic joints for morphing of micro air vehicles," *Bioinspiration & Biomimetics*, vol. 5, no. 4, p. 045007, Dec. 2010. [Online]. Available: http://stacks.iop.org/1748-3190/5/i=4/a=045007?key=crossref.2e3d133361f8e2a3318799ea60f7a32f

[17] G. J. J. Ducard and M. Allenspach, "Review of designs and flight control techniques of hybrid and convertible VTOL UAVs," *Aerospace Science and Technology*, vol. 118, p. 107035, Nov. 2021. [Online]. Available: https://www.sciencedirect.com/science/article/pii/S1270963821005459

[18] A. S. Saeed, A. B. Younes, C. Cai, and G. Cai, "A survey of hybrid Unmanned Aerial Vehicles," *Progress in Aerospace Sciences*, vol. 98, pp. 91–105, Apr. 2018. [Online]. Available: https://www.sciencedirect.com/science/article/pii/S0376042117302233

[19] "WindShape - Drone Test Equipment and Services - Wind Tunnel." [Online]. Available: https://www.windshape.ch/

[20] "Controller Diagrams | PX4 User Guide." [Online]. Available: https://docs.px4.io/main/en/flight_stack/controller_diagrams.html

[21] J. Hamilton, "Photo by Jeffrey Hamilton on Unsplash," Jul. 2019. [Online]. Available: https://unsplash.com/photos/qK0L-_1uH5g

[22] W. Hasselmann, "Photo by Wolfgang Hasselmann on Unsplash," Dec. 2019. [Online]. Available: https://unsplash.com/photos/aGZqOI9LNZU

[23] W. Romanowska, "Photo by Weronika Romanowska on Unsplash," May 2019. [Online]. Available: https://unsplash.com/photos/RXV1X3wEe8k

[24] L. Frantsevich, "Geometry of elytra opening and closing in some beetles (Coleoptera, Polyphaga)," *Journal of Experimental Biology*, vol. 208, no. 16, pp. 3145–3158, Aug. 2005. [Online]. Available: http://jeb.biologists.org/cgi/doi/10.1242/jeb.01753

[25] SgH, "Stag Beetle." [Online]. Available: https://pixabay.com/photos/stag-beetle-tree-wing-644129/

[26] M. Hassanalian and A. Abdelkefi, "Classifications, applications, and design challenges of drones: A review," *Progress in Aerospace Sciences*, vol. 91, pp. 99–131, May 2017. [Online]. Available: http://www.sciencedirect.com/science/article/pii/S0376042116301348

[27] J. Goczał, R. Rossa, and A. Tofilski, "Elytra reduction may affect the evolution of beetle hind wings," *Zoomorphology*, vol. 137, no. 1, pp. 131–138, Mar. 2018. [Online]. Available: http://link.springer.com/10.1007/s00435-017-0388-1

[28] P. Kornatowski, S. Mintchev, and D. Floreano, "An origami-inspired cargo drone," in *2017 IEEE/RSJ International Conference on Intelligent Robots and Systems (IROS)*, Sep. 2017, pp. 6855–6862, iSSN: 2153-0866. [Online]. Available: https://ieeexplore.ieee.org/document/8206607

[29] C. J. Salaan, Y. Okada, K. Hozumi, K. Ohno, and S. Tadokoro, "Improvement of UAV's flight performance by reducing the drag force of spherical shell," in *2016 IEEE/RSJ International Conference on Intelligent Robots and Systems (IROS)*, Oct. 2016, pp. 1708–1714, iSSN: 2153-0866. [Online]. Available: https://ieeexplore.ieee.org/document/7759274

[30] wildwatertv, "Ladybird taking off from a grass stalk." [Online]. Available: https://www.pond5.com/stock-footage/item/8658289-ladybird-taking-grass-stalk-slow-motion

[31] vexedart, "Tiny But Powerful Little Bug Getting Up From Being Stuck On Its Back. Lady Bug O." [Online]. Available: https://www.pond5.com/

[32] D. Costa, "Photo by Davi Costa on Unsplash," Dec. 2018. [Online]. Available: https://unsplash.com/photos/cG2JQnPfmAw

[33] H. Matthew, "Photo by Matthew Henry on Unsplash," Sep. 2016. [Online]. Available: https://unsplash.com/photos/yETqkLnhsUI

[34] T. Meritt, "Photo by Meritt Thomas on Unsplash," Oct. 2019. [Online]. Available: https://unsplash.com/photos/GktK3Jb9BRE

[35] J. Weirick, "Photo by Jake Weirick on Unsplash," Apr. 2020. [Online]. Available: https://unsplash.com/photos/krsmsfjjGgg

[36] J. Blackeye, "Photo by Jason Blackeye on Unsplash," May 2017. [Online]. Available: https://unsplash.com/photos/jq7Bsv4qvds

[37] "DJI Innovations' Drone Is Simple Enough for Anyone to Use - Bloomberg." [Online]. Available: https://www.bloomberg.com/news/articles/2014-05-15/dji-innovations-drone-is-simple-enough-for-anyone-to-use

[38] "Wingtra – The professional VTOL drone for mapping and surveying." [Online]. Available: https://wingtra.com/

[39] "Flyability — Drones for indoor inspection and confined space." [Online]. Available: https://www.flyability.com

[40] "senseFly – The Professional's Mapping Drone." [Online]. Available: https://www.sensefly.com/

[41] D. Floreano and R. J. Wood, "Science, technology and the future of small autonomous drones," *Nature*, vol. 521, no. 7553, pp. 460–466, May 2015. [Online]. Available: https://rdcu.be/cF47z

[42] P. E. Sitorus, H. C. Park, D. Byun, N. S. Goo, and C. H. Han, "The Role of Elytra in Beetle Flight: I. Generation of Quasi-Static Aerodynamic Forces," *Journal of Bionic Engineering*, vol. 7, no. 4, pp. 354–363, Dec. 2010. [Online]. Available: http://www.sciencedirect.com/science/article/pii/S1672652910602673

[43] C. Wang, C. Wang, Y. Ning, L. Chen, and X. Wang, "Design and Mechanical Analysis of Bionic Foldable Beetle Wings," *Applied Bionics and Biomechanics*, vol. 2018, pp. 1–10, Aug. 2018. [Online]. Available: https://www.hindawi.com/journals/abb/2018/1308465/

[44] T. Q. Le, T. V. Truong, H. T. Tran, S. H. Park, J. H. Ko, H. C. Park, and D. Byun, "How Could Beetle's Elytra Support Their Own Weight during Forward Flight?" *Journal of Bionic Engineering*, vol. 11, no. 4, pp. 529–540, Dec. 2014. [Online]. Available: http://link.springer.com/10.1016/S1672-6529(14)60065-2

[45] L. C. Johansson, S. Engel, E. Baird, M. Dacke, F. T. Muijres, and A. Hedenström, "Elytra boost lift, but reduce aerodynamic efficiency in flying beetles," *Journal of The Royal Society Interface*, vol. 9, no. 75, pp. 2745–2748, Oct. 2012. [Online]. Available: https://royalsocietypublishing.org/doi/10.1098/rsif.2012.0053

[46] D. Grimaldi, M. S. Engel, M. S. Engel, and S. C. a. P. M. S. Engel, *Evolution of the Insects*. Cambridge University Press, May 2005, google-Books-ID: Ql6Jl6wKb88C.

[47] J. R. Usherwood and F.-O. Lehmann, "Phasing of dragonfly wings can improve aerodynamic efficiency by removing swirl," *Journal of The Royal Society Interface*, vol. 5, no. 28, pp. 1303–1307, Nov. 2008, publisher: Royal Society. [Online]. Available: https://royalsocietypublishing.org/doi/10.1098/rsif.2008.0124

[48] E. Salami, T. A. Ward, E. Montazer, and N. N. N. Ghazali, "A review of aerodynamic studies on dragonfly flight," *Proceedings of the Institution of Mechanical Engineers, Part C: Journal of Mechanical Engineering Science*, vol. 233, no. 18, pp. 6519–6537, Sep. 2019, publisher: IMECHE. [Online]. Available: https://doi.org/10.1177/0954406219861133

[49] A. L. Thomas, "The Flight of Birds that have Wings and a Tail: Variable Geometry Expands the Envelope of Flight Performance," *Journal of Theoretical Biology*, vol. 183, no. 3, pp. 237–245, Dec. 1996. [Online]. Available: http://linkinghub.elsevier.com/retrieve/pii/S0022519396902179

[50] A. Ward-Smith, "Analysis of the aerodynamic performance of birds during bounding flight," *Mathematical Biosciences*, vol. 68, no. 1, pp. 137–147, Feb. 1984. [Online]. Available: http://linkinghub.elsevier.com/retrieve/pii/0025556484900774

[51] A. V. Birn-Jeffery and M. A. Daley, "Birds achieve high robustness in uneven terrain through active control of landing conditions," *The Journal of Experimental Biology*, vol. 215, no. 12, pp. 2117–2127, Jun. 2012. [Online]. Available: http://jeb.biologists.org/lookup/doi/10.1242/jeb.065557

[52] G. Glaeser, H. F. Paulus, and W. Nachtigall, *The Evolution of Flight*. Cham: Springer International Publishing, 2017. [Online]. Available: http://link.springer.com/10.1007/978-3-319-57024-2

[53] S. Mintchev and D. Floreano, "Adaptive Morphology: A Design Principle for Multimodal and Multifunctional Robots," *IEEE Robotics & Automation Magazine*, vol. 23, no. 3, pp. 42–54, Sep. 2016. [Online]. Available: http://ieeexplore.ieee.org/document/7565704/

[54] J. C. Gomez and E. Garcia, "Morphing unmanned aerial vehicles," *Smart Materials and Structures*, vol. 20, no. 10, p. 103001, Oct. 2011. [Online]. Available: http://stacks.iop.org/0964-1726/20/i=10/a=103001?key=crossref.e5fa7178d7019c83f888a731461802e9

[55] A. Concilio, I. Dimino, L. Lecce, R. Pecora, S. Ricci, F. Aliabadi, R. Botez, and F. Semperlotti, *Morphing Wing Technologies: Large Commercial Aircraft and Civil Helicopters*. Elsevier Science, 2017. [Online]. Available: https://books.google.gr/books?id=H3a0CwAAQBAJ

[56] A. Moosavian, F. Xi, and S. M. Hashemi, "Design and Motion Control of Fully Variable Morphing Wings," *Journal of Aircraft*, vol. 50, no. 4, pp. 1189–1201, Jul. 2013. [Online]. Available: http://arc.aiaa.org/doi/10.2514/1.C032127

[57] D. S. Ramrakhyani, G. A. Lesieutre, M. I. Frecker, and S. Bharti, "Aircraft Structural Morphing using Tendon-Actuated Compliant Cellular Trusses," *Journal of Aircraft*, vol. 42, no. 6, pp. 1614–1620, Nov. 2005. [Online]. Available: http://arc.aiaa.org/doi/10.2514/1.9984

[58] C. Vourtsis, V. C. Rochel, N. S. Müller, W. Stewart, and D. Floreano, "Wind Defiant Morphing Drones," *Advanced Intelligent Systems*, vol. n/a, no. n/a, p. 2200297, Jan. 2023, _eprint: https://onlinelibrary.wiley.com/doi/pdf/10.1002/aisy.202200297. [Online]. Available: https://onlinelibrary.wiley.com/doi/abs/10.1002/aisy.202200297

[59] C. Vourtsis, W. Stewart, and D. Floreano, "Robotic Elytra: Insect-Inspired Protective Wings for Resilient and Multi-Modal Drones," *IEEE Robotics and Automation Letters*,

vol. 7, no. 1, pp. 223–230, Jan. 2022, conference Name: IEEE Robotics and Automation Letters.

[60] C. Vourtsis, V. Casas Rochel, F. Ramirez Serrano, W. Stewart, and D. Floreano, "Insect Inspired Self-Righting for Fixed-Wing Drones," *IEEE Robotics and Automation Letters*, pp. 1–1, 2021, conference Name: IEEE Robotics and Automation Letters.

[61] "Modelling the Flying Bird, Volume 5 - 1st Edition." [Online]. Available: https://www.elsevier.com/books/modelling-the-flying-bird/pennycuick/978-0-12-374299-5

[62] C. Harvey, V. B. Baliga, P. Lavoie, and D. L. Altshuler, "Wing morphing allows gulls to modulate static pitch stability during gliding," *Journal of The Royal Society Interface*, vol. 16, no. 150, p. 20180641, Jan. 2019, publisher: Royal Society. [Online]. Available: https://royalsocietypublishing.org/doi/10.1098/rsif.2018.0641

[63] J. A. Cheney, J. P. J. Stevenson, N. E. Durston, J. Song, J. R. Usherwood, R. J. Bomphrey, and S. P. Windsor, "Bird wings act as a suspension system that rejects gusts," *Proceedings of the Royal Society B: Biological Sciences*, vol. 287, no. 1937, p. 20201748, Oct. 2020, publisher: Royal Society. [Online]. Available: https://royalsocietypublishing.org/doi/10.1098/rspb.2020.1748

[64] D. A. Olejnik, F. T. Muijres, M. Karásek, L. Honfi Camilo, C. De Wagter, and G. C. de Croon, "Flying Into the Wind: Insects and Bio-Inspired Micro-Air-Vehicles With a Wing-Stroke Dihedral Steer Passively Into Wind-Gusts," *Frontiers in Robotics and AI*, vol. 9, 2022. [Online]. Available: https://www.frontiersin.org/article/10.3389/frobt.2022.820363

[65] K. Z. Y. Ang, J. Cui, T. Pang, K. Li, K. Wang, Y. Ke, and B. M. Chen, "Development of an unmanned tail-sitter with reconfigurable wings: U-Lion," in *11th IEEE International Conference on Control & Automation (ICCA)*, Jun. 2014, pp. 750–755, iSSN: 1948-3457.

[66] G. Heredia, A. Duran, and A. Ollero, "Modeling and Simulation of the HADA Reconfigurable UAV," *Journal of Intelligent & Robotic Systems*, vol. 65, no. 1-4, pp. 115–122, Jan. 2012. [Online]. Available: http://link.springer.com/10.1007/s10846-011-9561-9

[67] M. Di Luca, S. Mintchev, Y. Su, E. Shaw, and K. Breuer, "A bioinspired Separated Flow wing provides turbulence resilience and aerodynamic efficiency for miniature drones," *Science Robotics*, vol. 5, no. 38, p. eaay8533, Jan. 2020. [Online]. Available: https://robotics.sciencemag.org/lookup/doi/10.1126/scirobotics.aay8533

[68] E. Ajanic, M. Feroskhan, S. Mintchev, F. Noca, and D. Floreano, "Bioinspired wing and tail morphing extends drone flight capabilities," *Science Robotics*, vol. 5, no. 47, Oct. 2020, publisher: Science Robotics Section: Research Article. [Online]. Available: https://robotics.sciencemag.org/content/5/47/eabc2897

[69] E. Chang, L. Y. Matloff, A. K. Stowers, and D. Lentink, "Soft biohybrid morphing wings with feathers underactuated by wrist and finger motion," *Science Robotics*, vol. 5, no. 38,

p. eaay1246, Jan. 2020. [Online]. Available: https://robotics.sciencemag.org/lookup/doi/10.1126/scirobotics.aay1246

[70] C. B. Jabeur and H. Seddik, "Neural networks on-line optimized PID controller with wind gust rejection for a quad-rotor," *International Review of Applied Sciences and Engineering*, vol. -1, no. aop, Nov. 2021, publisher: Akadémiai Kiadó Section: International Review of Applied Sciences and Engineering. [Online]. Available: https://akjournals.com/view/journals/1848/aop/article-10.1556-1848.2021.00325/article-10.1556-1848.2021.00325.xml

[71] J. F. Whidborne and A. K. Cooke, "Gust Rejection Properties of VTOL Multirotor Aircraft," *IFAC-PapersOnLine*, vol. 50, no. 2, pp. 175–180, Dec. 2017. [Online]. Available: https://linkinghub.elsevier.com/retrieve/pii/S2405896317335681

[72] Y. Yang, J. Zhu, X. Zhang, and X. Wang, "Active Disturbance Rejection Control of a Flying-Wing Tailsitter in Hover Flight," in *2018 IEEE/RSJ International Conference on Intelligent Robots and Systems (IROS)*, Oct. 2018, pp. 6390–6396, iSSN: 2153-0866.

[73] C. Montella and J. R. Spletzer, "Reinforcement learning for autonomous dynamic soaring in shear winds," in *2014 IEEE/RSJ International Conference on Intelligent Robots and Systems*, Sep. 2014, pp. 3423–3428, iSSN: 2153-0866.

[74] V. Bonnin, E. Benard, J.-M. Moschetta, and C. A. Toomer, "Energy-Harvesting Mechanisms for UAV Flight by Dynamic Soaring," *International Journal of Micro Air Vehicles*, vol. 7, no. 3, pp. 213–229, Sep. 2015, publisher: SAGE Publications Ltd STM. [Online]. Available: https://doi.org/10.1260/1756-8293.7.3.213

[75] I. Mir, A. Maqsood, S. A. Eisa, H. Taha, and S. Akhtar, "Optimal morphing – augmented dynamic soaring maneuvers for unmanned air vehicle capable of span and sweep morphologies," *Aerospace Science and Technology*, vol. 79, pp. 17–36, Aug. 2018. [Online]. Available: https://www.sciencedirect.com/science/article/pii/S1270963818300427

[76] Y. Zhao, A. Dutta, P. Tsiotras, and M. Costello, "Optimal Aircraft Trajectories for Wind Energy Extraction," *Journal of Guidance, Control, and Dynamics*, vol. 41, no. 2, pp. 488–496, 2018, publisher: American Institute of Aeronautics and Astronautics _eprint: https://doi.org/10.2514/1.G003048. [Online]. Available: https://doi.org/10.2514/1.G003048

[77] M. Shademan and A. Naghib-Lahouti, "Effects of aspect ratio and inclination angle on aerodynamic loads of a flat plate," *Advances in Aerodynamics*, vol. 2, no. 1, p. 14, Jun. 2020. [Online]. Available: https://doi.org/10.1186/s42774-020-00038-7

[78] R. C. Nelson, *Flight stability and automatic control*, 2nd ed. Boston, Mass: WCB/McGraw Hill, 1998.

[79] "Open Source Autopilot for Drones." [Online]. Available: https://px4.io/

[80] "Using the ECL EKF | PX4 User Guide." [Online]. Available: https://docs.px4.io/main/en/advanced_config/tuning_the_ecl_ekf.html#multicopter-wind-estimation-using-drag-specific-forces

[81] A. Briod, P. Kornatowski, J.-C. Zufferey, and D. Floreano, "A Collision-resilient Flying Robot," *Journal of Field Robotics*, vol. 31, no. 4, pp. 496–509, 2014, _eprint: https://onlinelibrary.wiley.com/doi/pdf/10.1002/rob.21495. [Online]. Available: https://onlinelibrary.wiley.com/doi/abs/10.1002/rob.21495

[82] C. J. Salaan, K. Tadakuma, Y. Okada, Y. Sakai, K. Ohno, and S. Tadokoro, "Development and Experimental Validation of Aerial Vehicle With Passive Rotating Shell on Each Rotor," *IEEE Robotics and Automation Letters*, vol. 4, no. 3, pp. 2568–2575, Jul. 2019, conference Name: IEEE Robotics and Automation Letters.

[83] D. Kumar, S. F. Ali, and A. Arockiarajan, "Structural and Aerodynamics Studies on Various Wing Configurations for Morphing," *IFAC-PapersOnLine*, vol. 51, no. 1, pp. 498–503, 2018. [Online]. Available: https://linkinghub.elsevier.com/retrieve/pii/S2405896318302489

[84] A. Klaptocz, A. Briod, L. Daler, J.-C. Zufferey, and D. Floreano, "Euler spring collision protection for flying robots." IEEE, Nov. 2013, pp. 1886–1892. [Online]. Available: http://ieeexplore.ieee.org/document/6696606/

[85] A. Kalantari and M. Spenko, "Design and experimental validation of HyTAQ, a Hybrid Terrestrial and Aerial Quadrotor," in *2013 IEEE International Conference on Robotics and Automation*, May 2013, pp. 4445–4450, iSSN: 1050-4729.

[86] P. Sareh, P. Chermprayong, M. Emmanuelli, H. Nadeem, and M. Kovac, "Rotorigami: A rotary origami protective system for robotic rotorcraft," *Science Robotics*, vol. 3, no. 22, p. eaah5228, Sep. 2018. [Online]. Available: https://robotics.sciencemag.org/lookup/doi/10.1126/scirobotics.aah5228

[87] D. Gandhi, L. Pinto, and A. Gupta, "Learning to fly by crashing," in *2017 IEEE/RSJ International Conference on Intelligent Robots and Systems (IROS)*, Sep. 2017, pp. 3948–3955, iSSN: 2153-0866.

[88] "eBee X," Sep. 2018. [Online]. Available: https://www.sensefly.com/drone/ebee-x-fixed-wing-drone/

[89] A. K. Stowers and D. Lentink, "Folding in and out: passive morphing in flapping wings," *Bioinspiration & Biomimetics*, vol. 10, no. 2, p. 025001, Mar. 2015. [Online]. Available: http://stacks.iop.org/1748-3190/10/i=2/a=025001?key=crossref.a8a11ecfbeb3c732dbd277e7e5d44c11

[90] Y. Chen, S. Xu, Z. Ren, and P. Chirarattananon, "Collision Resilient Insect-Scale Soft-Actuated Aerial Robots With High Agility," *IEEE Transactions on Robotics*, pp. 1–13, 2021, conference Name: IEEE Transactions on Robotics.

[91] L. Daler, S. Mintchev, C. Stefanini, and D. Floreano, "A bioinspired multi-modal flying and walking robot," *Bioinspiration & Biomimetics*, vol. 10, no. 1, p. 016005, Jan. 2015. [Online]. Available: http://stacks.iop.org/1748-3190/10/i=1/a=016005?key=crossref.f305bd49cb1d6cb9a009c91104061e28

[92] D. M. Linz, A. W. Hu, M. I. Sitvarin, and Y. Tomoyasu, "Functional value of elytra under various stresses in the red flour beetle, Tribolium castaneum," *Scientific Reports*, vol. 6, no. 1, pp. 1–10, Oct. 2016, number: 1 Publisher: Nature Publishing Group. [Online]. Available: https://www.nature.com/articles/srep34813

[93] B. Lee, H. Park, and S.-T. Kim, "Three-dimensional wing behaviors of a rhinoceros beetle during takeoff flights," *Journal of Mechanical Science and Technology*, vol. 29, no. 12, pp. 5281–5288, Dec. 2015. [Online]. Available: http://link.springer.com/10.1007/s12206-015-1130-x

[94] J. Anderson, *Fundamentals of Aerodynamics*. McGraw-Hill Education, 2010. [Online]. Available: https://books.google.de/books?id=xwY8PgAACAAJ

[95] T. Q. Le, T. V. Truong, S. H. Park, T. Quang Truong, J. H. Ko, H. C. Park, and D. Byun, "Improvement of the aerodynamic performance by wing flexibility and elytra–hind wing interaction of a beetle during forward flight," *Journal of The Royal Society Interface*, vol. 10, no. 85, p. 20130312, Aug. 2013. [Online]. Available: https://royalsocietypublishing.org/doi/10.1098/rsif.2013.0312

[96] W. F. Phillips, *Mechanics of flight*. John Wiley & Sons, 2004.

[97] R. Jones, D. J. Cleaver, and I. Gursul, "Aerodynamics of biplane and tandem wings at low Reynolds numbers," *Experiments in Fluids*, vol. 56, no. 6, p. 124, Jun. 2015. [Online]. Available: https://doi.org/10.1007/s00348-015-1998-3

[98] H. K. Versteeg and W. Malalasekera, *An introduction to computational fluid dynamics: the finite volume method*. Pearson education, 2007.

[99] B. D. Wilts, K. Michielsen, J. Kuipers, H. De Raedt, and D. G. Stavenga, "Brilliant camouflage: photonic crystals in the diamond weevil, Entimus imperialis," *Proceedings of the Royal Society B: Biological Sciences*, vol. 279, no. 1738, pp. 2524–2530, Jul. 2012, publisher: Royal Society. [Online]. Available: https://royalsocietypublishing.org/doi/10.1098/rspb.2011.2651

[100] M. M. D. Souza and D. E. Alexander, "Passive aerodynamic stabilization by beetle elytra (wing covers)," *Physiological Entomology*, vol. 22, no. 2, pp. 109–115, 1997, _eprint: https://onlinelibrary.wiley.com/doi/pdf/10.1111/j.1365-3032.1997.tb01147.x. [Online]. Available: https://onlinelibrary.wiley.com/doi/abs/10.1111/j.1365-3032.1997.tb01147.x

[101] E. Cuesta and J. M. Lobo, "Visible and near-infrared radiation may be transmitted or absorbed differently by beetle elytra according to habitat preference," *PeerJ*,

vol. 7, p. e8104, Nov. 2019, publisher: PeerJ Inc. [Online]. Available: https://peerj.com/articles/8104

[102] L. Frantsevich, "Righting kinematics in beetles (Insecta: Coleoptera)," *Arthropod Structure & Development*, vol. 33, no. 3, pp. 221–235, Jul. 2004. [Online]. Available: https://www.sciencedirect.com/science/article/pii/S1467803904000337

[103] J. Zhang, J. Li, C. Li, Z. Wu, H. Liang, and J. Wu, "Self-righting physiology of the ladybird beetle Coccinella septempunctata on surfaces with variable roughness," *Journal of Insect Physiology*, vol. 130, p. 104202, Apr. 2021.

[104] M. I. Wallace, J. F. Burn, R. A. Hyde, C. Melhuish, and T. Pipe, "Biologically Inspired Solutions for Compliant Limb UGVs." SEAS DTC, 2007.

[105] C. C. Kessens, D. C. Smith, and P. R. Osteen, "A framework for autonomous self-righting of a generic robot on sloped planar surfaces," in *2012 IEEE International Conference on Robotics and Automation*, May 2012, pp. 4724–4729, iSSN: 1050-4729.

[106] H. Tsukagoshi, M. Sasaki, A. Kitagawa, and T. Tanaka, "Design of a Higher Jumping Rescue Robot with the Optimized Pneumatic Drive," in *Proceedings of the 2005 IEEE International Conference on Robotics and Automation*, Apr. 2005, pp. 1276–1283, iSSN: 1050-4729.

[107] J. Zhang, G. Song, Z. Li, G. Qiao, H. Sun, and A. Song, "Self-righting, steering and takeoff angle adjusting for a jumping robot," in *2012 IEEE/RSJ International Conference on Intelligent Robots and Systems*, Oct. 2012, pp. 2089–2094, iSSN: 2153-0866.

[108] Q. Xuan and C. Li, "Randomness in appendage coordination facilitates strenuous ground self-righting," *Bioinspiration & Biomimetics*, vol. 15, no. 6, p. 065004, Oct. 2020, publisher: IOP Publishing. [Online]. Available: https://doi.org/10.1088/1748-3190/abac47

[109] C. S. Casarez and R. S. Fearing, "Dynamic terrestrial self-righting with a minimal tail," in *2017 IEEE/RSJ International Conference on Intelligent Robots and Systems (IROS)*, Sep. 2017, pp. 314–321, iSSN: 2153-0866. [Online]. Available: https://ieeexplore.ieee.org/document/8202174

[110] U. Saranli, A. A. Rizzi, and D. E. Koditschek, "Model-Based Dynamic Self-Righting Maneuvers for a Hexapedal Robot," *The International Journal of Robotics Research*, vol. 23, no. 9, pp. 903–918, Sep. 2004. [Online]. Available: https://doi.org/10.1177/0278364904045594

[111] S. Peng, X. Ding, F. Yang, and K. Xu, "Motion planning and implementation for the self-recovery of an overturned multi-legged robot," *Robotica*, vol. 35, no. 5, pp. 1107–1120, 2017, edition: 2015/12/23 Publisher: Cambridge University Press. [Online]. Available: https://doi.org/10.1017/S0263574715001009

[112] H. Schempf, E. Mutschler, C. Piepgras, J. Warwick, B. Chemel, S. Boehmke, W. Crowley, R. Fuchs, and J. Guyot, "Pandora: autonomous urban robotic reconnaissance system," in *Proceedings 1999 IEEE International Conference on Robotics and Automation (Cat. No.99CH36288C)*, vol. 3, May 1999, pp. 2315–2321 vol.3, iSSN: 1050-4729.

[113] Z. Guanghua, D. Zhicheng, and W. Wei, "Realization of a Modular Reconfigurable Robot for Rough Terrain," in *2006 International Conference on Mechatronics and Automation*, Jun. 2006, pp. 289–294, iSSN: 2152-744X.

[114] C. Li, C. C. Kessens, R. S. Fearing, and R. J. Full, "Mechanical principles of dynamic terrestrial self-righting using wings," *Advanced Robotics*, vol. 31, no. 17, pp. 881–900, Sep. 2017. [Online]. Available: https://www.tandfonline.com/doi/full/10.1080/01691864.2017.1372213

[115] A. Briod, A. Klaptocz, J. Zufferey, and D. Floreano, "The AirBurr: A flying robot that can exploit collisions," in *2012 ICME International Conference on Complex Medical Engineering (CME)*, Jul. 2012, pp. 569–574. [Online]. Available: https://ieeexplore.ieee.org/document/6275674

[116] A. Klaptocz, L. Daler, A. Briod, J.-C. Zufferey, and D. Floreano, "An Active Uprighting Mechanism for Flying Robots," *IEEE Transactions on Robotics*, vol. 28, no. 5, pp. 1152–1157, Oct. 2012, conference Name: IEEE Transactions on Robotics.

[117] A. Kossett and N. Papanikolopoulos, "A robust miniature robot design for land/air hybrid locomotion," in *2011 IEEE International Conference on Robotics and Automation*, May 2011, pp. 4595–4600, iSSN: 1050-4729.

[118] M. Kovac, M. Schlegel, J.-C. Zufferey, and D. Floreano, "Steerable miniature jumping robot," *Autonomous Robots*, vol. 28, no. 3, pp. 295–306, Apr. 2010. [Online]. Available: http://link.springer.com/10.1007/s10514-009-9173-4

[119] E. Beyer and M. Costello, "Performance of a Hopping Rotochute," *International Journal of Micro Air Vehicles*, vol. 1, no. 2, pp. 121–137, Jun. 2009, publisher: SAGE Publications Ltd STM. [Online]. Available: https://doi.org/10.1260/175682909789498242

[120] "Simulink - Simulation and Model-Based Design." [Online]. Available: https://www.mathworks.com/products/simulink.html

[121] "Tech Talk: Identify Drone Autonomy - Drone Industry Insights," Mar. 2019, section: Market. [Online]. Available: https://droneii.com/drone-autonomy

[122] "Beaufort wind force scale." [Online]. Available: https://www.metoffice.gov.uk/weather/guides/coast-and-sea/beaufort-scale

[123] N. US Department of Commerce, "Beaufort Wind Scale," publisher: NOAA's National Weather Service. [Online]. Available: https://www.weather.gov/mfl/beaufort

Curriculum Vitae

CHARALAMPOS VOURTSIS

Ph.D. Student in Aerial Robotics

Lausanne, Switzerland

http://www.harryvourtsis.com | +41 78 261 3585 | harry.vourtsis@epfl.ch

Passionate Ph.D. student with 5 years of experience in Aerial Robotics and interdisciplinary background, having worked both as a researcher to implement core technologies for aerospace systems in a combination of aircraft design, rapid prototyping, unconventional manufacturing, virtual reality, and robotics as well as a technical leader to leverage an innate ability to communicate complex topics, make rapid practical decisions and action plans, analyze data and collaborate with top-tier universities and companies such as Airbus, Fiat, KIT, OPTIS, and Intel.

RESEARCH EXPERIENCE

ÉCOLE POLYTECHNIQUE FÉDÉRALE DE LAUSANNE (EPFL) – LABORATORY OF INTELLIGENT SYSTEMS, SWITZERLAND *2018 – Current*

Doctoral Researcher

- Currently working on developing a semi-autonomous autopilot for a morphing VTOL platform
- Designed, developed, and flight-tested several bioinspired VTOL platforms for negotiating diverse operational requirements by utilizing wing-shapeshifting strategies
- Designed and developed a biplane platform featuring variable-sweep high-cambered wings for investigating the aerodynamics of hybrid morphing wing configurations in wind tunnel experiments

INTEL RESEARCH LABS – INTELLIGENT SYSTEMS LAB, GERMANY *2021 – 2022*

Research Intern

- Developed the aerodynamic simulation of a VTOL drone with morphing wings that was designed and manufactured at the Laboratory of Intelligent Systems
- Developed a flight simulator that would be used for flight control optimization of VTOL drones

UNIVERSITY OF PATRAS – LABORATORY FOR MANUFACTURING SYSTEMS AND AUTOMATION, GREECE *2014 – 2016*

Research Associate / Technical Project Leader

- Responsible for the technical developments of i-VISION; a 3-year, aeronautics, European-funded research project consisting of 7 companies and institutions (http://www.ivision-project.eu/)
- Managed a team of 4 software developers and collaborated with over 20 professionals from diverse fields and technical backgrounds
- Evaluated each partner's working results and reported to the Senior Management & European Commission

UNIVERSITY OF PATRAS – LABORATORY FOR MANUFACTURING SYSTEMS AND AUTOMATION, GREECE *2013 – 2014*

Research Assistant

- Designed a platform architecture for human–aircraft cockpit operations analysis in virtual environments
- Designed and manufactured prototype devices for laboratory and research applications using 3D scanning and 3D printing technologies
- Developed an aircraft cockpit database model that served as an early functional prototype and a basis to build a semantic cockpit model
- Researched and developed a method for measuring the aspect of coupling complexity in different aircraft–cockpit variants

UNIVERSITY OF PATRAS – LABORATORY OF AERODYNAMIC DESIGN OF AIR VEHICLES, GREECE *2012 – 2013*

Research Assistant

- Designed parametric models for the aerodynamic study and computational analysis of turbomachinery blades
- Analyzed the geometric structure and identified critical design parameters for centrifugal impellers and auxiliary turbine blades

Charalampos VOURTSIS

Laboratory of Intelligent Systems
Lausanne, Switzerland

harry.vourtsis@epfl.ch
+41 78 261 3585

EDUCATION

ÉCOLE POLYTECHNIQUE FÉDÉRALE DE LAUSANNE (EPFL), SWITZERLAND — *2018 – Current*

Doctorate (Ph.D.) in Aerial Robotics under a Marie-Curie Fellowship
Topic: Collision resilient drones for long-range operations
Thesis Advisor: Prof. Dario Floreano

UNIVERSITY OF PATRAS, GREECE — *2009 – 2016*

Diploma (5-year / BSc & MSc) in Mechanical and Aeronautics Engineering
Dissertation Title: A VR Method for the Measurement of Complexity in Product Design
Thesis Advisor: Prof. George Chryssolouris

SENIOR HIGH SCHOOL – LYKEION KATO KASTRITSIOU, GREECE — *2006 – 2009*

Apolytirion Lykeiou, GPA: 19.15/20 – Top 5%

SKILLS & INTERESTS

Programming: Python, JavaScript, CSS, HTML
Tools – Frameworks: Microsoft Office, CATIA, SOLIDWORKS, AutoCAD, Inventor, OpenCV, Robot Operating System (ROS)
Online Courses:
- *Machine Learning by Stanford University on Coursera*
- *Neural Networks and Deep Learning by DeepLearning.AI on Coursera*
- *Robotics: Aerial Robotics by University of Pennsylvania on Coursera*
- *Introduction to Computer Science and Programming Using Python by MITx on edX*

Software – Environments: Linux, Windows, MATLAB, Octave, 3DVIA Virtools
Manufacturing: Rapid Prototyping, 3D Printing, CNC Machining, Laser Cutting, Composite Layups
Languages: Greek (Native), English (Professional)
Interests: Painting, Mountain Biking, Chess, RC Piloting, Projects: https://www.harryvourtsis.com/projects/

SCHOLARSHIPS – AWARDS – ACHIEVEMENTS – VOLUNTEERING

EPFLINNOVATORS FELLOWSHIP, SWITZERLAND — *2018 – 2022*

- *Selected as one out of 7 from 538 applicants for an industry-oriented doctoral programme co-funded by Marie Skłodowska-Curie for 48months*

OTHONOS & ATHINAS STATHATOU FOUNDATION SCHOLARSHIP, GREECE — *2009 – 2015*

- *Ranked 3rd out of 144 admitted students in the Department of Mechanical Engineering & Aeronautics at the University of Patras*

GREEK STATE SCHOLARSHIPS FOUNDATION AWARD — *2009*

- *For the exemplary performance at the University of Patras*

1ST AWARD IN THE TECHNOLOGY & SCIENCE COMPETITION OF THE INSTITUTE OF CHEMICAL ENGINEERING SCIENCES, GREECE — *2006*

- *Participated with the design and construction of a homemade 2-stage rocket*

VOLUNTEER IN THE OLYMPIC GAMES 2004 IN ATHENS, GREECE — *2004*

- *Participated with Polyfoniki Choir of Patras to perform the Olympic Hymn in the Opening Ceremony*

SELECTED PUBLICATIONS

C. Vourtsis, V. C. Rochel, N. S. Müller, W. Stewart, and Dario Floreano, “Wind Defiant Morphing Drones”, in Advanced Intelligent Systems, Accepted and pending publication, Dec. 2022

C. Vourtsis, W. Stewart, and D. Floreano, "Robotic Elytra: Insect-Inspired Protective Wings for Resilient and Multi-Modal Drones," in IEEE Robotics and Automation Letters, vol. 7, no. 1, pp. 223-230, Jan. 2022, 10.1109/LRA.2021.3123378, https://ieeexplore.ieee.org/document/9591382

C. Vourtsis, V. C. Rochel, F. R. Serrano, W. Stewart, and D. Floreano, "Insect Inspired Self-Righting for Fixed-Wing Drones," in IEEE Robotics and Automation Letters, vol. 6, no. 4, pp. 6805-6812, Oct. 2021, 10.1109/LRA.2021.3096159, https://ieeexplore.ieee.org/document/9479684